Biomechanics of the Fibrillar Adhesive System in Insects

James Michael Rex Bullock

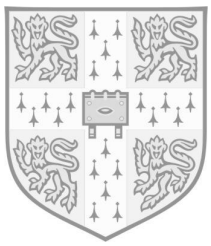

Biomechanics of the Fibrillar Adhesive System in Insects

James Michael Rex Bullock

Clare College

Supervised by Dr Walter Federle
This dissertation is submitted for the degree of
Doctor of Philosophy

Cambridge 2010

James M. R. Bullock, *Biomechanics of the fibrillar adhesive system in insects*
University of Cambridge, 2010

DECLARATION

This dissertation is submitted for the degree of Doctor of Philosophy. It is the result of my own work and includes nothing which is the outcome of work done in collaboration except where specifically indicated in the text and acknowledgements. It is not substantially the same as any previous material submitted for a degree at any other University. This thesis totals 151 pages (including bibliography and appendices) and does not exceed the prescribed word limit.

Cambridge, 30th September 2010

James Bullock

ACKNOWLEDGEMENTS

To my supervisor, Walter Federle, an enormous debt is owed. His help and guidance have been more than critical to the success of all that is contained within this thesis and his constant supply of ideas and inspiration have made him one of the best supervisors one could have, regardless of the field of research.

Uncountable thanks are due to all current and honorary members of the Cambridge Insect Biomechanics workgroups. It has been an immense privilege to have studied and worked with you; Ulrike Bauer, Holger Bohn, Christofer Clemente, Kristien de Clercq, Jan-Henning Dirks, Patrick Drechsler, Thomas Endlein, Nanna Evers, Jamie Gundry, David Labonte, Li Ming-he, Karin Moll, Sean Ng, Anne Peattie, Gregory Sutton, Filip Szufnarowski, Dan Thornham, Kerstin Tüchert and Yanjia Gao.

Many thanks go to Clare College and the Department of Zoology, who have both provided me with an exceptionally creative and friendly environment within which to live and work. In particular Sue Goodbody and Linda Wheatley deserve much credit.

Thanks to my advisors, Simon Laughlin and Ullrich Steiner, to my examiners, Jon Barnes and Simon Maddrell, and to the other members of the Department of Zoology that I have worked with during the course of my PhD, including Malcolm Burrows, Charlie Ellington, Felix Evers and Heather Whitney. Additionally I would like to thank the members of the Cambridge Engineering Department (Mechanics, Materials and Design Division), Nanoscience Centre and Multi Imaging Centre for technical help concerning several areas of this work.

Importantly thanks must go to Christofer Clemente, Saul Dominguez, Patrick Drechsler, Andreas Eckart, Thomas Endlein, Nanna Evers and Filip Szufnarowski for the initial and continued development of the LabVIEW motor control programmes and force feedback set-up. I would specifically like to express my deep gratitude to Christofer Clemente and Thomas Endlein for their continual guidance, advice and help with many of the technical and scientific aspects of this work.

Thanks to Dan Thornham and all at the Telamba Homestay in Brunei Darussalam for the indispensable guidance and incredible hospitality I received during my time spent working in the field.

This thesis was funded by research grants from the UK Biotechnology and Biological Sciences Research Council and the Cambridge Isaac Newton Trust. Additional funding was received from Clare College and the Cambridge Philosophical Society.

And to my family, Michael Bullock, Felicity Bullock, Charlie Bullock and Payel Das, who have given me constant love and support, everything else is owed.

Biomechanics of the fibrillar adhesive system in insects
- James Michael Rex Bullock

Many animals are able to scale smooth surfaces using adhesive structures on their feet. These organs are either soft pads with a relatively smooth surface or dense arrays of microscopic adhesive hairs with both designs having independently evolved in diverse taxa of arthropods and vertebrates. Biological adhesive pads out-perform conventional adhesives in many respects, making them important models for biomimetics. Hairy pads have attracted particular attention, because it has become feasible to fabricate similar synthetic microstructures. Nevertheless, the detailed performance and functional properties have not been characterised for any natural fibrillar adhesive system, and many fundamental aspects are still not understood. The aim of this thesis was therefore to investigate the fibrillar adhesive system of leaf beetles as a model.

To investigate the functional implications of hairy pad design, the attachment performance between hairy pads of the leaf beetle *Gastrophysa viridula* and smooth pads of stick insects (*Carausius morosus*) was compared. Adhesive and frictional stresses were found to be similar in smooth and hairy pads, inconsistent with contact splitting theory, which predicts higher adhesive stresses for fibrillar adhesives. Hairy pads showed a greater direction-dependence of friction forces than smooth pads, confirming the importance of the asymmetric design of individual setae for effortless detachment. Experiments with contaminating particles also showed that hairy pads removed contamination more rapidly and efficiently than smooth pads. Self-cleaning ability had not been previously documented for adhesive organs of insects. To investigate to what extent the hairy system is able to compensate for surface roughness, whole-body attachment forces were measured for varying roughness levels. Attachment was reduced for all length scales of surface roughness, but in particular for asperity sizes smaller than the diameter of individual seta tips.

Leaf beetles possess adhesive pads on three tarsal segments, which vary in setal morphology. However, the functional implications of this variation are unknown. The mechanical and adhesive properties of individual pads were therefore tested and their use during climbing observed. Proximal pads were shown to be stiffer than distal pads, conferring stability during pushing. In contrast, the softer distal pads allowed better attachment to rough surfaces. Hence the morphological variation is explained by an effective division of labour between the pads. To investigate an

extreme example of pushing in a hairy system, pad use was studied during jumping in flea beetles. The pushing forces needed during take-off were exclusively produced by the proximal pads, again confirming the division of labour. To characterise the effects of different hair morphologies and to understand how individual setae contribute to array and whole-animal performance, single hair forces were measured using a glass capillary cantilever. Male-specific discoidal hairs were shown to be both stiffer and more adhesive than pointed and spatula-tipped setae, likely affecting overall pad stability and attachment.

This thesis has shown that hairy pads are similar to smooth pads in the magnitude of adhesive stress supported yet outperform them in detachability and self-cleaning. It was also demonstrated that there are considerable differences in design and performance even within setal arrays of the same insect, indicating the limitations of general models of fibrillar adhesion and underlining the importance of specialised adaptations.

Some of the ideas and figures presented in this thesis have previously appeared in the following publications:

Journal Papers

Bullock, J. M. R., Drechsler, P. and Federle, W. (2008). Comparison of smooth and hairy attachment pads in insects: friction, adhesion and mechanisms for direction-dependence. *Journal of Experimental Biology* 211, 3333-3343.

Bullock, J. M. R. and Federle, W. (2009). Division of labour and sex differences between fibrillar, tarsal adhesive pads in beetles: effective elastic modulus and attachment performance. *Journal of Experimental Biology* 212, 1876-1888.

Clemente C. J., Bullock J. M. R., Beale A. and Federle W. (2009). Evidence for self-cleaning in fluid-based smooth and hairy adhesive systems of insects. *Journal of Experimental Biology* 213, 635-642.

Bullock, J. M. R. and Federle, W. (2010). The effect of surface roughness on claw and adhesive hair performance in the dock beetle Gastrophysa viridula. *Insect science* in press.

Abstracts

Bullock, J. M. R. and Federle, W. (2008). Friction forces in the hairy adhesive pads of beetles. *Comparative Biochemistry and Physiology - Part A: Molecular & Integrative Physiology* 150, 90-91. Society for Experimental Biology, 6-10th July, Marseille, France.

Bullock, J. M. R. and Federle, W. (2008). Comparison of Attachment Performance in the Hairy and Smooth Adhesive Pads of Insects. *Annual Meeting & Exhibition Final Program and Abstracts.* Society for Integrative and Comparative Biology, 3-7th January, Boston, MA, USA.

Bullock, J. M. R. and Federle, W. (2009). Why have more than one pad per leg? Determining the mechanical and adhesive properties of hairy attachment pads in beetles. *Comparative Biochemistry and Physiology - Part A: Molecular & Integrative Physiology* 153, 130. Society for Experimental Biology, 28th June – 1st July, Glasgow, Scotland.

Clemente, C. J., Beale, A., Bullock, J. M. R. and Federle, W. (2009). Evidence for self-cleaning in fluid-based smooth and hairy adhesive systems of insects. *Comparative Biochemistry and Physiology - Part A: Molecular & Integrative Physiology* 153, 123. Society for Experimental Biology, 28th June – 1st July, Glasgow, Scotland.

Bullock, J. M. R., Clemente, C. J. and Federle, W. (2010). Pushing and pulling: beetles use different tarsal pads to walk and climb. *Annual Meeting & Exhibition Final Programme and Abstracts*. Society for Integrative and Comparative Biology, 3-7th January, Seattle, WA, USA.

Clemente, C. J., Beale, A., Bullock, J. M. R. and Federle, W. (2010). Evidence for self-cleaning in fluid-based smooth and hairy adhesive systems of insects. *Annual Meeting & Exhibition Final Programme and Abstracts*. Society for Integrative and Comparative Biology, 3-7th January, Seattle, WA, USA.

Bullock, J. M. R. and Federle, W. (2010). How sticky is a single beetle hair? Measuring in vivo attachment forces from individual adhesive setae. *Annual Main Meeting Programme*. Society for Experimental Biology, 30th June – 3rd July, Prague, Czech Republic.

Labonte, D., Bullock, J. M. R. and Federle, W. (2010). Hairy vs. smooth: differences in fluid-based friction and adhesion between different pad designs. *Annual Main Meeting Programme*. Society for Experimental Biology, 30th June – 3rd July, Prague, Czech Republic.

Bullock, J. M. R., Clemente, C. J. and Federle, W. (2010). The hairy pads of insects; smart biological adhesives that can effortlessly attach, detach and clean themselves. *Congress Proceedings Programme and Abstracts*. 6th World Congress of Biomechanics, 1-6th August, Singapore.

CONTENTS

1

INTRODUCTION

"Every species is furnished with implements, adapted to its exigencies. What exquisiteness! What proportion in the several parts that compose the body of a fly! What precision, what mechanism in the springs and motion… to account for the remarkable ability of this creature to walk on smooth surfaces!"

Antoine Augustin Calmet (1730)

Humans have, since the earliest days of science, been fascinated by the natural world and have sought ways to both understand and mimic it. A good example of this is the past and recent interest focused on nature's impressive use of biological attachment structures. Natural adhesives are found in numerous places and display a great many forms. Dynamic structures are found on the foot pads of lizards, amphibians, mammals, spiders and insects. More static bonds are used by as diverse a range of organisms as marine mussels and climbing plants.

Given this ubiquity, it is perhaps not surprising to find in literature references to biological adhesives dating as far back as Aristotle, who commented on the gecko's ability to "*run up and down a tree in any way, even with the head downwards*" (Thompson, 1918). Further description has followed the progress of modern science, advancing as experimental techniques develop. Famously, in 1665, Robert Hooke described the adhesive structures on a fly's foot (see Fig. 1.1), one of the first specimens observed with the newly developed microscopic apparatus (Hooke, 1665)[1]. Present day scientific methodologies have brought further important

[1]In Hooke's original 1665 publication Micrographia he describes the fly's foot as "*of a most admirable and curious contrivance, for by this the Flies are inabled to walk against the sides of Glass, perpendicularly upwards, and to contain themselves in that posture as long as they please; …to stick or suspend themselves on the under surface of a Glass well polish'd and cleans'd; their suspension therefore is wholly to be ascrib'd to some Mechanical contrivance in their feet*." He additionally notes and warns that "*the Fly could so readily unglew and loosen its feet …that we might not be cast upon unintelligible explications of the Phænomena of Nature, at least others then the true ones, where our senses were able to furnish us with an intelligible, rational and true one*." (Hooke, 1665).

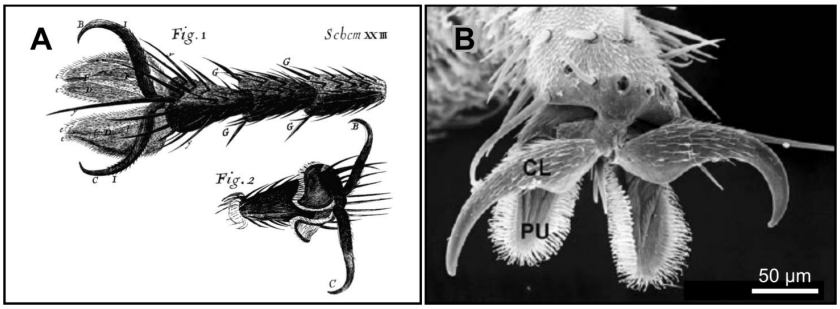

Figure 1.1: (A) Hooke's original illustration plate of a fly's foot from Micrographia (Hooke, 1665). (B) Scanning electron micrograph of the foot of the blowfly *Chrysomya chani*, showing the claws, CL and adhesive pulvilli, PU, adapted from Sukontason et al. (2006).

advances in the understanding of biological adhesives, with microscopic techniques finally allowing characterisation of many of the adhesives properties and parameters to be discussed below.

With the desire to describe and understand these systems comes the impulse to replicate them. Following on from rapid advances in material science, many attempts have been made to fabricate copies of the gecko or insect's adhesive structures, yet most fall short of their inspirations in several performance aspects (for reviews see: Bogue, 2008; del Campo and Arzt, 2007). Fabrication techniques now allow mimics of more and more complex designs (see Appendix A.1) making the replication of detailed adhesive morphologies increasingly feasible. However, many fundamental questions still remain as to the actual mechanisms, functions and principles of the systems being imitated. Hence this thesis attempts to address and answer some of the important and outstanding questions relating to the mechanisms of attachment and detachment in biological adhesives.

1.1 BIOLOGICAL ATTACHMENT DEVICES

In nature, the ability to grip and hold on to a wide variety of surfaces has proved a strong selection pressure for many species. It has allowed animals to avoid predation or forage for food and to prevent dislodgement or colonise otherwise inaccessible parts of their environment. The following section discusses the requirements for attachment in animals and the biological morphologies that have developed to overcome these challenges.

1.1.1 Requirements for animal attachment

Animals run and climb over almost every terrain on earth and usually must do this quickly enough to avoid predation or catch prey. In some cases the substrate possesses enough texture to allow

claws to grip and these structures are found in the vast majority of climbing animals. However, when the surface is smooth and comparatively stiff (for example a sheer rock face, or the smooth outer cuticle of a plant), claws will no longer support the animal (Dai et al., 2002) and adhesive devices are needed. A wide variety of natural adhesive organs have therefore evolved to cope with these problems (e.g. see: Scherge and Gorb, 2001) that demonstrate an array of impressive properties. For example, gecko and insect adhesives can provide strong adhesion with high safety factors (Autumn et al., 2000; Eisner and Aneshansley, 2000) yet also allow rapid and dynamic detachment (Autumn et al., 2006a; Autumn and Hansen, 2006; Autumn et al., 2006b; Federle, 2006). They can resist both wear and contamination (Hansen and Autumn, 2005; Ridgel et al., 2003) yet also remain compliant enough to attach to a wide range of smooth and rough surfaces (Autumn et al., 2006c; Persson and Gorb, 2003).

Specialised plant structures designed to prevent attachment produce further challenges. For example, *Macaranga* trees produce brittle and micro-rough waxy blooms to deter ants (Federle, 1999) and *Nepenthes* pitcher plants have developed slippery inner rims to

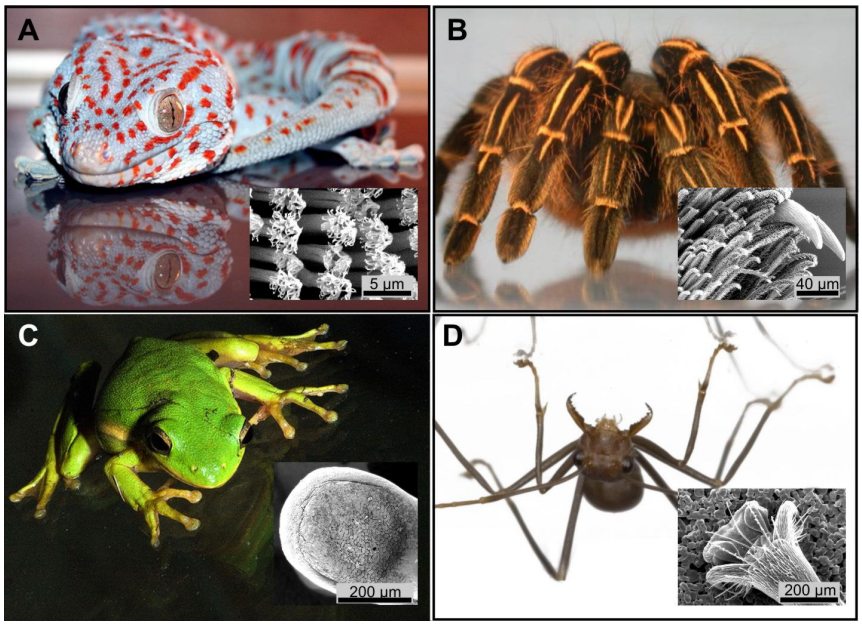

Figure 1.2: Whole animal photographs and inset scanning electron micrographs illustrating the broad variety of morphologies in hairy and smooth vertebrate and invertebrate adhesive pads. (A) Gecko (*Gekko gecko* pictured from flickr.com/jglitten, *L. picturatus* setae inset from A. Peattie) a vertebrate with hairy pads, (B) tarantula spider (*Aphonopelma seemanni* pictured adapted from Gorb et al. (2006), *Grammostola rosea* claw tuft inset from A. Peattie) an invertebrate with hairy pads, (C) tree frog (*Hyla cinerea* pictured from flickr.com/e_monk, *Litoria caerulea* toe pad inset from J. Smith) a vertebrate with smooth pads, (D) weaver ant (*Oecophylla smaragdina* pictured, tarsus inset from T. Endlein) an invertebrate with smooth pads.

trap insects (Bohn and Federle, 2004). Yet in both these cases animals have evolved to overcome these devices, with several species of *Crematogaster* and *Camponotus* ants able to climb waxy *Macaranga* stems (Federle et al., 1997; Federle et al., 2002a; Federle et al., 2000) and *C. schmitzi* ants able to run across the pitcher plant peristomes (Bohn and Federle, 2004).

The dynamic animal adhesives that have evolved to meet these challenges are highly diverse. However, to allow comparison they are generally grouped into two broad categories; smooth and fibrillar (Scherge and Gorb, 2001) (see Fig. 1.2) both of which are found in a wide number of vertebrates and invertebrates. Smooth systems make use of broad, compliant pads usually located on the toes or between claws. They are found on the feet of amphibians (in tree frogs (Barnes, 2007; Green, 1981) and arboreal salamanders (Green and Simon, 1986)), mammals (in arboreal possums (Rosenberg and Rose, 1999) and bats (Riskin and Racey, 2009)) and in many orders of insect (Beutel and Gorb, 2001; Gorb et al., 2002). Fibrillar or 'hairy' systems employ arrays of fine, flexible hairs or 'setae' densely packed on toe or foot pads. They are found in lizards (in geckos, anoles and skinks (Irschick et al., 1996; Ruibal and Ernst, 1965; Stork, 1983; Williams and Peterson, 1982)), spiders (Coddington and Levi, 1991; Hill, 1977; Rovner, 1978) and again in many insects (Beutel and Gorb, 2001; Gorb et al., 2002)[2].

These hairy and smooth systems can be further sub-divided by their adhesive mechanism as all rely on either a 'wet' or 'dry' model of adhesion. All smooth pads that have been so far studied are fluid covered and hence reliant on a form of wet adhesion derived from this secretion (e.g. Barnes et al., 2004; Federle et al., 2006; Federle et al., 2002b; Gorb and Scherge, 2000; Gorb, 2001; Jiao et al., 2000; Lees and Hardie, 1988; Vötsch et al., 2002). Hairy systems can be dry (e.g. geckos: Autumn et al., 2002) or wet and covered with a secreted fluid (e.g. insects: Betz, 2003; Eisner and Aneshansley, 2000; Gorb, 1998; Langer et al., 2004). Dry systems are reliant on dispersive intermolecular attraction (Autumn et al., 2002), whereas wet systems can additionally make use of capillary

[2]Other adhesive mechanisms also exist in nature and have been reported in several biological systems. These mechanisms are generally not regarded as being 'dynamic' as they are often semi-permanent or require relatively long detachment times, making them unsuitable for rapid locomotion. For example, natural glues are used by limpets and mussels (Crisp et al., 1985; Papov et al., 1995; Smith, 1992; Waite et al., 2005), echinoderms (Santos et al., 2005) and climbing plants (Groot et al., 2003). Suction cups are also used by some animals for grasping or hanging and allow both effective long term adhesion and some degree of controllable detachability during locomotion. These are commonly found underwater where tight seals are more easily made and shape changes are smaller (e.g. in diving beetles (Bergsten and Miller, 2007), cephalopods (Kier and Smith, 2002; Smith, 1996) or limpets (Smith, 1991)), but have also been observed on the feet of some species of hanging bats (Riskin and Fenton, 2001; Thewissen and Etnier, 1995).

and viscous forces to provide attachment (Hanna and Barnes, 1991). The principles governing dry and wet adhesion and friction are discussed in section 1.2.

The gecko hairy adhesive system is perhaps the most studied to date and information exists characterising its frictional and adhesive abilities (for reviews see: Autumn, 2006a; Autumn, 2006b). Indeed, a great many biomimetic studies have based synthetic adhesive designs on parameters derived from this system (see Appendix A.1). Insect adhesives are comparatively less well understood. They do however encompass a wide array of diversity of adhesive organs (Beutel and Gorb, 2001; Scherge and Gorb, 2001). Their ability to colonise almost every terrestrial habitat also makes them extremely important models for any research intended to improve our understanding of how animals climb in challenging environments.

1.1.2 Hairy and smooth adhesive pads in insects

As discussed in the preceding section, both hairy and smooth wet adhesive pads are found amongst the tarsal structures of insects (see Fig. 1.3). In hairy systems, the hairs or setae are made from cuticle and are found on the tarsal segments of insects of many orders, most prominently in flies (Diptera) and beetles (Coleoptera) (Scherge and Gorb, 2001). The pads may take many forms, for example the pulvilli of flies are flexible (Gorb, 1998), whereas the pads of leaf beetles are flat and planar (Stork, 1980c). Whilst the mechanical properties of the seta cuticle are largely unknown, it is generally believed to be a stiff, wear-resistant material (Federle, 2006; Orso et al., 2006). Flexibility, and hence the compliance required for intimate surface contact is therefore derived from the high aspect-ratio design of the hairs (Autumn et al., 2006c). Smooth pads are found in several other insect orders, including cockroaches (Blattodea), grasshoppers (Orthoptera), bugs (Hemiptera) and stick insects (Phasmatodea). These pads are also formed from cuticle, but unlike the rigid setae of hairy pads are soft and compliant (Gorb et al., 2000; Scholz et al., 2008) and filled with haemolymph (Beutel and Gorb, 2001).

Previous studies have made progress towards describing the composition and fluid properties of the secreted liquid (Dirks et al., 2009; Drechsler and Federle, 2006; Federle et al., 2002b; Vötsch et al., 2002). However, uncertainties still exist, particularly for hairy pads where many basic parameters such as attachment performance, detachability, resistance to contamination and substrate tolerance remain to be quantified, (Federle, 2006). Hairy insect adhesives and their comparison to smooth insect pads therefore form the principal focus of this thesis. The following section provides important background information on the basic

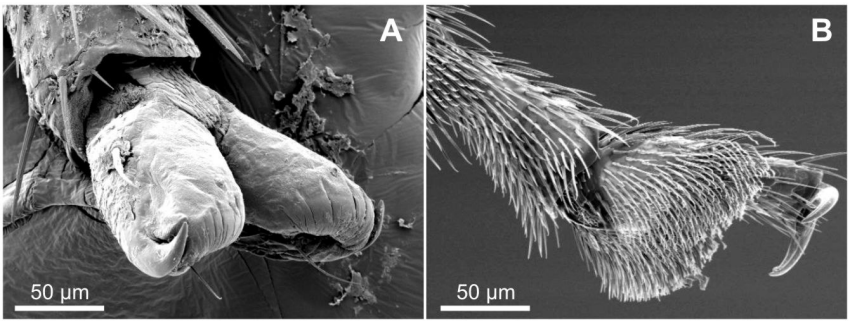

Figure 1.3: SEMs illustrating typical smooth and hairy tarsal adhesive structures in insects. (A) shows the smooth arolium of a leaf hopper bug from the genus *Aphrodes*, whereas (B) shows the hairy distal pad of the flea beetle of the genus *Altica*.

mechanics of adhesion and friction between solid deformable bodies.

1.2 MECHANISMS OF ADHESION AND FRICTION

Adhesive forces are an important feature of the interactions between solids and liquids. A fundamental property of all matter, electrostatic forces hold molecules together and on the macroscopic scale allow bulk materials to adhere. Generally the only factor preventing two bodies from adhering is the lack of contact made between uneven surfaces. Adhesion between solids also arises due to interactions with fluids, with viscous and surface tension properties capable of bonding lubricated surfaces. 'Adhesive force' quantifies the perpendicular force required to detach an object from a surface and therefore provides a measure of the attachment of two objects. 'Friction force' quantifies the shear force preventing two bodies from sliding freely and is of equal importance in most biological attachment systems. Most real examples of adhesion will take place between two deformable bodies and several theoretical contact or detachment models exist to explain this phenomenon.

1.2.1 Adhesion mechanisms

Adhesion mechanisms can be dry (relying on the formation of direct intermolecular bonds) or wet (mediated through an adhesive fluid) and both have been adopted by biological systems to provide strong dynamic attachment during locomotion.

Dry adhesion – intermolecular bonds

Dry adhesion relies on the formation of weak intermolecular van der Waals forces. These can be between polar (Keesom interactions) or non-polar (London dispersion forces) molecules, and depend

upon the weak interactions between permanent or induced dipoles. Dispersion forces form when fluctuating polarisations of electron clouds allow weak and temporary bonds to form between two molecules. These forces result in macroscopic adhesion, providing that close contact can be made between objects. The van der Waals force between two spheres of radius R_i therefore depends upon the polarisability of the molecules and on the distance between them and is given by (Hamaker, 1937):

$$F_{vdW} = -\frac{A_H R}{6h^2} \qquad [1.1]$$

where R is the reduced radius (given by R_1R_2/R_1+R_2), A_H is the Hamaker constant (which depends on the number of atoms per unit volume in two interacting bodies and the interaction between the molecules) and h the separation between surfaces. Given that the denominator falls off with the second power, it is clear that van der Waals forces will rapidly decrease with separation and are generally only relevant for very small separations (of the order of approximately 10 nm).

Wet adhesion – capillary and Stefan forces

When a wetting fluid is present between two surfaces, this mediates adhesion instead and forces depend upon the fluid properties of viscosity and surface tension. Capillary forces are a result of the surface tension of a fluid. When a fluid contacts a solid it will 'wet' the surface forming a droplet of defined contact angle. This angle depends on the interfacial energies between the solid, fluid and vapour (i.e. the surface energy of the solid and the surface tension of the fluid), as described by Young's equation (Young et al., 1855) which balances the tensions at each boundary. For example as water has a high surface tension, hydrophobic materials (low surface energies) are represented by high water droplet contact angles, whereas hydrophilic materials (high surface energies) are represented by low contact angles. If the contact angle of a fluid to the surface is known then the capillary force adhering two wetted solids can be calculated. Between two parallel surfaces a capillary bridge will form, with a radius of curvature given by:

$$r = \frac{h}{\cos\theta_1 + \cos\theta_2} \qquad [1.2]$$

where θ_i is the contact angle of the fluid with each surface and h the separation between surfaces. For a cylindrical volume of fluid (of radius R and height h) trapped between two surfaces, the wetting

will result in a pressure drop inside the fluid, given by Laplace's law (Laplace, 1806; Young, 1805) as:

$$\Delta p = \gamma_{LV}\left(\frac{1}{r}+\frac{1}{R}\right) \qquad [1.3]$$

where γ_{LV} is the surface tension of the fluid. Hence substituting for r and multiplying by the total area of contact (πR^2) gives the total attractive capillary force as:

$$F_{capillary} = -\pi R^2 \gamma_{LV}\frac{\cos\theta_1+\cos\theta_2}{h} - \pi R\gamma_{LV} \qquad [1.4]$$

which is a combination of the Laplace pressure and surface tension terms. The second term is relatively small and can in many cases be neglected. As noted above for van der Waals forces, the presence of h in the denominator means that the attractive force will decrease with separation. Hence a greater volume of fluid should serve to weaken the capillary bridges and reduce adhesion.

'Stefan adhesion' forces (Stefan, 1875) are a result of the viscosity of a fluid. This is modelled using fluid dynamics, assuming two plates of radius R, separated by a distance h filled with a fluid of (temperature-dependent) viscosity η. As the plates are pulled apart (with the separation increasing by an increment of dh), the fluid is treated as if flowing through a thin box with the 'no slip' condition applied at the fluid-solid boundary. This leads to the derivation of the Stefan adhesive force:

$$F_{stefan} = \pm\frac{dh}{dt}\frac{3\pi\eta R^4}{2h^3} \qquad [1.5]$$

Clearly in this case, the force is time dependent (i.e. non-static) as it depends on the velocity of separation dh/dt. Again, attractive force decreases with separation and adhesion is reduced in the presence of a thicker fluid layer.

The surface tension and viscosity terms can be combined to form a general wet adhesion model (e.g. see: Emerson and Diehl, 1980; Hanna and Barnes, 1991). It should be noted however that the models presented above for the adhesion mechanisms are only valid for the perpendicular separation of two rigid substrates. In many biological systems this will not be the case and some degree of peeling will take place. This is discussed for theoretical contact models and the peeling tape detachment model in section 1.2.3.

1.2.2 Friction mechanisms

Dry friction – classical and rubber friction

Dry friction is empirically described by 'classical' or Coulomb friction. This takes into account the parallel shear force that arises between two dry sliding materials containing some degree of surface roughness. It is quantified by Amontons' friction law which states that the friction force will be directly proportional to the applied normal force, and is independent of both 'projected' surface contact area and sliding velocity (Amontons, 1709). Hence:

$$F_{\parallel} = \mu F_{\perp} \qquad [1.6]$$

where μ, the proportionality constant, is termed the coefficient of friction. This is a result of both the adhesion (i.e. van der Waals forces that cause molecules to adhere to each other as discussed in section 1.2.1) and the 'ploughing' (deformation required to plough asperities of the harder surface through the softer one) components. As the normal force is increased, sliding surfaces are brought closer together and 'real' contact area increases. This brings more molecules into close contact. Enlarging the overall projected contact area but not the normal force will not increase friction as the pressure remains constant and the real contact area will not increase.

A distinction can be made between 'static' and 'kinetic' friction. Static friction describes the parallel force that must be applied to a body before the onset of sliding, whereas kinetic friction describes the force that must be applied to a body to keep it in stable motion. If the static friction force is larger than the kinetic friction force then a 'stick-slip' behaviour will be observed during sliding as the force must continually build during movement (Persson, 1999).

Rubber and other deformable materials will not obey Amontons' laws. Increasing their projected area will increase the friction force as they are already able to deform around surface asperities without high pressures, thus increasing the amount of real contact. If the material is highly deformable then it is termed an adhesive and will exhibit friction forces even under negative loads.

Wet friction – fluid properties

As for rubber friction, wet friction i.e. that between two lubricated surfaces, will also not obey Amontons' laws. In this case the presence of a fluid fills in the gaps between surfaces, and increasing the normal force will generally have no effect on real contact area.

Friction in a fully wetted, fluid based system is no longer solely reliant on the van der Waals interactions between surfaces but instead on the viscous and surface tension properties of the liquid as discussed in section 1.2.1 for the case of wet adhesion.

This must be treated in a slightly different way than the adhesion case as shearing fluids give rise to different effects. It is important to note that whilst the viscous component may account for much of the sliding friction force, it is, for a standard Newtonian fluid, rate dependent (see Equation 1.5) and will not give rise to any static friction. The surface tension component (capillary forces), will contribute static friction (due to the retention forces from the deformation of the liquid-solid contact angle; see Equation 1.4) but is likely to be relatively small in many systems (Federle et al., 2004; Geiselhardt et al., 2009a). If the fluid layer is very thin (of the order of ten molecules), the interactions become more complex and 'boundary lubrication' is described (Israelachvili, 1992a; Israelachvili, 1992b) which may involve direct contact and van der Waals interactions between the solids (i.e. 'de-wetting' of the surfaces). If however the liquid film is very thick then the surfaces can be considered 'lubricated' and forces will depend mostly on the bulk properties of the fluid (Israelachvili, 1992a).

1.2.3 Contact and detachment models

This section introduces some of the models describing contacting deformable bodies. These models put into context the adhesion mechanisms discussed above and provides the basis for the general principles of both the attachment and detachment of a flexible, peeling adhesive.

The Hertz model

The Hertz model is a basic contact model (Hertz, 1881) that defines the contact radius of two non-adhesive contacting elastic spheres. This depends on the mechanical properties of the spheres and the normal force pressing them together. Assuming two spheres of radius R_i and elastic modulus E_i, the contact radius, a is given by:

$$a^3 = \frac{RF_{\perp}}{K} \qquad [1.7]$$

where R is the radius of curvature (given by R_1R_2/R_1+R_2), $F_{\perp}$ the normal load force and K is the bulk elastic modulus given by:

$$\frac{1}{K} = \frac{3}{4}\left(\frac{1-\nu_1^2}{E_1} + \frac{1-\nu_2^2}{E_2}\right) \qquad [1.8]$$

Where v_i is the Poisson ratio of each sphere.

Johnson–Kendall–Roberts (JKR) theory

JKR theory (Johnson et al., 1971) extends the Hertz model to take into account the adhesive force existing between the two spheres. Hence a contact radius will exist, even without an external load force. The contact radius, *a* for two adhering elastic spheres of equal radius is found to be:

$$a^3 = \frac{R}{K}\left(F_\perp + 3\pi RW + \sqrt{6\pi RWF_\perp + (3\pi RW)^2} \right) \qquad [1.9]$$

Where *W* is the work of adhesion[3]. Clearly, for a non-zero work of adhesion term there is still contact even when the load force equals zero. The adhesive pull-off force can be further derived and is found to be:

$$F_{JKR} = -3\pi R\gamma \qquad [1.10]$$

where γ is the surface energy of the solids. Here it should be noted that adhesive force scales with the contact length *R*, and not with the contact area *A*. If there is no adhesion and the work of adhesion equals zero, the contact radius equation will simply reduce back to the Hertz model.

The peeling tape model

In addition to describing the contact between two elastic bodies, the above models also describe the separation between them. The peeling tape detachment model is presented here in addition to the JKR model as a further illustration of the scaling of adhesive force with contact length in a peeling adhesive. For an inextensible tape of width *B* peeling from a surface at a peel angle θ where the work of adhesion for the surfaces is *W*, the force that must be applied perpendicularly to the surface to cause detachment is given by (Kendall, 1971):

$$F_{tape} = -\frac{BW\sin\theta}{1-\cos\theta} \qquad [1.11]$$

[3]Adhesion is often quantified by the 'work of adhesion' *W*, defined as the work per unit area (Jm^{-2}) lost during the separation of two surfaces. *W* is simply an addition of the surface energies, γ of the adhering materials, i.e. the energy required per unit area to create each new surface (usually a solid-vapour interface).

As shown for JKR detachment, the peel force will be directly proportional to both the work of adhesion and to the width of the peel zone. These principles form an important basis for many theoretical arguments concerning animal adhesive systems and are discussed in section 1.4.

1.2.4 Application to biological adhesives

As discussed in section 1.1, most dynamic vertebrate and invertebrate adhesive systems fall within the broad grouping of 'smooth' or 'hairy'. Additionally, these can be dry or wet systems, the broad mechanics of which have been detailed above. In most cases however, the exact attachment system is to some extent unclear. For example for geckos, typically described as a 'dry' system, the main attachment mechanism has been shown to rely on intermolecular van der Waals adhesion (Autumn et al., 2002) formed from non-polar induced dipole interactions. This is suggested by an observed lack of dependence on surface chemistry, however the possibility of a contribution from capillary forces condensed from water vapour has also been discussed (Huber et al., 2005b).

The 'wet' systems of insects and tree frogs are likely based mainly on the contributions from viscous and surface tension forces as discussed above. However, the observed static and kinetic friction forces of many natural systems are too great to be explained by simple capillary and Newtonian Stefan forces (Federle et al., 2002b). It has instead been shown that for some insects, a two phasic emulsion exists within the foot secretion causing it to act as a non-Newtonian, Bingham fluid (Dirks et al., 2009; Federle et al., 2004; Federle et al., 2002b; Gorb, 2001; Vötsch et al., 2002). This causes a shear thinning, allowing static friction and highly rate-dependent friction forces (Dirks et al., 2009; Federle et al., 2004; Federle et al., 2002b). Additionally it is to some extent unclear whether close enough contact can be made between the adhesive pad and the substrate to allow van der Waals forces to contribute. For example direct contact has been proposed as a mechanism to prevent sliding in tree frogs and ants (Barnes, 1999; Federle et al., 2006; Federle et al., 2002b).

The detachment mechanism for animal adhesives is in most cases equally unknown. Whilst geckos deliberately unpeel their toes (digital hyper extension) whilst walking (Russell, 1975; Russell, 2002), it is not clear to what extent other animals are able to resist or cause peeling of their attachment pads. This has important consequences for the theoretical models governing the attachment of fibrillar adhesives (Federle, 2006). The most important of these models are discussed in the following section along with a

discussion of the potential benefits hairy systems confer over smooth systems.

1.3 FUNCTIONAL PROPERTIES OF THE HAIRY ADHESIVE SYSTEM

Many animals have developed a fibrillar system of adhesion and in insects alone, hairy adhesives have independently evolved at least three times (Beutel & Gorb 2001). It has therefore been argued that they represent an optimised form of attachment (Federle, 2006) and may confer several advantages over smooth systems. These possible advantages are summarised as an increase in maximal adhesion, an ability to produce controlled, directionally-dependent attachment and a mechanism for self cleaning. It has also been suggested that hairy adhesives may possess a strong ability to adapt to surface roughness. In this section, the theoretical ideas supporting these concepts are discussed.

1.3.1 Maximal overall adhesion

Many theoretical arguments attribute the wide distribution of hairy systems in animals to the mathematical concept of contact splitting. This describes the mechanisms by which adhesive force can be increased by dividing the surface of a material. This concept is derived from three separate models; the principles of 'crack arresting' and 'work of adhesion' and the concept of 'force scaling' (Federle, 2006). The crack arresting model explains that due to the small size of individual contacts, fractures cannot propagate across the pad. The work of adhesion model requires a peeling pad and demonstrates that due to the increased compliance of a fibrillar array the work required to stretch the hairs will increase the pull-off force. Both of these concepts are discussed in more detail in Appendix A.2.

The force scaling model however, is of particular relevance to the scaling of animal adhesive devices (Arzt et al., 2003). It provides a set of theoretical predictions for the attachment forces of hairy pads (Arzt et al., 2003; Jagota and Bennison, 2002) and employs established contact models, for example the Johnson-Kendall-Roberts theory (Johnson et al., 1971). This theory states that for a peeling flexible material with an evenly distributed load, adhesive force will scale with contact length and not area (see section 1.2). This implies that division of contact will enhance attachment as the total contact perimeter will increase (Arzt et al., 2003; Autumn et al., 2002; Spolenak et al., 2004).

Assuming that the force acting on a solid or smooth pad is proportional to its radius, R_{pad} gives:

$$F_{smooth} \propto R_{pad} \quad [1.12]$$

Hence for a simultaneous detachment of a hairy pad divided into multiple contacts of radius R_{hair}, the force on a hairy pad will be proportional to the force on each hair multiplied by the number of hairs, n (see Fig. 1.4). Hence:

$$F_{hairy} \propto nR_{hair} \quad [1.13]$$

n is given by the ratio of areas as:

$$n = \frac{\pi R_{pad}^{\ 2}}{(2R_{hair})^2} \approx \frac{R_{pad}^{\ 2}}{R_{hair}^{\ 2}} \quad [1.14]$$

Hence, substituting for R_{hair} shows an increase of approximately $\sqrt{n}$ over the smooth system:

$$F_{hairy} \propto \sqrt{n} R_{pad} \quad [1.15]$$

$$F_{hairy} \propto \sqrt{n} F_{smooth} \quad [1.16]$$

Therefore the hairy system should be capable of producing significantly higher maximal adhesive forces than an otherwise identical smooth system. This concept is certainly of much theoretical interest and has received a degree of experimental verification with increased normal forces resulting from the division of contacts of a synthetic adhesive surface (Gorb et al., 2007; Peressadko and Gorb, 2004a; Varenberg et al., 2006). However, the situation will change if the load on the pad is not

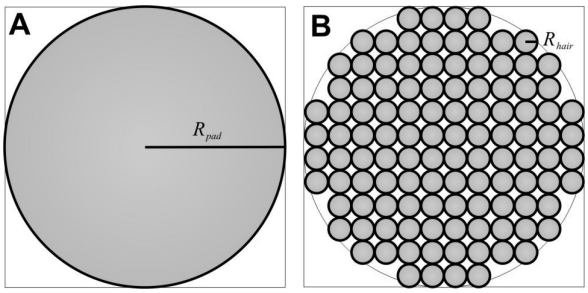

Figure 1.4: layout showing the theoretical (A) smooth or solid and (B) hairy or fibrillar pads. R_{pad} indicates the total pad radius, whereas R_{hair} is the radius of a single hair. As evident from B, the hairy system presents a smaller overall contact area, but a far greater contact perimeter.

evenly distributed, causing the pad to peel from one edge, rather than detach simultaneously, (i.e. contrary to the requirements of the work of adhesion model, see Appendix A.2). In this case, force will be concentrated along the peel edge and the model will break down (Federle, 2006; Hui et al., 2004). In effect then, the model requires peeling of the individual contacts (which will scale with contact perimeter) but not of the whole array. Arzt et al. (2003) have suggested that contact splitting may explain the observed scaling of seta density with body mass in some animals with hairy adhesive pads. However, other studies have found little evidence to support this with the relation being better explained by phylogeny or adhesive mechanism (Federle, 2006; Peattie and Full, 2007). The contact splitting model is also limited by the 'self-matting' constraint (Glassmaker et al., 2004; Persson, 2003; Sitti and Fearing, 2003; Spolenak et al., 2005) which states that if hairs are made too thin their increased flexibility will allow them to clump together, reducing performance (see Appendix A.2). It therefore remains unclear to what extent animal adhesive pads are able to resist peeling and maximise forces via the force scaling principle. If the scaling effect were present in nature then a hairy adhesive insect pad should be capable of generating higher adhesive stresses than a smooth pad. This has not previously been tested in any natural system.

1.3.2 Controllable attachment and detachment

For any animal using its adhesive organs to climb across a smooth surface, the ability to detach will be just as important as the ability to attach. Pads have therefore evolved to allow an extremely dynamic form of adhesion providing high attachment forces yet negligible detachment forces (Autumn and Peattie, 2002). Whilst the exact detachment mechanisms are still unclear, several studies have found evidence of a direction-dependence of adhesive organs. Direction-dependence allows a contacting pad to attach when pulled (typically towards the body) and detach when pushed and has been observed in both smooth and hairy animal adhesives (Autumn et al., 2006a; Clemente and Federle, 2008; Federle et al., 2001; Federle and Endlein, 2004; Gorb and Scherge, 2000; Hanna and Barnes, 1991; Hill, 1977; Niederegger and Gorb, 2003; Niederegger and Gorb, 2006).

However, it has been argued that the fibrillar system is inherently better designed for this task as the presence of individual contacts allows for the development of specialised tip designs (Federle, 2006). These are likely crucial parameters for controllable detachment and many hairs possess spatula-like tips which are both asymmetrical and non-parallel to the surface in their default state (Autumn and Hansen, 2006; Stork, 1980c). The

asymmetrical design will aid peeling in one (usually the distal or 'pushing') direction. The non-parallel tips lead to a 'non-adhesive' default position requiring a lateral pull for alignment (Autumn and Hansen, 2006; Autumn et al., 2000; Gao et al., 2005; Gravish et al., 2008). This results in many independent contact elements, each of which will have a tendency to detach by elastic force. These properties of fibrillar adhesives may therefore help in the regulation of attachment, allowing detachment via simple distal movements of the leg. However, although direction dependence has been observed in several insect pads (Federle et al., 2001; Gorb and Scherge, 2000; Niederegger and Gorb, 2003) the details of this mechanism have not been fully clarified. In addition, no previous study has compared the direction-dependence of smooth and hairy systems. Hence it is unclear whether hairy pads actually allow a more dynamic form of adhesion.

A further important question concerns the need for pushing during locomotion. If, as suggested by previous studies (Autumn et al., 2006a; Federle et al., 2001; Federle and Endlein, 2004; Gorb and Scherge, 2000; Hanna and Barnes, 1991; Niederegger and Gorb, 2003), pads detach when moved distally then how is an animal able to push with its pads when moving? This would, for example, be necessary when the leg is below the centre of mass in a climbing animal.

1.3.3 Self-cleaning ability

An ability to resist contamination is essential as without it any adhesive would foul and become useless after relatively few applications. However, despite its importance, for example in the design of synthetic adhesives, this is a relatively poorly understood area with few studies addressing the problem. A self-cleaning effect has been demonstrated for gecko pads contaminated with microspheres (Hansen and Autumn, 2005). However, for insects, which in many cases groom their adhesive organs (Farish, 1968; Stork, 1983) there has been no experimental verification of self-cleaning in their pads.

Suggestions as to the self-cleaning mechanism in geckos have been made, emphasising the importance of the fine (≤ 200 nm) setae tips. It has been proposed that due to reduced contact with the small hair tips particles may adhere better to the substrate than to each seta (Hansen and Autumn, 2005). The spatula design of the tip may also allow them to peel and detach from the dirt particles (Persson, 2007). Divided contacts are therefore potentially less susceptible to contamination than a connected single pad would be (Hui et al., 2005; Persson, 2003). No previous study has documented the presence of self-cleaning in any smooth animal

pad and it has not been compared in smooth and hairy biological attachment pads.

1.3.4 Rough surface adaptation

Most studies on biological adhesives have only focused on the problems of attaching to smooth surfaces. However, most, if not all, natural surfaces will display a degree of substrate roughness and this presents additional problems for adhesion. When roughness levels are so small that claws cannot interlock to support the animal (Dai et al., 2002), the adhesive system must instead be used. An ability to adapt to varying levels of substrate roughness is therefore critical for a natural adhesive to maintain a firm hold to a range of surfaces.

Compliance is an essential property of any adhesive allowing it to conform to a real surface exhibiting roughness on different size scales (Persson, 2003). Without this, the elastic energy required to deform the material will outweigh the gain of surface energy and separation will occur. An adhesive fluid, should help to compensate for roughness by filling gaps in the surface (Drechsler and Federle, 2006; Federle, 2006). However this will result in an increased fluid height which weakens attachment forces (as shown in section 1.2) and a flexible pad material is still beneficial. The required compliance has been quantified using the Dahlquist criterion which states that a pressure-sensitive material may exhibit a 'tacky' or adhesive property if its effective elastic modulus falls within approximately 100 kPa (Dahlquist, 1969). Hence all natural adhesives must achieve a bulk compliance to allow contact with rough substrates. Smooth pads have therefore been shown to possess a low elastic modulus (Gorb et al., 2000). The use of soft adhesive pads does however imply a trade-off, as enhanced compliance may increase susceptibility to creep, wear and contamination (Federle, 2006).

The fibrillar design on the other hand appears well suited for this purpose for several reasons and may be able to achieve compliance at many different length scales. Firstly, due to their high aspect ratio, setae bend easily so that their tips can make contact with an irregular substrate without the need for high normal forces. The array will therefore exhibit an effective elastic modulus orders of magnitude lower than that of its bulk material (Autumn et al., 2006c; Glassmaker et al., 2004; Peattie et al., 2007; Persson, 2003) whilst maintaining a wear resistant structure. This property should allow compliance on substrates with large scale asperities. Secondly, the small size of the seta tips makes the fibrillar pad insensitive against roughness with an intermediate length scale. Thirdly, contact to even smaller length scales of surface roughness may be facilitated by the better ability of small

hair tips to deform laterally (Eimüller et al., 2008; Gorb and Varenberg, 2007; Niederegger et al., 2002; Persson and Gorb, 2003). It is however as yet unclear to what extent many hairy insect systems are able to compensate surface roughness and the precise limitations arising from both fine and large scale surface asperities are not fully understood.

1.4 THE MECHANICS OF SETA DEFORMATION

In order to allow a quantitative treatment of the behaviour of insect hairy pads discussed above, further models are needed to explain and predict their behaviour under compression. Hence, this section contains a brief description of two important approaches describing the bending of both individual hairs and the setal array.

1.4.1 The small-strain cantilever model

The small strain cantilever model treats a single seta as an angled, uniform cantilever and can be used to calculate the displacement of the hair when a perpendicular force is applied to the tip. Under a vertical deflecting force the perpendicular bending of the beam is given by (Glassmaker et al., 2004; Persson, 2003; Sitti and Fearing, 2003):

$$\delta_{bending} = \frac{4F\cos\theta l^3}{3\pi R^4 E} \qquad [1.17]$$

where $F\cos\theta$ is the tangential component of the applied force, l the beam length, R the radius and E the elastic modulus (see Fig. 1.5). The longitudinal stretching of the beam on the other hand is proportional to the length and to the ratio of stress to strain, hence:

$$\delta_{stretching} = \frac{F\sin\theta l}{\pi R^2 E} \qquad [1.18]$$

where $F\sin\theta$ is the parallel component of the applied force. In order to calculate the total vertical deflection of the beam (i.e. along the force vector), each deflection component must be resolved giving vertical deflection as:

$$\delta = \delta_{bending}\cos\theta + \delta_{stretching}\sin\theta \qquad [1.19]$$

$$\delta = \frac{4F\cos^2\theta l^3}{3\pi R^4 E} + \frac{F\sin^2\theta l}{\pi R^2 E} \qquad [1.20]$$

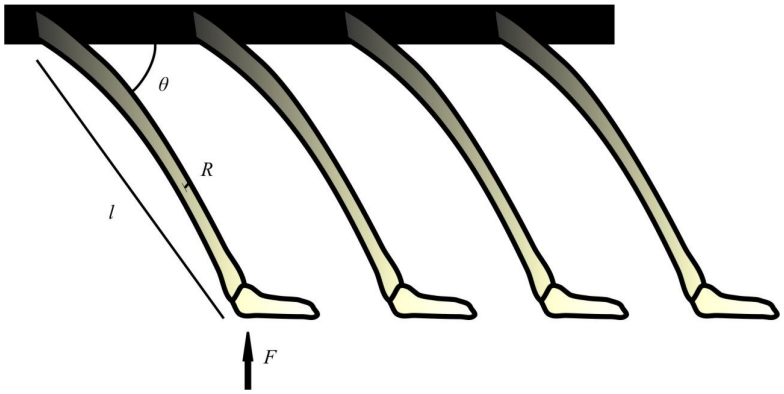

Figure 1.5: Diagram showing dimensions and angles of an array of stiff setae with radius *R*, length *l*, angle to the horizontal θ and elastic modulus *E*, under an applied vertical force of *F*. The mechanical deflection of the hair can then be modelled as a simple cantilever bending beam.

In most cases the stretching component is insignificant when compared to the bending component of deflection and can be ignored.

1.4.2 The effective elastic modulus of a setal array

The effective elastic modulus of an array of bending hairs can subsequently be determined given that elastic modulus is defined as the ratio of stress to strain. Hence:

$$E_{eff} = \frac{stress}{strain} = \frac{F_{pad} / A}{\delta / h} \qquad [1.21]$$

where *A* is the total projected area of the array, F_{pad} the perpendicular force across the array and *h* the height of the array (hence $h = l \sin\theta$). Given that the compressive force across the pad is simply the force on each hair multiplied by the number of hairs *N*, the force over displacement term (i.e. the pad spring constant) can be substituted for the small strain Equation 1.20 to relate the effective elastic modulus of the array to the parameters of each hair. Hence, neglecting the stretching component of Equation 1.20 effective array modulus is given by:

$$E_{eff} = N \frac{3\pi R^4 E \sin\theta}{4 l^2 A \cos^2\theta} \qquad [1.22]$$

This allows calculation of the setal modulus or pad effective modulus if the other basic hair morphological parameters are known.

1.5 OPEN QUESTIONS OF THE THESIS

As discussed above, several questions remain concerning the performance of the hairy adhesive systems of insects; for example how do they compare with smooth systems in terms of attachment, detachment and reusability and how well are they able to compensate surface roughness? In addition many detailed aspects of the setal morphology are poorly understood with the roles and functions of different pads or hair types still unclear. This not only presents a significant gap in the understanding of the biology of these animals but also limits any attempt to replicate their attachment systems. In the following chapters many of these outstanding issues are addressed with the focus placed on quantifying and explaining the fundamental performance mechanisms of hairy pads in insects. The green dock beetle, *Gastrophysa viridula* De Geer (Coleoptera) was used as the model study organism for much of this thesis. Coleoptera represent an extremely successful order of insects and provide a wide diversity of seta and pad morphology (Stork, 1980c). The tarsal adhesive pads of leaf beetles in particular have been used as subjects for many previous studies (Eimüller et al., 2008; Gorb, 2001; Peressadko and Gorb, 2004b; Voigt et al., 2008).

As discussed in section 1.3, many advantages have been proposed for hairy systems, such as maximal yet controllable adhesion and resistance to contamination. However in most cases these predictions have not been tested or quantified. In Chapters 2 and 3, three fundamental measures of attachment performance were therefore tested; the ability of the pads to attach (and the forces and stresses involved), the ability to detach and the ability to self-clean. To test the supposed advantages of the fibrillar design and to allow further insight into the mechanics of the pads, comparisons were then made with the smooth adhesive pads of insects for each case. The arolium of the Indian stick insect, *Carausius morosus* Brunner (Phasmatodea) was used as the model smooth system for this comparative work.

It is also not fully known how insect hairy attachment systems are able to cope with surface roughness. This is an important feature of any biological adhesive as few if any natural surfaces are perfectly smooth. In Chapter 4 the ability of the adhesive pads of the dock beetle to adapt to rough substrates (and in which instances the claws were instead used to support the animal) was therefore investigated.

Generalised models of fibrillar adhesion face important limitations when addressing biological systems. Both pads and hairs demonstrate considerable differences in design both between and within species and the importance of this morphological variation has not previously been investigated. Leaf beetles, for

example, possess three distinct adhesive pads on each leg, which vary greatly in setal morphology. The mechanical and adhesive properties of these pads were therefore tested and their use during climbing and jumping investigated in Chapters 5 and 6. The differing hair morphologies were investigated in Chapter 7 in order to gain a better understanding of the contribution of individual setae to the array level performance parameters quantified and discussed in the other chapters.

2

MECHANISMS FOR ATTACHMENT AND DETACHMENT IN FIBRILLAR AND SMOOTH INSECT ADHESIVE SYSTEMS

Summary

Adhesive pads on the legs of animals can be classified as either 'smooth' or 'hairy' (fibrillar). It has been proposed that the hairy design conveys superior and controllable adhesion. However, no study has yet compared the basic performance of both systems. As such single-pad friction and adhesion forces were measured in sample hairy (*Gastrophysa viridula*) and smooth (*Carausius morosus*) pads and contact area simultaneously recorded. Adhesion and friction forces per unit pad area were very similar in smooth and hairy systems. Insect pads of both types adhere via a thin film of liquid secretion. As found previously for the smooth system, forces in the fibrillar system strongly decreased with larger amounts of fluid secretion present, suggesting that the fluid mainly serves to maximize contact on rough substrates. One essential prerequisite for the control of surface attachment during locomotion is the direction-dependence of adhesive pads. The mechanisms of direction-dependence in smooth and hairy systems were compared by performing pulling and pushing slides. Both types of pad exhibited a large drop in friction when moved away from the body, although this effect was more extreme for the hairy system. Direction-dependence is explained in both smooth and fibrillar systems by the instability of the tarsal chain, causing the whole pad to peel off. In the fibrillar pads, anisotropy additionally arises from the direction-dependence of individual setae.

2.1 INTRODUCTION

Many arthropods and vertebrates possess tarsal attachment systems, which broadly divide into two principal groups, namely hairy (fibrillar) and smooth adhesive pads (Scherge and Gorb, 2001). Fibrillar adhesive systems have recently attracted much attention from the engineering and physical sciences because they are considered promising models for novel, biomimetic adhesives (Aksak et al., 2007; Glassmaker et al., 2004; Gorb et al., 2007; Hui et

al., 2004; Jagota et al., 2007; Kim and Sitti, 2006; Lee et al., 2008; Menon and Sitti, 2006; Schubert et al., 2008). The fibrillar design is thought to convey a number of specific advantages such as superior performance on rough substrates (Persson and Gorb, 2003), effortless detachment (Autumn et al., 2006a; Autumn and Hansen, 2006; Autumn et al., 2006b; Federle, 2006), self-cleaning properties (Hansen and Autumn, 2005) and increased adhesion due to contact splitting (Arzt et al., 2003). However, fibrillar and smooth adhesive pads have evolved repeatedly in different taxa (Beutel and Gorb, 2001; Gorb et al., 2002), and it appears that both designs fulfil the requirements for successful climbing on diverse substrates. Surprisingly, it is still unclear whether the performance of the two designs is any different and if so, in what respect. Smooth and fibrillar adhesive systems have been the subject of recent reviews (Autumn, 2007; Barnes, 2007; Federle, 2006; Gorb, 2007; Persson, 2007) However, no previous study has explicitly compared the performance of these systems under controlled conditions, and there exists a lack of information regarding the forces that can be supported by these systems in insects. This study has attempted to address this by comparing a representative example of each: the hairy pads of the leaf beetle *Gastrophysa viridula* De Geer (Coleoptera) and the smooth arolium of the stick insect *Carausius morosus* Brunner (Phasmatodea) (Fig. 2.1).

Unlike the 'dry' adhesives of geckos, both smooth and fibrillar adhesive systems in insects require the use of a secreted fluid (Betz, 2003; Eisner and Aneshansley, 2000; Federle et al., 2002b; Gorb, 1998; Langer et al., 2004). This mediates attachment through capillary and viscous forces and may help overcome the problem of rough substrate attachment by filling in surface crevices. It has, however, been shown for smooth pads that a build-up of fluid is detrimental to their performance on smooth substrates due to the smaller forces resulting from a thicker fluid layer (Drechsler and Federle, 2006). As such it was tested here whether a similar effect occurs in the hairy system.

Insects with hairy and smooth pads can generate very high attachment forces (Eisner and Aneshansley, 2000; Federle et al., 2000). While strong adhesion may be beneficial in many situations, it can make locomotion more difficult. The problem of how to effect a controlled, energy efficient detachment is of particular importance to leaf dwelling insects which must be capable of adhering to a range of demanding substrates whilst still being able to rapidly detach (for example during the pursuit or evasion of other animals). A fundamental property of adhesive structures that helps to achieve rapid and controllable adhesion during locomotion is their direction-dependence. It has been observed that friction and adhesion forces of most animal attachment organs are higher when pulled towards the body (i.e. proximally) rather than pushed away

from it (i.e. distally). Previous studies have shown this to be the case in hairy adhesives of geckos, spiders and flies (Autumn et al., 2006a; Autumn et al., 2000; Hill, 1977; Niederegger and Gorb, 2003) as well as in smooth adhesive pads of ants, bushcrickets and cockroaches (Clemente and Federle, 2008; Federle et al., 2001; Federle and Endlein, 2004; Gorb and Scherge, 2000).

However, the detailed mechanisms underlying direction-dependence are still not sufficiently understood in either smooth or fibrillar systems. It is unclear whether direction-dependence is achieved through changes in contact area or through a change in shear stress (i.e. friction force per unit contact area). Analysing the smooth euplantulae of the bushcricket *T. viridissima*, Gorb & Scherge (2000) proposed that friction is direction-dependent due to the bending and reorientation of the inner rods of the pad cuticle. However, this hypothesis does not specify whether the action of the rods during a proximal pull is thought to increase pad contact area or shear stress. Large direction-dependent changes of contact area can occur in adhesive pads that can be unfolded. It has been shown for ants and bees that changes of adhesive contact area are mediated both by the action of the claw flexor muscle and by the passive unfolding of the pad when legs are pulled toward the body (Federle et al., 2001; Federle and Endlein, 2004). However, even in the absence of such an unfolding mechanism, direction-dependent changes of contact area can be brought about by the flexibility of the chain-like tarsus. This has been shown for the cockroach *N. cineraea*, where a distal movement of the unrestrained tarsus caused a peeling detachment of the smooth arolium (Clemente and Federle, 2008).

For the fibrillar adhesive system, previous explanations of direction-dependence have focused on the behaviour of individual setae. Adhesive hairs of geckos are non-symmetrical and feature distally pointing setae and spatulae which have been shown to generate higher friction and adhesion when aligned with a proximal pull (Autumn et al., 2006a; Autumn and Hansen, 2006; Autumn et al., 2000; Gravish et al., 2008). Without a proximal pull, only the ends of the spatulae will contact the surface, representing only a small fraction of the total possible contact area. This results in a highly direction-dependent friction on the level of individual hairs. However, fibrillar adhesive systems have a hierarchical structure and attachment and detachment may not only be controlled on the level of individual setae/spatulae but also on the level of setal arrays (pads) and the foot (tarsus) as a whole. It is still unclear what contribution each of these levels make to directional dependence and to attachment and detachment during locomotion.

The fibrillar systems of beetles are similar to those of geckos in many aspects. Although several other hair types exist, spatula-tipped setae represent the prevalent design (Stork, 1980c) and may

well exhibit similar properties to gecko setae. Tarsal movements involved in attachment and detachment have been recorded in flies (Niederegger and Gorb, 2003). However, no observations have been made on the dynamic changes of adhesive contact area in any fibrillar system and the presence of a directional dependence has yet to be confirmed for beetles with hairy adhesive pads.

The aim of this study was therefore to compare the performance of smooth and fibrillar systems in insects and to clarify their mechanisms of direction-dependence. By measuring frictional and adhesive forces in two model organisms, the leaf beetle *G. viridula* and the stick insect *C. morosus*, the following questions were addressed: 1. How do smooth and hairy systems compare in terms of their adhesive and frictional performance? 2. How does the fluid pad secretion influence attachment in fibrillar systems? 3. Are forces in these smooth and hairy pads direction-dependent? 4. What is the mechanism for this direction-dependence if present?

2.2 METHODS

2.2.1 Study animals

As the material properties of arthropod cuticle are strongly dependent on its state of hydration (Jiao et al., 2000; Vincent and Wegst, 2004) the functional properties of insect adhesive pads can only be investigated *in vivo*. As such, live adult stick insects, *C. morosus* and male dock beetles, *G. viridula* were taken from laboratory colonies, weighed and mounted on glass cylinders. Stick insects (body mass 898 ± 31 mg, mean ± s.e.m.) were enclosed inside

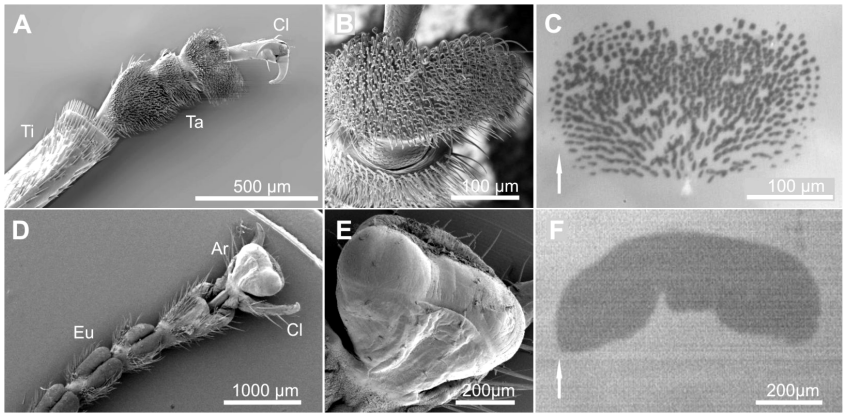

Figure 2.1: Adhesive pad morphology in *Gastrophysa viridula* (A-C) and *Carausius morosus* (D-F). Hind (A) and front tarsi (D), the distal-most adhesive pad (B,E) and the contact area of each of the pads in contact with glass, as viewed via epi-illumination (C,F). Arrows indicate distal direction. Ti, tibia; Cl, claws; Ta, tarsal segments; Eu, euplantulae; Ar, arolium.

the glass cylinder so that a single leg protruded. The leg was isolated using plasticine and secured to a firm piece of wire (attached to the glass cylinder) using dental cement ESPE Protemp II (3M, St Paul, MN, USA). The claw tips were clipped with micro-scissors to prevent them from obstructing the arolium. Beetles (body mass 10.4 ± 0.4 mg, mean ± s.e.m.) were immobilised by enclosing them in blu-tack and parafilm tape, with the blu-tack (Bostik, Leicester, UK) used to isolate the leg. Front and rear legs were used.

The tarsus of *C. morosus* has five segments, the first four of which bear euplantulae on the ventral side. The leg terminates with a pretarsus that bears the claws and the smooth adhesive arolium (see Fig. 2.1E-G). The tarsus of *G. viridula* consists of five segments and a distal pretarsus bearing the claws. The fourth segment is reduced and sunken into the larger third tarsomere. The ventral sides of the first three tarsomeres are densely covered by adhesive setae. Setae are typically curved and oriented distally and belong to three principal types: a) pointed, with a tapered end, b) flat spatula-tipped and c) disk-tipped with a marginal bulge. Due to sex-specific variation in the abundance of the different types of setae, only male beetles were used in this study. The distal-most pad on the third tarsomere was used throughout this study for force measurements (Fig. 2.1B-D).

To investigate the role of both the tarsal chain and the adhesive pads, two restraining conditions were used for the legs; either the 'footloose' condition where the legs were fixed only up to the tibia, or the 'immobilised' condition where the legs were fully encased (including the dorsal side of the pretarsus in *Carausius* and the dorsal side of the tarsus in *Gastrophysa*), leaving only the pad free (Fig. 2.2). Additionally for *G. viridula*, lateral instabilities became apparent during footloose slides, causing the pad to significantly rotate. Therefore, further observations were taken whereby the tarsus was fixed laterally as for the immobilised condition, but left movable in the dorsal-ventral direction.

2.2.2 General set-up

Following Drechsler and Federle (2006) a force transducer set-up was used to measure friction forces of the pad, whilst simultaneously recording contact area (Fig. 2.3). Forces were measured with a two-dimensional force transducer employing 350 Ω foil strain gauges 1-LY13-3/350 (Vishay, Malvern, PA, USA) and fixed to a three-dimensional, DC motor stage M-126PD (Physik Instrumente, Karlsruhe, Germany). The force transducer was calibrated with calibration weights and by applying defined displacements to obtain the spring constant at different lever arm lengths. The stage was controlled with custom made LabVIEW

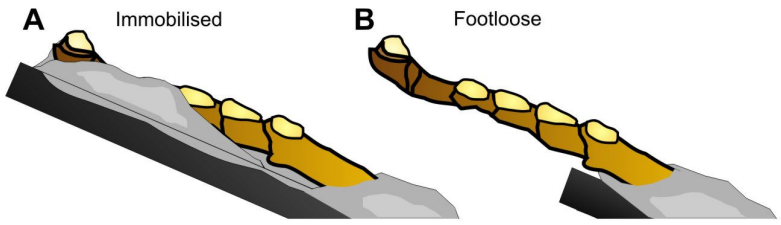

Figure 2.2: Diagram showing the two restraining conditions for the stick insect tarsus. (A) immobilised: the pretarsus is fully restrained using dental cement. (B) footloose: the leg is fixed at the tibia, leaving the tarsus free to move.

(National Instruments, Austin, TX, USA) software that allowed a precise set of user defined movement patterns. Voltage output was amplified (ME-Meßsysteme, Henningsdorf, Germany) and sampled at 1000 Hz with an I/O board PCI-6035E (National Instruments). The LabVIEW programme included a normal force feedback mechanism that allowed friction experiments to be performed whilst keeping the normal force constant. The force feedback mechanism consists of a 50-Hz feedback loop, in which the programme computes the deviation between a setpoint force and the actual force and passes this on to a discrete PID control algorithm to compute a displacement which would compensate the error. The distal-most foot pad was brought into contact with a glass plate (18mm x 18mm x 0.1mm) attached to the strain-gauge transducer. Contact area was visualised using a coaxially-illuminated stereomicroscope, which shows actual contact as a high contrast silhouette (Federle et al., 2002b). Images were recorded using either a Redlake PCI 1000 B/W camera (Redlake, Tallahassee, FL, USA) (for smooth pads) or a high-speed digital HotShot PCI 1280 B/W camera (NAC image technology, Simi Valley, CA, USA) (allowing the higher resolution necessary to image hairy pads) and were analysed with MATLAB (The Mathworks, Natick, MA, USA) scripts. For the hairy pads, a 'projected' pad area was also measured by manually plotting a solid polygon around the outermost setae in contact to allow the basic frictional force per total pad area to be compared between hairy and smooth systems.

2.2.3 Measurements of attachment and detachment

For both animals, proximal friction slides (corresponding to a pull of the leg towards the body) were performed at 500 μms^{-1} over 10 mm. The relatively large sliding distance was chosen to ensure that the pads were sliding at the same velocities and to be able to test the effects of fluid accumulation and depletion. Distal friction slides (corresponding to a push of the leg away from the body) were done in the same way, but were preceded by a short, 0.5 mm proximal slide. This was done because previous studies (Autumn et

al., 2000; Gravish et al., 2008) and preliminary observations had suggested that a proximal movement following contact was beneficial in aligning the foot pads and ensuring proper contact. For the beetles, the normal force feedback kept the load constant at 0.1 mN during the slide, corresponding to 98% of the beetle's body weight and to a load stress (force per projected contact area) of 1.7 kPa. This was raised to 1 mN for the stick insects (corresponding to 11% of the body weight and a load stress of 9.8 kPa) to achieve a compromise between a comparable fraction of the insect's body weight and a comparable load stress. These results show that this difference of normal forces and load stresses has a negligible effect on friction and shear stresses (see below). Otherwise, conditions were kept identical for both insects during all slides. For the footloose condition, no feedback was used during the slide as otherwise the flexibility of the tarsal chain caused the leg to bend and bring other pads into contact. Adhesion area was not recorded for the pushing slides as in most cases the visible contact area at the end of the slide had dropped below a range that could produce meaningful, noise resistant results. Similarly, projected area was not calculated for pushing slides as the pad outline was often small and irregular.

To investigate the function of the pad secretion in the hairy system (and to control for its effects), repeated pulling slides were performed as above for the immobilised dock beetle. Nine consecutive slides (separated by a 3 s pause following each pull-off) were carried out on either the same area of the glass plate (intended to allow the fluid to build up) or on a fresh area (intended to allow

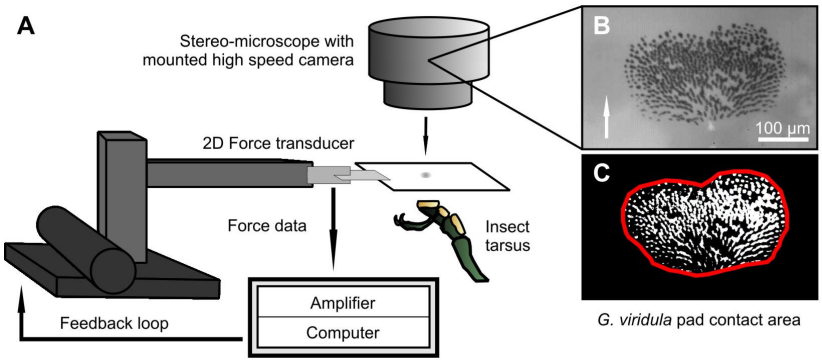

Figure 2.3: (A) Experimental setup for recording friction, adhesion and contact area of insect adhesive pads. The pad is brought into contact with a glass cover slip attached to a 2D strain gauge force transducer. The transducer is moved by a three-dimensional motorised positioning stage. Force signals are amplified and recorded on a computer. A feedback mechanism allows a constant normal force to be maintained. Contact area is recorded using a stereo microscope with coaxial illumination. (B) *Gastrophysa viridula* pad contact area. Arrow shows distal direction. (C) Threshold image providing a measure of the real contact area. The red frame shows the estimate of projected pad area.

the fluid to deplete). The fluid accumulation on the glass substrate was visualized using Interference Reflexion Microscopy (λ=546 nm, 20x magnification, Leica DRM) (Leica Microsystems GmbH, Wetzlar, Germany). Consecutive slides were statistically analysed using Page's non-parametric L test (Page, 1963), where the indices $L_{m,n}$ indicate the number of conditions (m) and the sample size (n).

Due to the considerable influence of the amount of secretion on friction forces, all immobilised slide movements were repeated following two regimes: a) 'little secretion': each slide was performed on a clean area of glass plate, b) 'accumulated secretion': four consecutive, pulling slides were performed first on the same area of the glass plate to allow the pad secretion to build up. Forces were recorded in both conditions in order to reduce variation caused by variable amounts of secretion present in the contact zone. At the end of every slide a 5 s pause was left to allow friction to drop before performing a 500 μms^{-1} perpendicular pull-off. This allowed adhesion forces to be measured.

To test the effect of applied normal force on sliding friction and shear stress, forces were measured for *G. viridula* and compared with already published, analogous measurements for stick insects (Drechsler and Federle, 2006). Pulling and pushing slides (little secretion) were performed as above, but with the

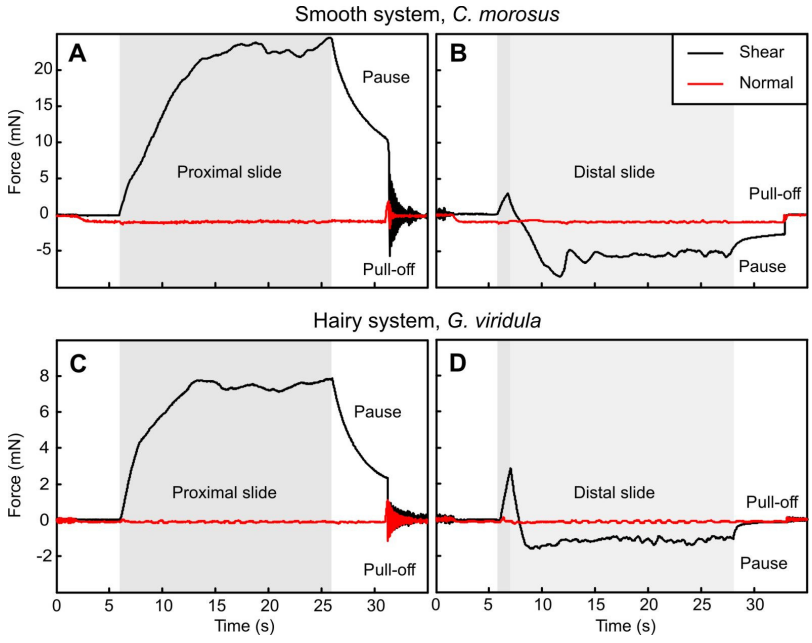

Figure 2.4: Example force curves for the stick insect (A,B) and the dock beetle (C,D). (A) and (C) pulling slides (displayed as a positive force), (B) and (D) pushing slides (displayed as a negative force), preceded by a short proximal movement. Dark grey background denotes pulling, light grey background denotes pushing movements. Sliding velocity 500 μms^{-1}, each slide followed by a 5 s pause before pull-off.

applied normal force varied at 0.1, 1.0 and 5.0 mN.

2.3 RESULTS

2.3.1 Attachment performance

To measure frictional and adhesive forces in pads of stick insects (*C. morosus*) and beetles (*G. viridula*), long-distance sliding movements of adhesive pads on glass were performed. When pads were sliding in the proximal direction, friction and shear stress increased steadily in the course of each slide and slowly tended to a plateau after approximately 15 s (see Fig. 2.4). When moved in the pushing direction, however, pad forces increased only briefly and then remained on a very low level (Fig. 2.4). Pads started to slide within less than 1 s of the beginning of the motor movement; there was no friction force peak at the onset of sliding.

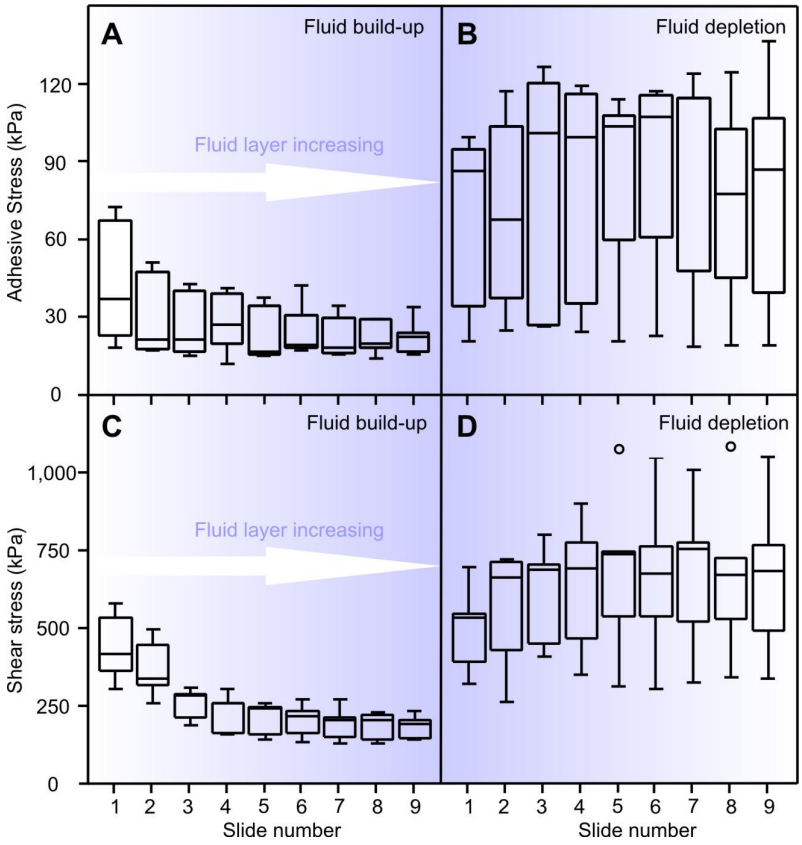

Figure 2.5: Effect of build-up or depletion of secretion on pad adhesive stress (A,B) and shear stress (C,D) for *Gastrophysa viridula* (*n*=5). (A) and (C) show the result of multiple slides on the same area of glass allowing the fluid to build up, (B) and (D) show repeated slides, each time on a fresh area, depleting the fluid. Centre lines denote medians, boxes the inner two quartiles and error bars the largest and smallest values that are not outliers (>3 standard deviations from the mean), marked as circles.

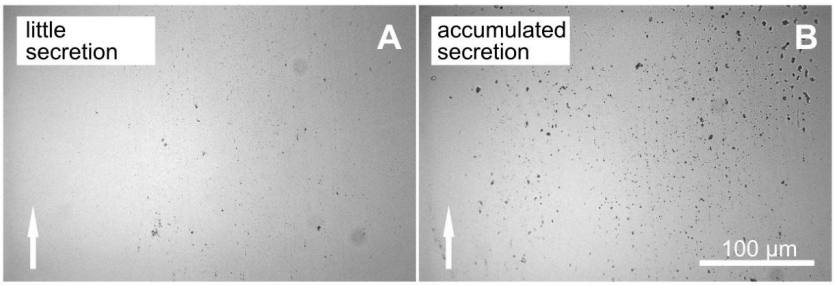

Figure 2.6: Build-up of pad secretion on glass after one slide (A, little secretion) or five consecutive slides (B, accumulated secretion) visualised by Interference Reflexion Microscopy. The dark marks indicate droplets of fluid secretion, and fluid build up is evidenced by the increased number of 'spots' visible in B. The sliding direction of the pad is indicated by arrows.

Effect of fluid secretion on friction and adhesion in the hairy system

To evaluate the effect of the amount of adhesive secretion in the hairy system, friction and adhesion were measured during pulling slides under two different regimes in *Gastrophysa*. When slides were repeated on the same area of glass (fluid build-up), friction and adhesion strongly decreased from slide to slide until they approached a plateau (mean shear force dropping to 42% from

Table 2.1: Comparison between the results regarding fluid build-up and normal forces between *Carausius morosus* (data from Drechsler and Federle (2006)) and *Gastrophysa viridula* (this study).

Effect of:	*Gastrophysa viridula*	*Carausius morosus*
fluid accumulation on shear stress	Decrease to 44% (Page's *L* test: $L_{10,5} = 1888$, $P < 0.001$)	Decrease to 32% (Page's *L* test: $L_{7,10} = 1037$, $P < 0.001$)
fluid depletion on shear stress	Increase to 123% from 1st to 3rd (Page's L test: $L_{3,5} = 68$, $P = 0.009$) No significant effect from 3rd slide (Page's L test: $L_{8,5} = 816$, $P > 0.05$)	No significant effect (ANOVA, $F_{1,7} = 0.284$, $P > 0.1$)
increased normal force on friction force	no significant effect (ANOVA: $F_{2,15}$=2.015, $P > 0.05$)	significant increase (ANOVA, $F_{1,19} = 8.05$, $P < 0.01$)
increased normal force on contact area	no significant effect ($F_{2,15}$=2.482, $P > 0.05$)	significant increase ($F_{1,19} = 45.8$, $P < 0.001$)
increased normal force on shear stress	no significant effect ($F_{2,15}$=0.748, $P > 0.05$)	no significant effect ($F_{1,19} = 0.09$, $P > 0.05$)
Loads:	0.1, 1, 5 mN	-0.1, 0.5, 1, 2 mN
Reference:	this study	(Drechsler and Federle 2006)

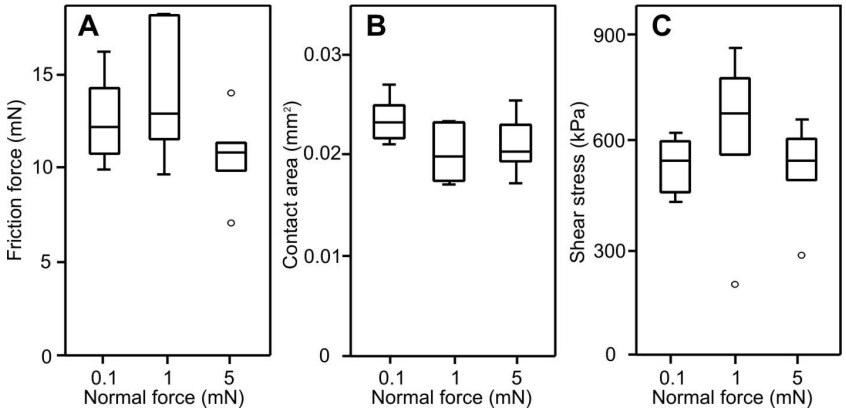

Figure 2.7: Effect of applied normal force on friction force (A), contact area (B) and shear stress (C) in *Gastrophysa viridula* (*n*=6).

slide one to nine; adhesive force dropping to 52%). As contact area remained largely unchanged, this effect was due to a highly significant decrease of both adhesive stress (adhesion per unit area) and shear stress (friction per unit area) (Page's L test, adhesive stress: $L_{9,5} = 1310$, $P < 0.001$, shear stress: $L_{10,5} = 1888$, $P < 0.001$, Fig. 2.5A,C). On the other hand repeated slides each time on a fresh area of glass (fluid depletion) showed no significant drop and in fact a significant upwards trend in shear stress (Page's L test, adhesive stress: $L_{9,5} = 1138$, $P = 0.396$, shear stress: $L_{10,5} = 1665$, $P = 0.007$, Fig. 2.4B,D). The increase in shear stress mainly occurred from the first to the third slide (Page's L test from 1st to 3rd slide, $L_{3,5} = 68$, $P = 0.0089$) and subsequent forces remained constant, producing highly reproducible curves between consecutive slides (Page's L test from 3rd to 10th slide, $L_{8,5} = 816$, $P = 0.44$). This indicates that the amount of fluid in the contact zone was depleted over the first three slides and reached a constant level after that. An example image of the build up of pad secretion is presented in Fig. 2.6. It can be seen that there were many more fluid droplets deposited on the glass surface in the accumulated condition. These droplets represent the persistent, hydrophobic component of adhesive secretion (Federle et al., 2002b). Fluid build-up and fluid depletion have a similar effect in *C. morosus* (see Table 2.1 and Drechsler and Federle, 2006), and the results presented here demonstrate that this is equally present and conspicuous in the fibrillar pads of *Gastrophysa*.

Effect of applied normal forces on friction, contact area and shear stress

The effect of normal force was investigated in *G. viridula* by performing pulling slides at three different applied forces (0.1, 1.0 and 5.0 mN). Despite a 50-fold variation of load, no significant change in friction, contact area or shear stress (Fig. 2.7) was observed. The lack of an increase in contact area with load differs

markedly from the previous findings for stick insects (Drechsler and Federle (2006); see Table 2.1). This finding is consistent with the morphology of both types of attachment pad (Fig. 2.1). The seta tips in *G. viridula* are almost coplanar so that even at very small normal forces, all setae make contact if the pad is properly aligned with the substrate. By contrast, the arolium of *C. morosus* is hemispherical, resulting in an increase of contact area with load as predicted by the JKR theory (Johnson et al., 1971). Both in *G. viridula* and *C. morosus*, however, shear stress was independent of load, confirming that friction forces are fully determined by contact area in both systems (Table 2.1). As a consequence, the comparison of shear stress between the smooth and hairy adhesive systems in this study is not affected by changes to normal force.

2.3.2 Direction-dependence and frictional anisotropy

The level of the adhesive pad

The effect of sliding direction in smooth and hairy systems was quantified by performing pulling and pushing slides in randomised order. Both the maximum friction during the slide and the adhesion force peak during the pull-off at the end of each slide were evaluated. As friction forces of beetles and stick insects were strongly dependent on the amount of fluid present in the contact zone (*Carausius*: Drechsler and Federle 2006; *Gastrophysa*: see above), slides were performed in both the little secretion and the accumulated secretion regimes (see Fig. 2.8). In both animals and both conditions, maximum friction was significantly lower in the pushing direction (see Table 2.2 and Fig. 2.8). However, frictional forces decreased more strongly in the hairy system (means little secretion: 7.8-fold in *G. viridula* vs. 2.3-fold in *C. morosus*; accumulated secretion: 3.4-fold vs. 2.7-fold).

Contact area was measured simultaneously, allowing friction forces to be normalised for area (see Table 2.2). In both systems, contact area visibly decreased during distal pushes (most differences significant, Table 2.2). The contact area of the hairy system showed conspicuous changes during the slides. During pulling slides, adhesive contact area was maximal and any hair tips not already in contact after the initial preload were brought into full contact at the start of the slide. However during pushing slides, hair tips appeared to peel off individually, and decreased in contact area (Fig. 2.9). This resulted in the pushing slides taking place with only what appeared to be the setal tips in contact. The tips appeared to remain in contact with the surface, the hairs bending or tilting to allow this. The deflection of setae was manifested visually by a movement of the contact zones relative to the pad. This displacement was measured by comparing the positions of the

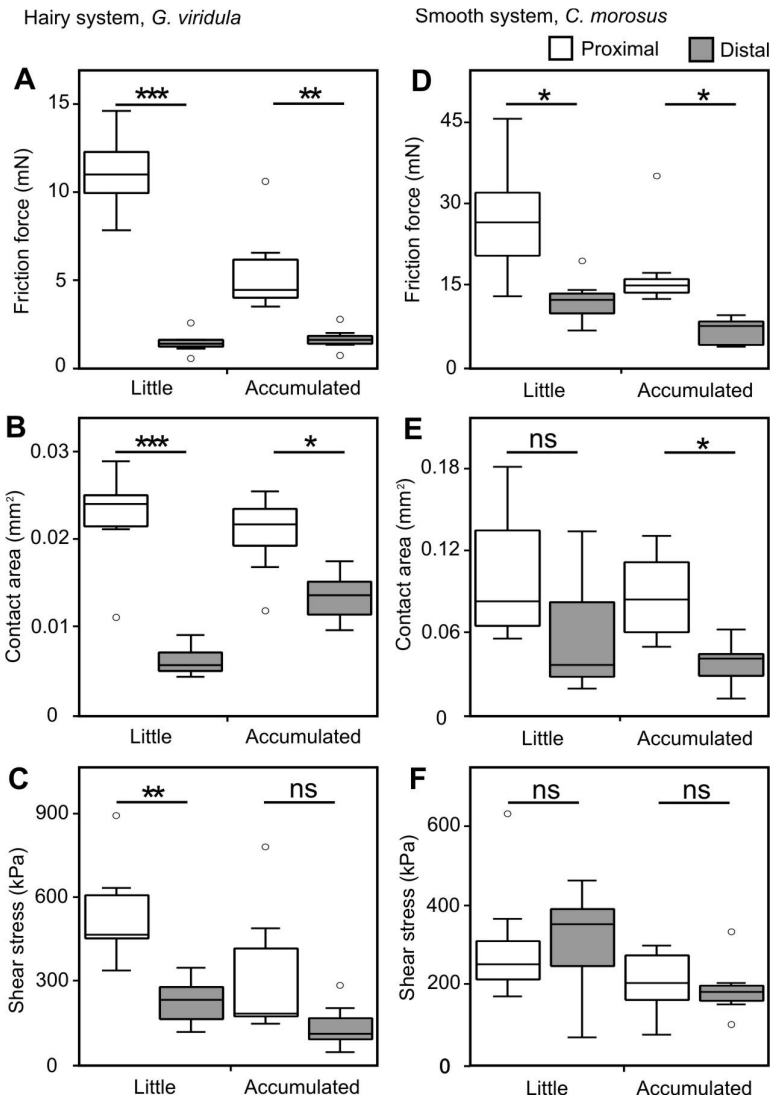

Figure 2.8: Direction-dependence of friction (A,D), contact area (B,E) and shear stress (C,F) for *Gastrophysa viridula* (hairy system, A-C) and *Carausius morosus* (smooth system, D-F) for proximal pulls and distal pushes of immobilised pads (n=7) in both little and accumulated secretion regimes. Significance levels: * P<0.05, ** P<0.01, *** P<0.001, N.S. not significant.

distal end of the contact zone during the short pull and subsequent pushing slides (measured at the force peaks) using a MATLAB script. Excluding three slides where the movement of the distal edge was difficult to track reliably, the hair contacts moved by 68.1 ± 4.4 μm in the proximal-distal direction (little secretion, mean ± s.e.m. n=4). This is greater than the length of the setae (40-50 μm; Orso et al. (2006)) and corresponds to a large bending or rotation of the hairs from being distally to being proximally angled.

Shear stress was computed using real observed contact area. For the stick insects shear stress showed no significant change

Table 2.2: Comparison of friction (Fr.) force (mN), contact area (μm²) and shear stress (kPa) as well as adhesion (Ad.) between proximal and distal slides in single pads of stick insects and beetles. Forces were measured for immobilised pads in the little (Lit.) and accumulated (Acc.) secretion regimes. Values show means ± s.e.m., all tests paired *t*-tests, df=6.

Smooth system *Carausius morosus*			Pulling slide	Pushing slide	test statistic
Fr.	Lit.	Force	27.1 ± 4.2	11.9 ± 1.6	T=3.30, p=0.016
		Contact area	102400 ± 19890	57830 ± 18850	T=2.22, p=0.068
		Shear stress	298.9 ± 60.2	307.1 ± 54.3	T=-0.13, p=0.898
	Acc.	Force	17.3 ± 3.0	6.30 ± 0.96	T=3.17, p=0.019
		Contact area	96650 ± 20450	36680 ± 6445	T=2.54, p=0.044
		Shear stress	205.8 ± 31.0	189.1 ± 27.5	T=0.59, p=0.574
Ad.	Lit.	Force	4.25 ± 0.96	0.47 ± 0.17	T=4.48, p=0.001
	Acc.	Force	2.28 ± 0.47	0.38 ± 0.16	T=4.41, p=0.001
Hairy system *Gastrophysa viridula*			Pulling slide	Pushing slide	test statistic
Fr.	Lit.	Force	11.1 ± 0.9	1.43 ± 0.23	T=11.17, p<0.001
		Contact area	22450 ± 2132	6117 ± 650	T=6.06, p=0.001
		Shear stress	518.5 ± 48.9	233.0 ± 28.6	T=3.72, p=0.010
	Acc.	Force	5.53 ± 0.94	1.62 ± 0.24	T=3.91, p=0.008
		Contact area	20630 ± 1786	13390 ± 1105	T=3.04, p=0.023
		Shear stress	293.8 ± 63.9	134.9 ± 31.0	T=2.03, p=0.089
Ad.	Lit.	Force	1.78 ± 0.27	0.17 ± 0.09	T=5.71, p=0.001
	Acc.	Force	1.05 ± 0.08	0.21 ± 0.09	T=6.85, p<0.001

between pulling and pushing slides (Table 2.2 and Fig. 2.8). This shows that the higher friction forces in the pulling direction are not explained by shear stress but by an increase in contact area. For the beetles, however, shear stresses were higher in the pulling direction (difference significant in the little secretion regime, see Table 2.2). Thus, the frictional direction dependence in *Gastrophysa* is based not only on a higher contact area but also on an increased shear stress during pulling slides.

Similar to the friction forces, adhesion was much smaller after a pushing slide in both smooth and hairy systems (differences highly significant, Table 2.2). This clearly confirms that adhesion is strongly influenced by shear forces towards the body or away from it, thus providing a way of controlling attachment and detachment.

It should be noted that despite the 3 s stop of the motor movement at the end of each slide, there was still a significant shear force present during the pull-off movement. Thus the effective force vector was not perpendicular to the surface but the mean detachment angles were: *C. morosus* 20.61 ± 2.64° pulling, 168.44 ± 3.91° pushing; *G. viridula* 32.36 ± 2.76° pulling, 114.52 ± 4.80° pushing (all presented for little secretion).

For both animals, the frictional force generated by a single pad in the pulling direction was more than sufficient to support the

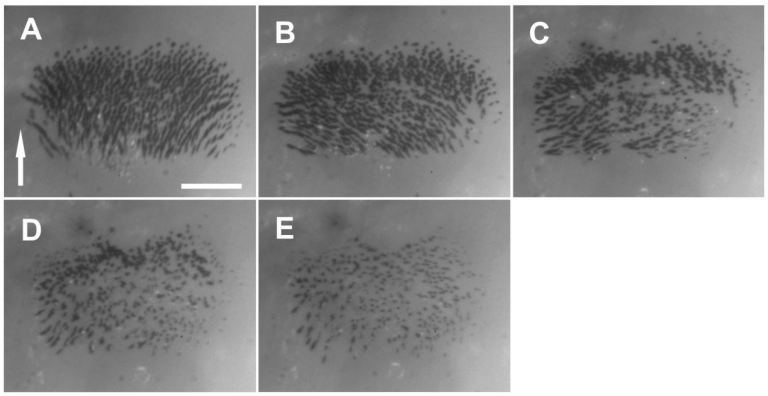

Figure 2.9: *Gastrophysa viridula*, changes in adhesive contact area during proximal and distal slides. (A) Full contact during a pulling slide. (B-E) The following pushing slide. Note that many individual tips have significantly decreased in contact during the movement. Contact visualised by epi-illumination. Scale bar = 100 μm, arrow shows distal direction.

body mass of the animal. However, this was not the case for the pushing adhesion of *C. morosus* (mean weight approx., *C. morosus*: 8.81 ± 0.30 mN, *G. viridula*: 0.102 ± 0.004 mN).

The level of the whole tarsus

Footloose slides (where the tarsal chain was left free to move) were performed for both pulling and pushing. This was done in order to investigate whether and how the flexible tarsus contributes to the observed direction-dependence of friction forces. Slides were performed in the same way as for the immobilised condition, with the exception that the feedback had to be left out to prevent the proximal tarsus or the tibia from touching the substrate. Footloose trials were therefore performed with a constant z-position of the motor after an initial force feedback preload. In both systems during a proximal pull, good contact was made and maintained throughout the slide (Fig. 2.10A,C). However during a distal push, tarsal instabilities were apparent. For *C. morosus* a distal push caused the tarsus to buckle upwards, thereby peeling off the arolium from the proximal side and detaching it rapidly from the surface (Fig. 2.10B). For *G. viridula*, the lateral flexibility of the tarsal chain caused the leg to bend, mainly laterally, rotating the foot by almost 180°, and preventing it from detaching (Fig. 2.10D). This behaviour is however never observed in freely walking beetles and may be an artefact resulting from the relaxed claw flexor muscle and the fixed tibia. As such, additional observations were made where the beetle was mounted in blu-tack as for the immobilised condition, but with greater freedom in the dorsal-ventral direction. In this condition, a pulling slide showed good contact as before (Fig. 2.10E, as imaged from above, given that the side view was

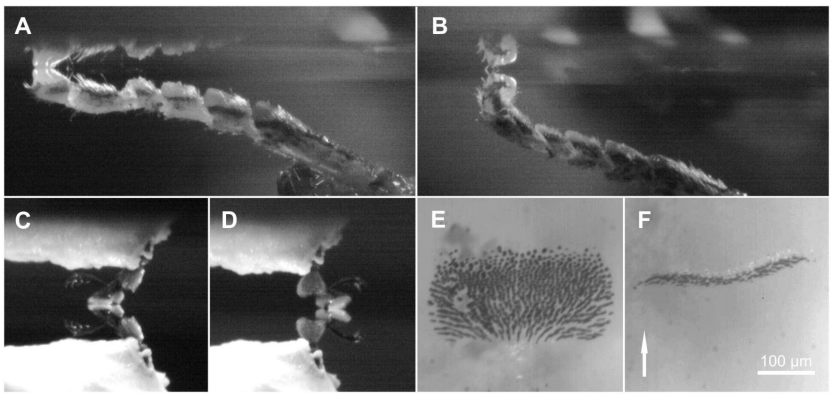

Figure 2.10: Tarsal movements during pulling and pushing slides in *Carausius morosus* and *Gastrophysa viridula* in the footloose condition. In the stick insect (A proximal, B distal), a distal slide resulted in buckling, peeling off the contact area from its proximal side. In the beetle (C proximal, D distal), a distal push caused the whole pad to rotate due to its lateral instability. When fixed in all but the vertical direction (E proximal, F distal), proximal to distal peeling of the entire pad was observed. (A-D) side views, (E,F) contact recorded via epi-illumination: arrow shows distal (pushing) direction.

obstructed with blu-tack), whereas a distal push caused the entire pad to peel off from the pulling to the pushing side (Fig. 2.10F). As for *C. morosus* this prevented any recording of friction forces in the pushing direction. Adjacent setae peeled and detached together and the propagation of 'peeling fronts' across the pad contact zone as a whole was observed. However, this propagation was very fast and peeling of individual setae occurred almost simultaneously over large contiguous areas of the pad contact zone. This detachment of the whole pad was apparently caused by a rotation of the tarsal segment within the sagittal plane, due to the torque introduced by the distal push.

2.3.3 Contrasts in the beetle and stick insect systems

The data for pulling slides presented above was used (Table 2.3) to compare the performance between smooth and hairy pads. Shear stress was approximately 1.7 times greater in *G. viridula* when calculated as force per unit real contact area of the hairs (difference significant, Table 2.3). For the hairy system, a projected area of the pad was also measured to allow comparisons with smooth pads in terms of force per available pad area. Projected area was ca. 2.6 times larger than spatula contact area (little secretion), corresponding to an area fraction of the seta tips of 38%. When shear stress was calculated from the projected pad area (see Table 2.3), it was 1.5 times lower in the fibrillar system (not significant, Table 2.3). This is similarly true for adhesive stress which was 1.9 times higher in the hairy system for real contact (difference

Table 2.3: Comparison of shear stress and adhesive stress between the hairy and smooth systems, for the little (Lit.) and accumulated (Acc.) regimes and taking both real and projected contact areas into account for the hairy system of *Gastrophysa viridula*.

		Contact area	Hairy system *G. viridula*	Smooth system *C. morosus*	test statistic *t*-test
Shear Stress (kPa)	Lit.	real	518.5 ± 48.9	298.9 ± 60.2	$T_{11.5}$=2.83, p=0.016
		projected	196.2 ± 14.5		$T_{6.7}$=1.66, p=0.143
	Acc.	real	293.8 ± 63.9	205.8 ± 31.0	$T_{8.7}$=1.24, p=0.248
		projected	95.21 ± 20.41		$T_{10.4}$=2.98, p=0.013
Adhesion Stress (kPa)	Lit.	real	86.93 ± 11.34	44.59 ± 9.07	$T_{11.5}$=-2.92, p=0.014
		projected	35.49 ± 5.18		$T_{9.5}$=0.87, p=0.405
	Acc.	real	62.90 ± 14.06	24.88 ± 2.25	$T_{6.3}$=-2.67, p=0.035
		projected	20.32 ± 3.33		$T_{10.5}$=1.14, p=0.281

significant, Table 2.3), but 1.3 times lower for projected contact (not significant, Table 2.3).

2.4 DISCUSSION

2.4.1 Comparison between hairy and smooth systems

Whilst obviously limited to only one representative of each adhesive system, insight can be gained through a comparison of the hairy system of *G. viridula* and the smooth system of *C. morosus*. These findings indicate that in both systems, the fluid secretion plays a similar role. Forces in the smooth and the hairy system decreased when fluid had accumulated over several slides on the same area. Forces however increased or stayed constant when fluid was depleted. A recent study on stick insects showed that this effect is only present on smooth surfaces (Drechsler and Federle, 2006). However, the opposite effect was found on a rough substrate, suggesting that the fluid mainly serves to maximize contact on rough substrates. This conclusion is also likely to hold for hairy pads of insects, where the contact of relatively large seta tips is supplemented by a fluid secretion.

To compare adhesive and frictional performance between *G. viridula* and *C. morosus*, the most direct contrast is of the shear and adhesive stresses supported by each adhesive. Table 2.3 shows that stresses were slightly higher in *G. viridula* when calculated from spatula contact area, suggesting that the hairy system may represent a more efficient attachment mechanism. However, it is biologically more relevant to compare forces per projected pad area, because this is the area available to the animal for generating adhesion and friction. Shear and adhesive stresses calculated from projected pad area for the hairy system were in most cases no longer significantly different and even slightly lower.

It has been proposed that the adhesive stress of fibrillar adhesives increases as the dimensions of the individual contact elements decrease (Arzt et al., 2003). This 'force scaling' idea is based on the assumption that the adhesion of an individual subcontact scales linearly with its radius of curvature (for spherical contacts) or its width (for tape-like spatulae). The model further assumes that the total adhesion of an array of setae is the product of the force of a single seta and the number of setae. Thus, if the adhesive force of a single subcontact scales with its width B and the number of contact elements per pad area with $1/B^2$, then adhesive stress F/A should increase when the subcontacts are made smaller:

$$\frac{F}{A} \propto \frac{1}{B} \qquad [2.1]$$

This concept has been used to explain differences of contact size and density across a range of animals with different body sizes, because larger animals with relatively less available surface area (such as geckos) are expected to require a more effective adhesive system per unit pad area than smaller animals such as insects (Arzt et al., 2003; Spolenak et al., 2004). The fact that fibrillar adhesive pads of lizards are characterised by a much higher contact density than those of beetles has been seen as a confirmation of the force scaling hypothesis (Arzt et al., 2003). However, Equation 2.1 predicts the adhesive stress of *G. viridula* (spatula width ca. 6 μm) to be 30 times smaller than that of a Tokay gecko (*Gekko gecko*, spatula width ca. 0.2 μm (Williams and Peterson, 1982)). The mean adhesive stress of arrays of gecko setae has been measured as 53 ± 7.6 kPa (Gravish et al., 2008), which is only slightly higher than the values for *G. viridula* and *C. morosus*. As the adhesive stress values compared here were measured under different conditions, any conclusions have to be treated with caution. The comparison is also being made between different species and adhesive systems (wet vs. dry) and this is an important caveat. However despite this, these values certainly suggest that gecko pads do not in fact have a much higher efficiency per unit attachment area, in contrast to the prediction from Equation 2.1. This conclusion is consistent with recent data on the scaling of adhesive hair dimensions across different taxa (Peattie and Full, 2007), which suggest that differences in seta density are mainly explained by phylogenetic background and the presence or absence of an adhesive fluid (as is the case here for the dry gecko and the wet insect system), rather than by force scaling. Equation 2.1 is also inconsistent with the almost identical adhesive stress in a smooth (*C. morosus*) and a hairy system (*G. viridula*), as found in this study.

A possible explanation is that the assumptions of the force scaling model do not hold for animal adhesive pads. First, load may not be 'shared' equally by all the setae of an array. If hairy pads detach from a surface by peeling (as observed during the footloose experiments), stress is concentrated at the edge of the pad so that only a small number of setae contribute to the total force (Hui et al., 2004). In this case, pad pull-off forces would not be correctly predicted by the force scaling model. Second, the adhesive forces of individual subcontacts might not scale with their width or radius but with contact area, removing any scaling advantage from seta miniaturisation (Gao and Yao, 2004; Spolenak et al., 2004). This could be achieved for example through spatulae that have an optimised concave shape, giving rise to a uniform stress distribution in the adhesive contact zone at pull-off (Gao and Yao, 2004; Spolenak et al., 2004). In fact, adhesive setae in several insects (including *G. viridula*) are known to have concave spatulae (Haas and Gorb, 2004; Langer et al., 2004).

If the efficiency of gecko and beetle pads is indeed of similar magnitude, it is unclear how geckos compensate the size-related loss of mass-specific adhesion. Assuming isometry, the surface-to-volume ratio of *G. gecko* can be estimated to be ca. 16 times smaller than that of *G. viridula* (body masses 10.4 mg vs. 43.4 g (Irschick et al., 1996)). Geckos may partly compensate for this through disproportionately larger adhesive pads (estimated total pad areas: 0.47 mm^2 vs. 227.1 mm^2 (Irschick et al., 1996)). However, given that the pull-off forces of *G. viridula* are extreme, with the force of a single pad on a smooth surface corresponding to more than 10 times the beetle's body weight (Table 2.2), geckos may simply have a smaller 'safety factor' and still adhere perfectly well.

The above argumentation applies only to smooth substrates. Most biologically relevant substrates, however, possess some degree of surface roughness. Theory predicts that fibrillar systems, and in particular arrays of branched setae with fine endings as found in geckos, should make better contact to rough substrates (Persson, 2003; Persson and Gorb, 2003). However, it still remains to be investigated experimentally whether the performance on rough substrates differs between smooth and wet or dry fibrillar pads.

2.4.2 Mechanisms for direction-dependence and detachment

In order to consolidate fast running with effective attachment, an adhesive system must allow rapid and energy efficient detachments. Both smooth and hairy adhesive pads of insects possess this ability. The direction-dependence of adhesive and frictional forces is probably a key adaptation for the dynamic control of surface attachment. These findings demonstrate that

smooth and hairy systems both showed this anisotropy when comparing proximal (a pull of the leg towards the body) and distal (a push of the leg from the body) slides. Pushing friction forces were always much lower in both little and accumulated secretion regimes and showed a significant drop in contact area. Adhesion forces were also greatly reduced following a pushing slide and, for the conditions used, demonstrate an increased ease of detachment.

The mechanism for this direction-dependence therefore makes for an interesting contrast. For the smooth pads, although forces dropped comparing pulling to pushing slides, the contact area also fell. This resulted in no significant change in shear stress (in either little or accumulated secretion) and argues against a change in the inherent pad efficiency. Thus, a drop in contact area due to the flexibility of the pad is the only explanation for the direction-dependence, consistent with findings in the smooth pads of cockroaches (Clemente and Federle, 2008). However, in the hairy system of the beetles, the higher friction in the pulling direction was not only due to a strongly increased area of contact but also due to a higher shear stress. This suggests that the 'quality' of the adhesive contact differed between pulls and pushes.

Fig. 2.9 shows that the changes in contact area occurred at the level of each individual hair. During the proximal pull (Fig 2.9A) all hairs made good contact with the surface and a high resultant force was observed. However, during the start of a distal push (Fig 2.9B-E) the spatulae of each hair began to lose contact. They appeared to peel from the surface and remain with this small fraction of contact during the slide. The hairs are typically angled in the distal direction (Beutel and Gorb, 2001) and as such the resulting steeper peel angle may aid detachment during a distal push, allowing individual hairs to peel from the proximal side. In contrast, a proximal pull would put the hairs into tension, the

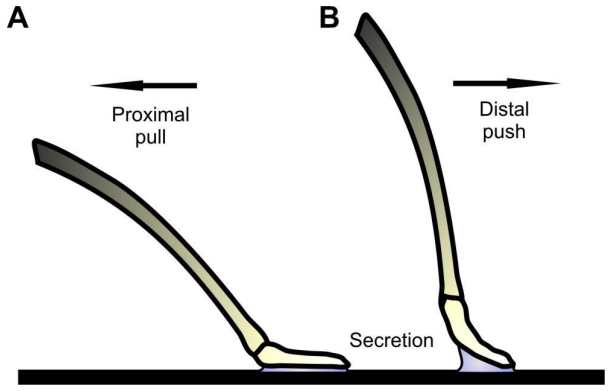

Figure 2.11: Diagram of setal movement during a proximal pull (A) and a distal push (B). During distal movements hairs appeared to contact only with their tips. The thicker fluid film may explain the observed distal decrease in shear stress.

shallow angle acting against contact peeling (Autumn et al., 2006a; Federle, 2006) (see Fig. 2.11). For immobilised pads, the fibrillar design had a more pronounced direction-dependence, with a 7.8 fold drop in friction, a considerable decrease compared with the 2.3 fold drop for the smooth system (little secretion). Unlike the smooth system which can detach at just one peel edge, the beetles' hairy system has several hundred contacts that can peel independently and almost simultaneously, which may aid rapid detachment.

The observed decrease in shear stress may be partly a result of overestimating the area of the seta tips that is in close contact. This could arise from fluid filled near-contact being observed in the coaxial illumination and being included in the contact area calculation (see Fig. 2.11). This idea gains support when taking into account the calculated change in contact area for both secretion regimes. The change for accumulated secretion was considerably less than the corresponding drop for little secretion (a 1.5 times decrease compared to a 3.7 times decrease) implying that the increased presence of fluid may well contribute to the measured area.

The footloose slides of the stick insect showed that the tarsus itself contributes to a loss of contact area in the pushing direction through buckling. Instabilities in the tarsal chain rapidly increase the angle between the leg and the surface, allowing the pad to peel from the proximal side. This adds to previous observations of the same effect in cockroaches (Clemente and Federle, 2008) and implies that due to their construction, the tarsus, and to some degree the pad itself are unstable against pushing. The foot as a whole also contributed to pad detachment in the beetles, adding to the direction-dependence of individual setae. This was less clearly demonstrated by the original footloose experiments but further observations made with a semi-restrained tarsus showed a similar proximal-distal peeling detachment as observed for the footloose stick insects.

These results show that adhesion strongly depends on the sliding direction before pull-off. When pull-off and proximal/distal shear forces act simultaneously, the effect is very similar. Recent work on geckos has shown the presence of a critical detachment angle at the level of single setae, arrays of setae and the whole toe (Autumn et al., 2006a; Autumn and Peattie, 2002; Gravish et al., 2008). Detachment occurs as soon as the angle of the force vector exceeds the critical angle. As some proximal shear is required for the setae to adhere, this effect has been termed 'frictional adhesion' (Autumn et al., 2006a). Direction-dependence of adhesive structures is the precondition for controlling attachment and detachment via the amount of proximal or distal shear force. The present results suggest that both *C. morosus* and *G. viridula* might

control adhesion in a similar way as the gecko. However, further work is needed to determine the detailed angle dependence of adhesion in both systems

The directional behaviour of the hair tips represents a specialised passive mechanism to control adhesion. Biomimetic directional adhesives have many possible applications and first prototypes have already been fabricated (Autumn et al., 2006a; Lee et al., 2008; Schubert et al., 2008). However, before design principles can be effectively transferred into technical applications, a greater understanding is needed of their precise function in the natural systems. This study illustrates that there is still much to investigate about both smooth and fibrillar adhesive systems in animals.

3

EVIDENCE FOR SELF-CLEANING IN FIBRILLAR AND SMOOTH INSECT ADHESIVE SYSTEMS

This work was conducted in collaboration with Christofer J. Clemente and Andrew Beale. All force measurements and statistical analyses in this study were performed in conjunction with them.

Summary

Insects possess adhesive organs that allow attachment to diverse surfaces. Efficient adhesion must be retained throughout their lifetime even when pads are exposed to contamination. Many insects groom their adhesive structures, but self-cleaning properties are also likely to play an important role. Attachment forces of insect pads on glass were measured after contamination with microspheres and both smooth pads (stick insects: *Carausius morosus*) and hairy pads (dock beetles: *Gastrophysa viridula*) were found to exhibit self-cleaning behaviours. Contaminated pads recovered high levels of adhesion after only eight simulated steps; this was accompanied by the deposition of spheres. Self-cleaning was strongly enhanced by shear movements, and only beetle pads showed the ability to self-clean during purely perpendicular pull-offs. Hairy pads also self-cleaned more efficiently than smooth pads for both large (45 μm) and small (1 μm) particle sizes. However, the beetles' self-cleaning was not superior to smooth pads when contaminated with 10-μm beads. This limitation of self-cleaning is explained by the coincidence of bead diameter and inter-seta distance, which caused beads to remain trapped in between setae.

3.1 INTRODUCTION

Many insects are capable of climbing and walking upside down on diverse substrates using adhesive organs on their legs (Scherge and Gorb, 2001). Despite the enormous diversity of insects, tarsal adhesive organs are regularly grouped into two alternative design categories; hairy and smooth (Federle, 2006). 'Hairy' pads are densely covered with flexible, micron-sized setae and occur in

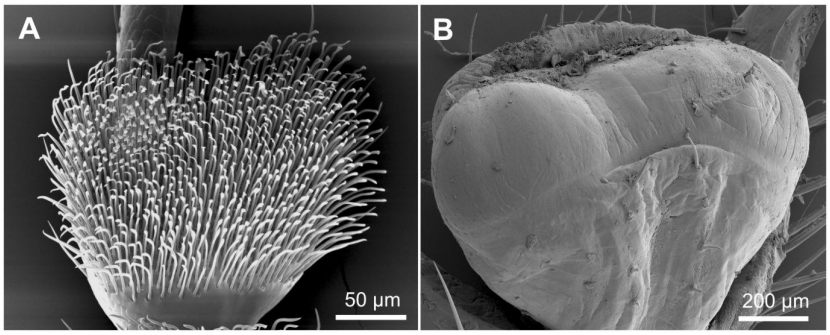

Figure 3.1: Scanning electron microscopy images of the distal, fibrillar adhesive pad of (A) the dock beetle (*Gastrophysa viridula*) and (B) the smooth pad (arolium) of the Indian stick insect (*Carausius morosus*).

several insect orders, including flies, beetles and earwigs (Beutel and Gorb, 2001; Fig. 3.1A). 'Smooth' adhesive pads have a relatively even surface profile and a specialised, soft cuticle; they are present in many insects including ants, bees, cockroaches and stick insects (Beutel and Gorb, 2001; Scherge and Gorb, 2001; Scholz et al., 2008; Fig. 3.1B). In both systems, adhesion is mediated by a fluid that is secreted into the contact zone (Gorb, 2001).

Hairy adhesive systems have evolved independently multiple times in arthropods and invertebrates (Federle, 2006). The frequent occurrence of hairy adhesive systems suggests that this design is optimised for surface attachment. As discussed in Chapter 1, several theoretical studies have suggested that the hairy pad design allows not only close contact to rough surfaces (Persson, 2003; Persson and Gorb, 2003), but also increased adhesion due to contact splitting (Arzt et al., 2003) and a more effortless detachment (Chapter 2; Autumn and Hansen, 2006; Autumn et al., 2006b; Federle, 2006; Gravish et al., 2008). These benefits raise the question of whether fibrillar adhesives are superior to smooth pads. However, insects with smooth pads have to fulfil largely the same biological requirements, i.e. they also need to be able to conform well to rough substrates and to detach efficiently. In Chapter 2 hairy pads of beetles and smooth pads of stick insects were compared directly for the first time, and it was found that there was little difference in friction or adhesive stresses. Moreover, both smooth and hairy systems showed a strong direction-dependence.

Hence a further possible advantage that hairy systems might have over smooth systems is an ability to self-clean as they walk, without the need for active grooming. Insects are continuously exposed to various contaminating particles such as dust, microorganisms, spores and pollen grains. Some plants have evolved leaf or stem surfaces covered by epicuticular wax crystals which easily exfoliate and thus contaminate insect adhesive structures. Indeed, contamination by wax crystals has been shown

to disrupt attachment both for insects with smooth and hairy adhesive systems (Edwards, 1982; Federle et al., 1997; Gaume et al., 2004; Stork, 1980b). Although adhesive pads can degenerate with age due to a loss of compliance (Ridgel et al., 2003), insects usually retain the ability to adhere to substrates throughout their life. Clearly, insects must be able to remove contamination from their adhesive pads.

Many insects are known to groom their body, including the legs (Farish, 1972), and it is likely that grooming removes particles from adhesive structures. However, many insects with adhesive pads do not or only rarely perform cleaning behaviours (e.g. stick insects) and even insects that groom more frequently take numerous steps between cleaning movements. It is therefore likely that many insects would quickly accumulate contamination and lose their adhesive ability if they only relied on active grooming to clean their pads.

A possible alternative mechanism for removing contaminating particles from adhesive pads is self-cleaning by contact. It was reported that gecko adhesive pads are able to self-clean within just a few steps after being contaminated by particles (Hansen and Autumn, 2005). Not only live geckos but also isolated setal arrays lost particles and recovered adhesion in simulated steps following contamination. Hansen and Autumn (2005) explained the geckos' ability to self-clean by the contact geometry of the hairy system. They argued that dirt particles adhere more strongly to the substrate than to fine seta endings on the foot. This balance of forces would remove the dirt and clean the pad with every step taken. A similar model was used to explain an observed force recovery in synthetically produced adhesive arrays of polypropylene microfibres, an important advance in the development of biomimetic self-cleaning adhesives (Lee and Fearing, 2008).

However, the assumptions of this model may only be plausible on smooth surfaces. On rough surfaces the real contact area between the particles and the substrate can be very small. This should cause the particles to adhere more strongly to the setae, making self-cleaning unlikely. As an alternative, it was suggested that self-cleaning could occur by small shear movements of the adhesive setae (Persson, 2007), which scratch away particles. In fact, Hansen and Autumn's (2005) demonstration of self-cleaning in geckos involved shear movements and it is unclear whether gecko pads would also self-clean without shear. From their model, Hansen and Autumn (2005) predicted that self cleaning in geckos should occur for contaminating particles of all sizes. However, it is still unclear whether and how the self cleaning ability of insect pads, if present, is influenced by particle size; this question was addressed experimentally in this study.

So far, self-cleaning has only been studied and modelled for fibrillar adhesive systems. It is unknown whether animals with smooth adhesive systems possess a similar self-cleaning ability. Insects also differ significantly from geckos in that they secrete an adhesive fluid into the contact zone. Does this fluid impede or facilitate self-cleaning? It was shown that the fluid secretion does not act to increase adhesion on smooth surfaces, but does so only on rough substrates where it fills in crevices and thus maximises contact area (Chapter 2; Drechsler and Federle, 2006). However, the fluid may have additional functions, and it is possible that it is involved in the deposition of contaminating particles by continuously 'washing' the pad.

Here the self-cleaning ability of fluid-based adhesive pads of insects was investigated by addressing the following questions: 1. Can smooth and hairy pads of insects remove contaminating particles by self-cleaning? 2. Is the self-cleaning ability of smooth and hairy pads different? 3. Does self-cleaning require a shear movement? 4. What is the effect of particle size on self-cleaning?

3.2 METHODS

3.2.1 Study animals

As in Chapter 2, adult stick insects *Carausius morosus* Brunner (Phasmatodea) and adult male beetles *Gastrophysa viridula* De Geer (Coleoptera) were tested. Both insects were taken from laboratory colonies kept at 24°C. Adhesive and frictional forces were measured for the distal adhesive pads (i.e. the pretarsal arolium of *C. morosus* and the pad on the third tarsal segment in *G. viridula*). For performing force measurements, the insects were restrained and their adhesive pads fixed as per the 'immobilised' condition described in Chapter 2. Stick insects were enclosed in a hollow glass tube, taking advantage of their typical stick-like camouflage position, with their front legs protruding from the open end. The dorsal side of the pre-tarsus of the front leg was attached to a piece of solder wire using dental cement ESPE Protemp II (3M, St Paul, MN, USA). Beetles were fastened to a mount using parafilm tape, and their front leg immobilised in blu-tack (Bostik, Leicester, UK).

3.2.2 Measurements of self-cleaning performance

Contamination

To contaminate the pads, polystyrene microspheres of nominal diameters 1 μm, 10 μm and 45 μm (Polysciences Inc., Warrington, PA, USA) were used. The actual diameters given by the manufacturer are 0.992 ± 0.026 μm, 9.606 ± 0.763 μm and 43.33 ±

2.23 μm, respectively. A single drop (~ 5 μl) with 2.6% of solid beads was placed near the corner of a glass coverslip (18 mm x 18 mm x 0.1 mm); the droplet was then freeze-dried for 2 hours at –20°C over Silica Gel. This resulted in a circular patch on the glass cover slip (5 mm diameter) densely covered by spheres. Freeze-drying minimised the aggregation of spheres into colloidal crystals along the contact line of the evaporating fluid; the treatment was performed to achieve a dispersed distribution of the particles.

Single-pad force measurements

The experimental setup used was similar to that described in Chapter 2 and a schematic of the force measurement device can be found there. Friction and adhesion forces were measured using a two-dimensional bending beam (spring constant 33 Nm^{-1}) equipped for each direction with two 350 Ω foil strain gauges 1-LY13-3/350 in a half-bridge configuration (Vishay, Malvern, PA, USA). Adhesion forces alone were measured with a one-dimensional full-bridge bending beam (spring constant 150 Nm^{-1}) equipped with 540 Ω semiconductor strain gauges SS-060-033-500PU, affording higher sensitivity (Micron Instruments, Simi Valley, CA, USA). The glass cover slip containing the patch with spheres was attached to the distal end of the bending beam and brought into contact with the insect foot. The adhesive contact area was recorded under reflected light using an externally triggered (10 Hz) Redlake PCI 1000 B/W camera (Redlake, Tallahassee, FL, USA) mounted on a Leica MZ16 stereo microscope (Leica Microsystems GmbH, Wetzlar, Germany) with coaxial illuminator (Federle and Endlein, 2004). Video analysis was performed with custom-made software using MATLAB (The Mathworks, Natick, MA, USA). Force input signals were amplified GSV1T8 (ME-Systeme, Henningsdorf, Germany) and recorded to a data acquisition board PCI-6035E (National Instruments, Austin, TX, USA) with a sampling frequency of 1000 Hz. As described in Chapter 2, the bending beam was mounted on a computer-controlled three-dimensional positioning stage M-126PD (Physik Instrumente, Karlsruhe, Germany). Motor movements, video trigger and force recording were synchronized using a custom-made LABVIEW (National Instruments) program that allowed a 50 Hz feedback control of the normal force.

To measure the attachment forces of pads before and after a contamination event, a series of consecutive press-downs and pull-offs ('steps') were performed. Each step was made at a new position on the glass plate. Steps lasted 5 s with a feedback-controlled load of 1 mN for the stick insects and 0.3 mN for the beetles (see Chapter 2 for explanation of feedback forces chosen) the duration between steps was 20 seconds. To quantify forces without contamination, four pull-offs from the clean glass plate were

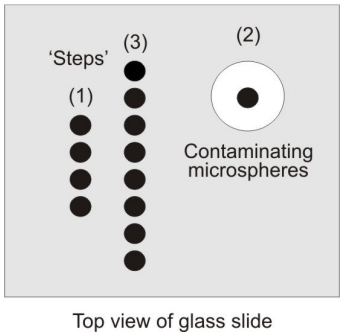

Figure 3.2: Order and pattern of steps performed on the glass-plate to test the effect of contamination and self-cleaning. Four initial steps were followed by a 'contamination step' and eight steps on clean areas of the glass plate.

initially performed. The pad was then brought in contact with the patch of spheres in the same way as for the other steps. After this contamination event, eight consecutive pull-offs were performed to assess the effect of the contamination and the extent of recovery in adhesion and friction forces. The order and location of steps on the glass plate are shown schematically in Figure 3.2.

To examine whether self-cleaning requires a shear movement of the pad, experiments with two different types of consecutive 'steps' were performed: 1. without shear: the movement consisted only of a perpendicular approach and pull-off (velocity 0.5 mms^{-1}), 2. with shear: approach and pull-off were performed as before, but after the initial approach phase and before the pull-off, the pad was dragged horizontally over a distance of 0.5 mm (velocity 0.5 mms^{-1}). The shear movement was performed in the proximal direction, corresponding to a pull of the pad towards the insect's body (Chapter 2). A pull in this direction is observed during the attachment and stance phase in freely running insects; it brings the adhesive pad structures in contact and maximises their adhesive contact area (for *C. morosus* and *G. viridula*, see Chapter 2).

Count of deposited spheres

After each series of consecutive force measurements, images of the footprints on the glass plate were taken using a 12 bit monochrome digital camera QIC-FM12 (QImaging, Surrey, BC, Canada) mounted on a Leica DMR-HC (Leica Microsystems GmbH) upright microscope. For the smaller 1 μm and 10 μm spheres, the counting was automated using a custom made Matlab script. Spheres were visible as black objects on a bright background, and a greyscale threshold was applied to obtain the total area of the image occupied by beads. After quantifying the area equivalent to a single bead, the total number of spheres in a footprint image was calculated. If beads were deposited on top of each other in layers, each stacked

layer was captured at a different focal plane and the spheres in them were counted manually. All force measurements and sphere counts were performed in conjunction with C. J. Clemente.

3.2.3 Statistics

To test the effect of contamination, adhesion and friction forces were converted to a percentage of the force before contamination in order to reduce size-related variation between insects. For other analyses comparing the efficiency of self-cleaning between bead sizes and between insects, the measured force F_n (adhesion or friction) of the n^{th} step was converted into a recovery index, $R_n = (F_n - F_{contaminated})/(F_{clean} - F_{contaminated})$, which is identical to the recovery index used by Hansen and Autumn (2005). Page's L tests (Page, 1963) were performed to test the hypothesis that the recovery index increased for consecutive steps. Pearson's correlation was used to test whether adhesion force was correlated with the number of deposited spheres. All statistical analyses were performed in conjunction with C. J. Clemente

3.3 RESULTS

3.3.1 Effect of contamination

Contamination strongly reduced adhesive and frictional forces in both insects. Forces for the first step after contamination were always smaller (*t*-tests for both insects and all three bead sizes $P<0.001$), and decreased by 50-90%. The effect of contamination on adhesion and friction is a result of the variation in adhesive contact area. Contamination strongly reduced both force and adhesive contact area (Fig. 3.3) such that adhesive stress (force per unit contact area) did not change over the course of each trial (10 μm beads, repeated measures ANOVA comparing the first step before, as well as the first and eighth step after contamination: stick insects $F_{2,6}=3.65$, $P=0.069$; beetles $F_{2,10}=1.53$, $P=0.248$). Similarly, shear stresses also showed no significant changes during each trial (stick insects $F_{2,6}=1.83$, $P=0.214$; beetles $F_{2,10}=1.74$, $P=0.208$). Thus, the loss of attachment forces after contamination is not based on a decrease of adhesive or shear stress but on the loss of contact area.

Pads of both insects exhibited a clear recovery of forces by self-cleaning in subsequent steps, but this recovery was influenced by the presence or absence of a shear movement before the pull-off.

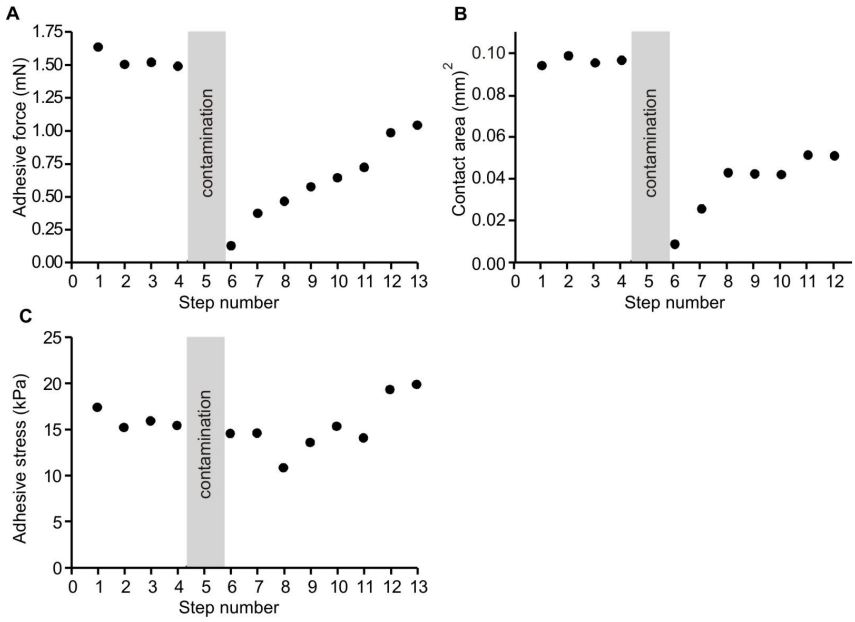

Figure 3.3: (A) Adhesive force, (B) contact area and (C) adhesive stress (adhesive force per unit contact area) for a stick insect contaminated with 10 μm beads. The initial four steps represent values for a clean uncontaminated pad. The fifth step is used to contaminate the pad with beads. Steps 6-13 show eight steps after contamination. An increase was seen in adhesive force which related to an increase in contact area. Adhesive stress remained unchanged.

3.3.2 Can insect adhesive pads self-clean?

Pull-offs without shear

Pull-offs without a preceding shear movement were performed only with the 10 μm diameter beads. For the smooth pads of stick insects, no evidence of a recovery of adhesion forces over consecutive pull-offs was found (Page's L-test $L_{8,6}$=910, P=0.946). However, the hairy pads of beetles tested under the same conditions exhibited a 50% recovery of adhesion, by the eighth step after contamination, providing evidence for self-cleaning (Page's L-test $L_{8,6}$=1109, P<0.001).

Pull-offs with a shear movement

When the experimental steps included a proximal shear movement (corresponding to a pull of the foot towards the insect's body), not only the hairy pads of beetles but also the smooth pads showed a significant recovery of adhesion, friction and contact area over eight steps. Forces recovered by self-cleaning in both stick insects and beetles for all three tested bead sizes (Page's L-test P<0.05 for all insects and bead sizes).

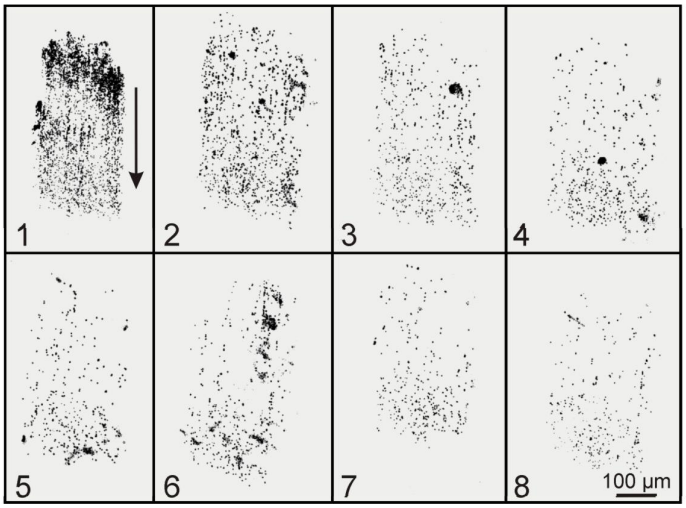

Figure 3.4: 1 µm spheres deposited by *Gastrophysa viridula* in eight consecutive footprints after contamination. The steps included a 0.5 mm proximal (pulling) sliding movement. Arrow shows direction of pad movement.

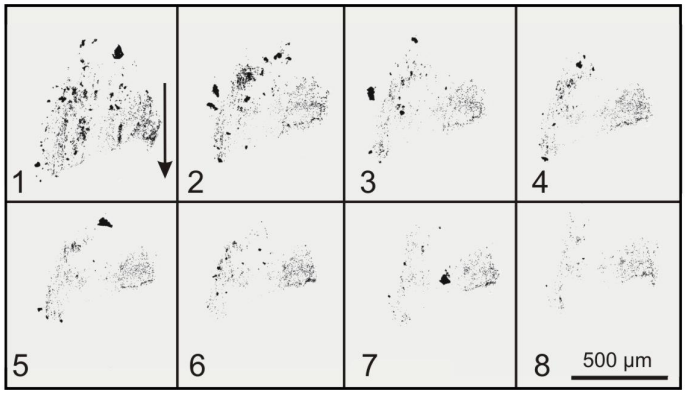

Figure 3.5: 1 µm spheres deposited by *Carausius morosus,* conditions as for Figure 3.4.

In beetles, the shear movement did not appear to increase the efficiency of self-cleaning; there was no significant difference between the corresponding recovery slopes of adhesion, with or without a shear movement (10 µm beads; $F_{1,12}$=0.737, P=0.407).

3.3.3 Deposition of particles

Examination of the footprints left on the glass plate revealed that many spheres were deposited with every step, together with liquid and solid footprint material. Figures 3.4 and 3.5 show that spheres were deposited throughout the entire slide so that the effect of the shear movement was to 'wipe' spheres off the pad. This pattern was observed both in beetles and stick insects. The number of spheres per footprint was highest in the first step and decreased in consecutive slides, correlating to the increase in friction and

Table 3.1: Rate of recovery (regression slopes of Fig. 3.8) after contamination with different-sized beads in smooth pads of stick insects and hairy pads of beetles.

	Friction slope comparison		Adhesion slope comparison	
C. morosus	regression	$df = 2$, MS = 0.001	regression	$df = 2$, MS = 0.011
	error	$df = 18$, MS = 0.008	error	$df = 18$, MS = 0.004
		$F_{2,18} = 0.123$, $P = 0.885$		$F_{2,18} = 2.736$, $P = 0.092$
G. viridula	regression	$df = 2$, MS = 0.264	regression	$df = 2$, MS = 0.092
	error	$df = 10$, MS = 0.017	error	$df = 13$, MS = 0.008
		$F_{2,10} = 15.600$, $P < 0.001$		$F_{2,13} = 11.100$, $P = 0.002$

adhesion (10 µm beads; stick insects: adhesion r=-0.82, P=0.012, friction r=-0.89, P=0.003; beetles: adhesion r=-0.88, P=0.003, friction r=-0.95, P<0.001).

3.3.4 Effect of sphere size on self-cleaning ability

To test the effect of bead size on self-cleaning ability, linear regressions of the recovery index for the steps after contamination in each insect were performed and the slopes (rate of recovery) compared. Steps were included until the recovery index was no longer significantly different from 1 as judged by a one-tailed t-test. Later steps were not included in the regression, as the forces had almost completely recovered.

For stick insects, the rate of recovery did not significantly depend on bead size (Table 3.1). By contrast, bead size had a

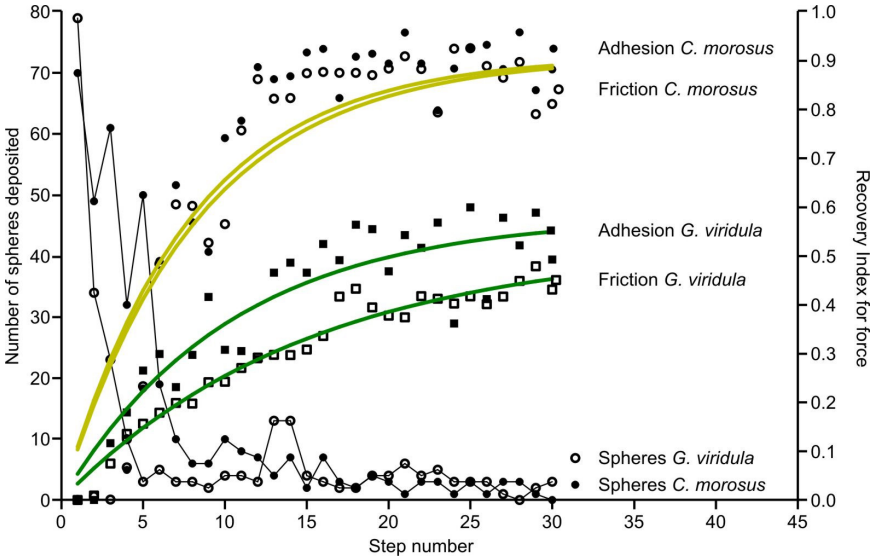

Figure 3.6: Recovery of adhesion and friction over 30 steps in stick insects (*Carausius morosus*) and beetles (*Gastrophysa viridula*) when contaminated with 10 µm diameter beads. The lines are exponential data fits of the form $C_n=C_\infty(1-e^{-\beta n})$, where n is the step number after contamination, β the exponential decay constant and C_∞ the value to which the recovery index may converge over an infinite number of steps.

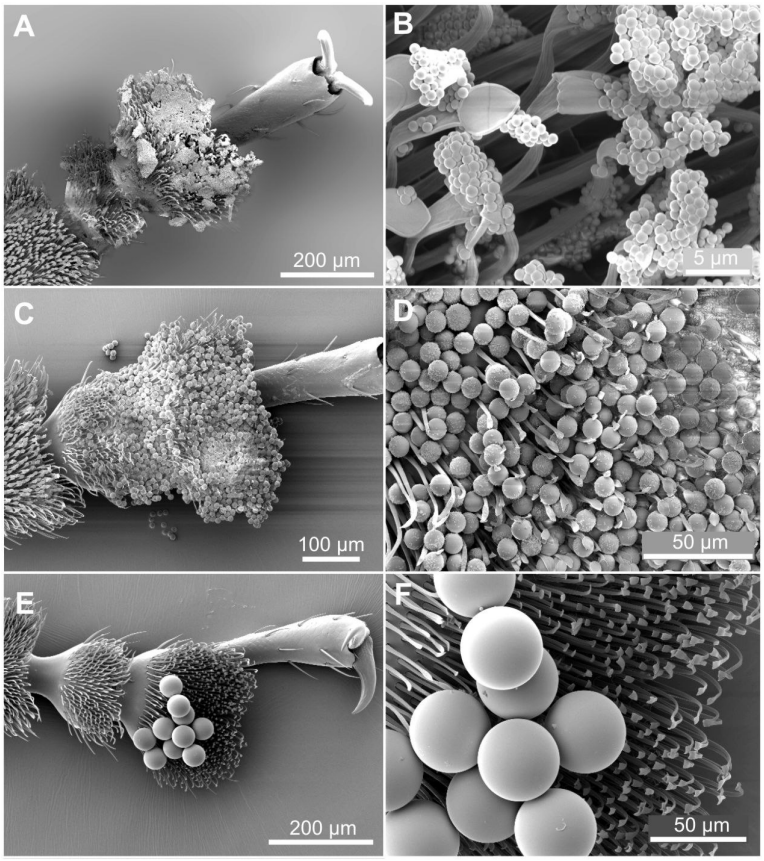

Figure 3.7: SEM images of adhesive pads of *Gastrophysa viridula* after contamination with beads of different sizes, followed by eight consecutive steps to allow self-cleaning. (A,B) 1 µm diameter beads; (C,D) 10 µm diameter beads; (E,F) 45 µm diameter beads. As pads contaminated with 45 µm beads did not contain any beads after self-cleaning, (E) and (F) show a freshly contaminated pad.

striking effect on the rate of recovery in beetles (Table 3.1). While forces recovered quickly for the 1 µm and the 45 µm spheres, recovery was much weaker and slower for pads contaminated with 10 µm diameter spheres, significantly different from the other bead sizes (SNK post hoc tests $P<0.05$ for both comparisons).

To further characterise the beetle pads' poor ability to self-clean for the 10 µm beads, a longer series of 30 consecutive steps in both *C. morosus* and *G. viridula* was performed. Figure 3.6 shows that while adhesion and friction for the stick insect pad completely recovered within ca. 15 steps, the forces of the beetle pads did not return to their initial values even over 30 steps. The forces exponentially approached an asymptote of about 50% force, indicating that little or no further recovery would occur even for larger numbers of consecutive steps.

To understand the underlying mechanism of this effect, pads were imaged after eight consecutive steps using SEM (Fig. 3.7). It is clear that the 45 µm spheres were too large to fit between

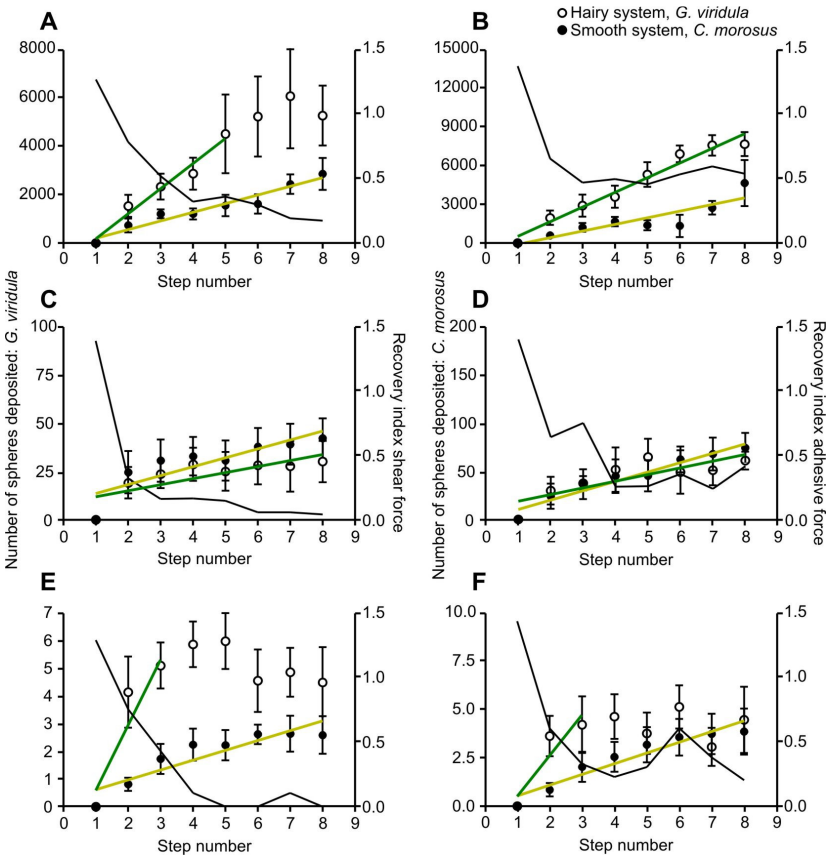

Figure 3.8: Comparison of the rate of adhesion and friction force recovery after contamination of smooth pads (closed circles) and hairy pads (open circles) for different particle sizes. (A,B) 1 μm beads, (C,D) 10 μm beads, (E,F) 45 μm beads. Lines show least square regression fits for all steps where the forces were significantly different from 1 using a one-tailed *t*-test, *n*=6 for all points.

setae, and they can therefore be rapidly removed by self-cleaning. By contrast, many 1 μm and 10 μm beads were still adhering to the setae after eight steps. While the 1 μm beads adhered loosely to the seta-stalks and left the setae free to move, the 10 μm spheres made contact with several setae simultaneously and thus likely immobilised them. The 10 μm spheres became trapped in between setae, because their diameter approximately corresponded to the inter-seta distance, which for dock beetles is 10.19 ± 1.16 μm (see Chapter 2 and Fig. 3.1).

3.3.5 Contrasts in the beetle and stick insect systems

The initial reduction of adhesion and friction forces due to contamination was not significantly different between smooth and hairy pads for any bead size (*t*-tests, $P>0.05$ for all bead sizes). However, the rate of force recovery after contamination differed significantly between beetles and stick insects (Table 3.2). The beetles' pads recovered more than two times faster when

Table 3.2: Comparison of the rate of recovery between smooth and hairy pads (of *Carausius morosus* and *Gastrophysa viridula*) for the three different bead sizes used.

		Friction				Adhesion			
1 μm	rate of recovery	*C. morosus:* 0.067 *G. viridula:* 0.193				*C. morosus:* 0.051 *G. viridula:* 0.113			
		df	MS	*F*	*P*	*df*	MS	*F*	*P*
	regression	1	0.13	48.5	0.00	1	0.08	20.0	0.00
	residual	9	0.00			12	0.00		
10 μm	rate of recovery	*C. morosus:* 0.069 *G. viridula:* 0.047				*C. morosus:* 0.072 *G. viridula:* 0.052			
		df	MS	*F*	*P*	*df*	MS	*F*	*P*
	regression	1	0.01	0.9	0.36	1	0.01	1.6	0.24
	residual	12	0.01			12	0.01		
45 μm	rate of recovery	*C. morosus:* 0.076 *G. viridula:* 0.504				*C. morosus:* 0.083 *G. viridula:* 0.314			
		df	MS	*F*	*P*	*df*	MS	*F*	*P*
	regression	1	0.35	15.9	0.01	1	0.1	12.0	0.01
	residual	7	0.02			7	0.01		

contaminated with 45 μm and 1 μm beads, but no difference and even a trend towards slower recovery in the beetles was found for the 10 μm beads (Fig. 3.8, Table 3.2).

3.4 DISCUSSION

3.4.1 Self-cleaning in insect adhesive systems

This study has confirmed that insect adhesive pads were able to self-clean with repeated steps. The ability was present both in insects with smooth and hairy adhesive organs. Adhesion and friction forces often returned to 100% of the force before contamination within only a few steps. The insects' self-cleaning ability was comparable to that previously observed for dry gecko adhesives (Hansen and Autumn, 2005) and may even exceed it in terms of efficiency. Under similar experimental conditions, whole digits of geckos recovered over eight steps 35.7% of the lost shear force (5 μm diameter particles: Hansen and Autumn, 2005), whereas smooth stick insect pads recovered 53.4% and hairy beetle pads recovered 98.4% (1 μm particles).

3.4.2 Mechanisms for self-cleaning

These results show that the effects of both contamination and recovery were based on changes of adhesive contact area. Neither shear nor adhesive stress increased for recovering pads (nor did they decrease following contamination). Instead, the increase in

forces seen with each step after contamination was matched by an increase in contact area.

Effect of shear

Smooth and hairy adhesive pads of insects were able to self-clean over consecutive steps when these included a shear movement. It is likely that sliding movements helped to dislodge spheres from the useful contact zone. Previous studies (Hui et al., 2006; Persson, 2007) have suggested that shear movements of fibrillar pads are important, and in particular the cyclical pulling and pushing movements that control attachment and detachment. Spheres may be transported to the edge of the contact zone by scratching, sliding or rolling, and may be removed by further sliding or when the seta or pad detaches from the surface (Persson, 2007).

The smooth pads of stick insects exhibited self-cleaning only in the presence of a shear movement. By contrast, forces for the hairy pads of beetles were able to recover even when steps consisted only of pull-offs. This suggests that beetles might self-clean by a mechanism similar to the one proposed for dry gecko setae by Hansen and Autumn (2005). Hansen and Autumn suggested that self-cleaning results from the greater attraction of particles to the surface than to the tips of the setae, resulting from the contact geometry, stiffness and low surface energy of fibrillar adhesive systems. Self-cleaning in the beetles' adhesive pads may be further enhanced by microscale shear movements of the setae. In a hairy adhesive system, contaminating particles need to be moved by only a very small distance to reach the edge of a seta's adhesive contact zone. When pressed onto the substrate, the tip of a seta may simply push particles aside, thereby moving them to a place where they adhere more strongly to the substrate and less to the seta. By contrast, a soft, smooth pad pressed onto the substrate will deform and enclose a contaminating particle, leaving the particle within the contact zone and with a stronger adhesion to the pad than to the surface.

Role of adhesive fluid

The presence of adhesive fluid differentiates the insects' 'wet' adhesive systems from that of the gecko. The greater efficiency of self-cleaning found in this study suggests that the fluid secretion facilitates the deposition of contaminating particles. In fact, many particles are found in fluid droplets left behind by insect pads after contamination. As footprint secretion is produced and deposited continuously with every adhesive pad surface contact, the fluid may effectively ‘wash’ particles off the pad.

Effect of particle size

These findings demonstrate a significant effect of particle size on the self-cleaning ability of the hairy system of the beetle, but not on the smooth system of the stick insect. While smooth pads appeared to work equally well for all sphere sizes, hairy pads showed a significantly slower recovery for 10 μm size beads when compared to smaller or larger bead sizes. Even in longer trials of 30 repeated steps, beetle pads were unable to fully recover when contaminated by particles of this size. One probable reason for this may be that the 10 μm particles became trapped in between setae, because their diameter approximately corresponded to the inter-seta distance. This condition not only makes the removal of particles very difficult, but it also immobilises setae and restricts their lateral movements. As discussed above, such microscale shear movements may be important for the recovery of fibrillar adhesives in that they allow setae to push particles aside.

Particles with diameters larger than the inter-seta distance such as the 45 μm spheres in this study can not or only partly penetrate the setal arrays. Such particles may therefore have a relatively small contact area with the setae, resulting in faster removal by self-cleaning. This is the situation investigated by Hansen & Autumn (2005); the spatula density of 3.79 μm^{-2} reported for the tokay gecko corresponds to an inter-spatula distance of ca. 0.55 μm, considerably less than the 5-μm diameter of the tested particles.

The dependence of self-cleaning ability on particle size is unlikely to be a phenomenon restricted to beetles but may also occur in hairy pads of other animals. However, self-cleaning ability in diverse animals may be influenced by the very different seta dimensions (Peattie and Full, 2007). Specifically, self-cleaning may be slowest for particles matching the inter-seta distance, and fastest for particles larger than it.

It is additionally important to note that all contaminating particles used in this study were smooth and of a perfect spherical shape. Whilst standardised spheres allow for a test of the effect of particle size, 'natural' particles (such as stone or dust fragments) are rarely smooth and spherical, leading to a reduced area of contact between the particles and the substrate. An interesting extension of this study would therefore be to investigate contamination with rough particles of a specified average size. In general, surface roughness and surface chemistry (of both substrate and particles) are likely to have important implications on self-cleaning performance and need to be investigated in future work.

3.4.3 Comparison between hairy and smooth systems

Hairy adhesive pads have arisen frequently throughout the animal kingdom. Several predictions have been proposed as to their possible benefits, including a superior self-cleaning ability (Federle, 2006; Hansen and Autumn, 2005). In the previous chapter comparing smooth and hairy pads, similar adhesion and friction stresses in both pads was found, however increased direction dependence was seen in hairy pads (Chapter 2). The results presented here thus provide the more direct evidence for a superior performance of hairy systems. Hairy pads of beetles not only outperformed the smooth pads of stick insects in their ability to self-clean without a shear movement but they also recovered more rapidly from contamination. For 1 and 45 μm particles, beetle pads recovered 2-10 times faster than the smooth pads of stick insects. In fact, despite the reduced rate of recovery for forces of beetle pads when contaminated with 10 μm beads, recovery rate was still not significantly lower than that of the stick insects. This suggests that even the slowest rates of recovery for hairy pads are not much worse than rates seen for smooth pads. The excellent ability of hairy pads to recover from contamination may be an important factor explaining the widespread appearance of hairy pad morphology across different taxa.

Possible reasons why the fibrillar design might allow a more efficient self-cleaning have been discussed above. However, the detailed mechanisms of self-cleaning in animal adhesive pads are still not fully understood, and further experimental and theoretical work is needed to clarify them.

A self-cleaning ability is an important property of biological adhesive systems and will be an important criterion for the design of bio-inspired adhesives. Scotch tape is a prime example of an adhesive that is not self-cleaning and consequently it is of no use after several applications. Efforts are underway to manufacture a fibrillar adhesive that is effective after more than one use (Gorb et al., 2007; Lee and Fearing, 2008; Sethi et al., 2008). The hard polymer adhesive developed by Lee and Fearing (2008) demonstrated the first example of self-cleaning in an artificial fibrillar adhesive. However, despite these advances, the currently existing technology still falls vastly short of the impressive self-cleaning ability of insects.

4

THE EFFECT OF SURFACE ROUGHNESS ON CLAW AND ADHESIVE HAIR PERFORMANCE

Summary

Natural adhesive systems are adapted to attach to rough surfaces, but the underlying mechanisms have not been fully clarified. Attachment forces for the beetle *Gastrophysa viridula* were recorded on epoxy casts of surfaces with different roughness using a centrifuge device. Replicas were made of standardised polishing paper with asperity sizes ranging from 0.05 to 30 μm and of dock leaves (*R. obtusifolius*). Beetles adhered with a safety factor of up to 36 times body weight on smooth substrates or on casts of leaves of their host plant. On the rough substrates, forces were much lower and a minimum at small scale roughness (0.05 to 1 μm asperity size, with a mean safety factor of 5) was observed. Removal of the claws led to a significant reduction in force for rough substrates with asperity sizes ≥ 12μm. Attachment forces of the hairy adhesive system itself (without the claws) slightly increased from small-scale to large-scale surface roughness, but remained below the level seen on the smooth substrate. This is explained by the inability of setal tips to make full contact with the surface.

4.1 INTRODUCTION

Insects have developed many adaptations to move quickly and efficiently on natural surfaces. In order to cling to a wide range of substrates, many species have evolved sophisticated adhesive pads in addition to the pretarsal claws. Adhesive pad structures have independently developed in multiple lineages such as tree frogs, lizards, spiders and many insect orders; they broadly divide into 'smooth' (soft pads) and 'hairy' (arrays of microscopic setae) (Beutel and Gorb, 2001; Scherge and Gorb, 2001). Both systems are highly compliant, which is essential as it allows adaptation to real surfaces exhibiting roughness (Persson, 2003). A low effective elastic modulus of an adhesive is a necessary requirement for good surface contact and sufficient attachment. Most adhesives fail on rough surfaces where intimate contact requires significant

deformation. This results in competing elastic forces which reduce the overall adhesion (Peressadko et al., 2005; Persson and Gorb, 2003). If a material is compliant enough, the gain in surface energy exceeds the work required to deform the adhesive and it can easily adapt to a substrate.

However, very soft materials are more susceptible to creep, wear and contamination. In hairy adhesive systems, a low 'effective' elastic modulus can be achieved through the fibrillar structure, despite each hair consisting of a very stiff material in the GPa range (Autumn et al., 2006c; Glassmaker et al., 2004; Persson, 2003). A high stiffness has been shown for the fine setae of geckos (Autumn et al., 2006c) allowing a combination of compliance and wear-resistance. The small tips of the hairs (with widths ranging from more than 5 μm in beetles down to ca. 100 nm in spiders and geckos) also allow for good contact to surfaces with finer roughness. If the hairs are fine enough, the hair tips can come so near to the surface that they are in the reach of van der Waals forces. In the wet systems of insects, a fluid secretion is used to fill the remaining microscopic gaps (Barnes et al., 2002; Drechsler and Federle, 2006; McFarlane and Tabor, 1950; Persson, 2007; Persson et al., 2005). As large volumes of fluid can weaken attachment (Chapter 2; Drechsler and Federle, 2006), close contact (and hence a flexible pad material and small amounts of fluid) is still desirable.

Adhesive hairs need to be both long enough to deform around large asperities, and sufficiently fine to accommodate small scale surface roughness. However, overly long and thin hairs will tend to clump and adhere to one other, detrimental to adhesive function (Glassmaker et al., 2004; Persson, 2003; Sitti and Fearing, 2003; Spolenak et al., 2005). A solution to this problem has evolved in geckos, spiders and some beetles, which possess branched hairs. Such a design allows high compliance and very fine tips without the risk of self-matting, because the length of the thinnest endings is reduced (Federle, 2006; Yao and Gao, 2006). At the same time, the hierarchical design allows good adhesion to surfaces with roughness on different length scales, because setae, spatula stalks and the flexible spatula tips each compensate surface features of different size (Persson, 2003; Persson and Gorb, 2003).

This study aims to clarify the effect of surface roughness in the hairy adhesive of the green dock beetle *Gastrophysa viridula* De Geer (Coleoptera). It is still unclear how the two components of the beetle's tarsal adhesive system, claws and fibrillar adhesive (see Fig. 4.1), are affected by surface roughness, and to what extent. Previous authors have investigated the impact of a range of surface profiles, either natural (e.g. Gorb and Gorb, 2002; Gorb and Gorb, 2009) or artificial (e.g. Gorb, 2001; Peressadko and Gorb, 2004b; Stork, 1980a; Voigt et al., 2008). Force measurements in beetles and flies revealed a minimum of attachment force at small roughness

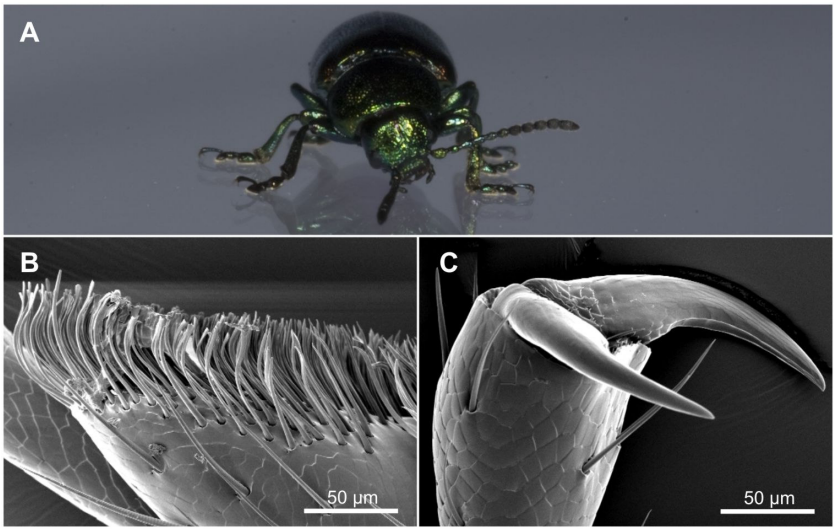

Figure 4.1: (A) The green dock beetle *Gastrophysa viridula* and scanning electron microscope detail of (B) the distal hairy adhesive pad and (C) the claws.

scales between 0.3 and 3 µm, which has been explained by the inability of the adhesive hairs to make full contact to surface features smaller than the size of their tips (Peressadko and Gorb, 2004b; Voigt et al., 2008). The higher forces on both smooth and coarse rough surfaces were interpreted by a closer contact of the adhesive hairs. A similar minimum has been reported for the adhesion of single gecko spatulae (Huber et al., 2007).

However, it is well-known that insect claws can increase the friction forces of insects for large surface asperities. The ability of claws to grip depends on the relationship between claw tip diameter and the size of asperities (Dai et al., 2002). Removal of claws in beetles resulted in a decrease of forces on rough surfaces such as plant leaves, filter paper or cloth but not on smooth glass or perspex (Betz, 2002; Stork, 1980a). However, a recent study on *L. decemlineata* leaf beetles reported that friction forces of claw-amputated beetles were smaller than those of intact beetles on most surfaces (smooth, micro-rough and coarse-rough) (Voigt et al., 2008). This result suggests that both components of the beetle's attachment system, claws and hairy pads, are similarly affected by different length scales of surface roughness. To clarify the role of adhesive hairs and claws in the insects' attachment to surfaces with small and large-scale surface roughness, friction forces on *G. viridula* were measured using similar methods as Voigt et al. (2008).

4.2 METHODS

4.2.1 Substrate preparation

In order to investigate the effect of varying roughness scale on insect attachment forces, a variety of substrates were prepared as epoxy casts (Green and Linstead, 1990). Aluminium oxide polishing paper, of varying particle size (30, 16, 12, 1, 0.5, 0.3 and 0.05 μm) (Ultra Tec, Santa Ana, CA, USA) and smooth glass cover slips were used as templates. Negatives were taken using dental impression polymer (Zhermack, Badia Polesine, Italy), and filled with 2-Ton epoxy resin cement (Devcon Corp, Danvers, MA, USA), providing rigid (modulus of elasticity > 1 GPa) surfaces of uniform material and surface chemistry. The same procedure was used to replicate the surfaces of fresh broad-leaved dock leaves (*Rumex obtusifolius*), the host plant of *G. viridula*. Surface profiles were measured using a Form Talysurf 120 stylus profiler (Taylor Hobson Ltd., Leicester, UK). 200 μm line scans (n=5 per surface) were performed of each surface allowing roughness parameters to be obtained (see Table 4.1). Due to the limitations in resolution of the profilometer used (stylus tip radius 2 μm), no roughness data was obtained for the 0.3 and 0.05 μm surfaces.

4.2.2 Whole insect centrifuge measurements

A centrifuge force testing device was used to measure adhesive forces of insects as detailed in Federle et al. (2000) (see Fig. 4.2). This method has the advantage that the insects are unconstrained and assume a natural 'attachment' position, which is essential for a meaningful assessment of the relative roles of claws and adhesive pads.

Table 4.1: Roughness parameters for the epoxy surfaces used for attachment force measurements. Amplitude parameters quoted are: R_a (arithmetic mean roughness value), RMS (root mean square) roughness and R_t (maximum profile height); the spacing parameter quoted is S_m (mean spacing of adjacent peaks at the mean line). For definitions see Gadelmawla et al. (2002). Values represent means ± s.e.m. (n=5 measurements from each surface).

Nominal asperity	Amplitude parameters			Spacing parameter
size (μm)	R_a (μm)	RMS (μm)	R_t (μm)	S_m (μm)
30	5.44 ± 0.69	6.66 ± 0.67	25.28 ± 1.47	66.08 ± 3.63
16	3.08 ± 0.25	3.75 ± 0.35	15.57 ± 1.64	60.66 ± 10.28
12	2.60 ± 0.17	3.25 ± 0.21	13.08 ± 0.64	51.93 ± 10.16
1	0.32 ± 0.02	0.40 ± 0.02	2.10 ± 0.15	19.79 ± 1.97
0.5	0.11 ± 0.01	0.13 ± 0.01	0.65 ± 0.03	17.91 ± 2.86
smooth	0.01 ± 0.00	0.01 ± 0.00	0.09 ± 0.01	20.31 ± 2.70
dock leaf	1.63 ± 0.31	1.96 ± 0.38	8.35 ± 1.87	101.97 ± 29.35

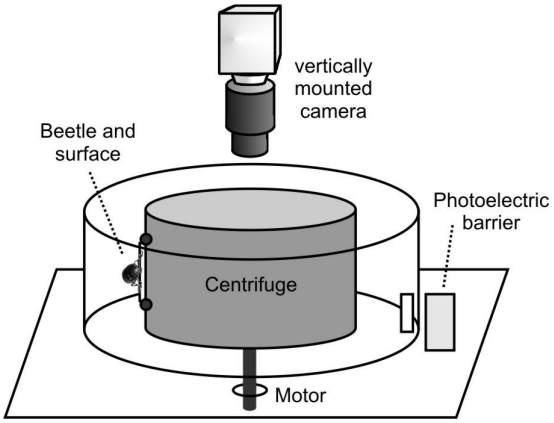

Figure 4.2: Schematic of the centrifuge force measurement set-up used.

Adult male dock beetles were taken from a laboratory colony and weighed to the nearest mg (average mass 10.93 ± 0.23 mg, mean ± s.e.m.). Forces were measured in beetles with their claws intact (n=13) or clipped (n=9 beetles). Claws were removed under a high magnification stereomicroscope using micro-scissors. Beetles were given 24 hours with a supply of dock leaves to ensure full recovery. Only the claws were removed so that the fifth tarsomere was left undamaged. The two treatment groups consisted of different beetles, avoiding any effect of order in the experiments. The dock beetles were placed on one of the epoxy substrates, mounted on the centrifuge (Fig. 4.2). Trials were only commenced when the animal had remained in place for 5 seconds. Rotation speed was slowly increased until the insect was observed to detach. The centrifuge was filmed from above with a Basler A602f camera (Basler Vision Technologies, Ahrensburg, Germany) triggered with a photoelectric barrier, so that it recorded one frame per rotation. The rotation frequency and the position of the beetle were measured from the video recording, and the beetle's force at the time of detachment was calculated. Each beetle was tested once on all surfaces (in a randomised order to control for fatigue effects). A smaller number of intact beetles only were tested on the dock leaf replica surface.

Differences in force between beetles with and without claws were analysed using independent t-tests. The dependence of attachment forces on different degrees of surface roughness was investigated using Page's L test (Page, 1963), where the indices $L_{m,n}$ indicate the number of conditions (m) and the sample size (n).

4.2.3 Morphology

To investigate basic morphological parameters for the claws of the beetle, the tarsal segments of *G. viridula* were imaged using

scanning electron microscopy (SEM). Tarsi from the rear legs of beetles were mounted on SEM stubs, sputter-coated with 20-nm thick gold and viewed with an FEI XL30-FEG (FEI, Hillsboro, OR, USA). The lengths of the claws (measured from the base to the tip) and claw tip radius were recorded using a custom MATLAB (The Mathworks, Natick, MA, USA) script.

4.3 RESULTS

4.3.1 Attachment forces of beetles

Attachment forces of intact beetles were high both on smooth and coarse rough substrates, but were minimal on surfaces with small scale roughness (0.05 – 1 μm particle size; see Fig. 4.3 and Table 4.2). For the smooth surface the safety factor (the ratio of adhesive force to body weight) was 36.2 ± 3.6. Even at the smallest particle size, forces were still high enough to support the beetle's body weight (mean safety factor 5.0 ± 1.1), although beetles did have visible difficulty attaching when initially placed on the 0.05 μm surface. For the beetles with clipped claws, a similar pattern was

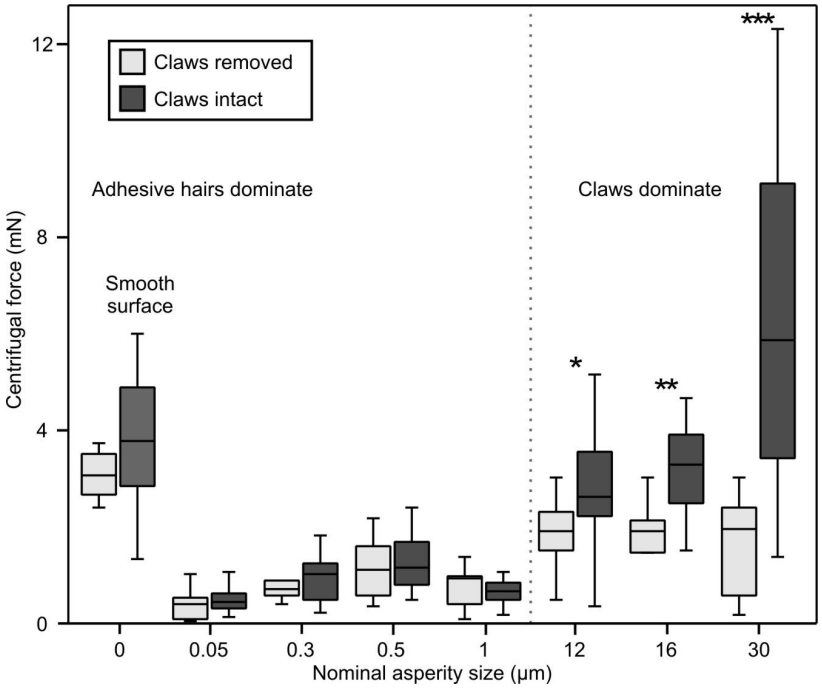

Figure 4.3: Centrifuge measurements of whole body detachment forces of male *Gastrophysa viridula* on epoxy substrates of varying roughness (*n*=13 claws intact, *n*=9 claws removed). Asperity size is approximate and corresponds to the average nominal particle size of the original polishing paper. Plot shows medians (centre lines), interquartile ranges (boxes), and the largest and smallest values (whiskers) that are not outliers (>3 standard deviations from the mean). Significance levels: * $P<0.05$, ** $P<0.01$, *** $P<0.001$, all others not significant.

Table 4.2: Summary of *t*-tests comparing attachment forces of beetles with (n=13) and without (n=9) claws on surfaces of different roughness.

Particle size (μm)	Independent samples *t*-test	
30	$t_{15.6}$=4.511	P<0.000
16	$t_{19.0}$=3.114	P=0.006
12	$t_{19.8}$=2.508	P=0.021
1	$t_{15.8}$=-0.277	P=0.785
0.5	$t_{17.9}$=0.733	P=0.473
0.3	$t_{13.6}$=-0.030	P=0.977
0.05	$t_{19.6}$=1.243	P=0.228
smooth	$t_{17.6}$=1.460	P=0.162

found, with attachment again minimal on the micro-rough substrates. On the smooth and the micro-rough (0.05 – 1 μm) substrates no significant difference in force between beetles with and without claws (Table 4.2) was found.

However, intact beetles produced significantly larger forces than clawless ones on surfaces with large scale roughness (12-30 μm particle size). Here, forces increased with particle size (Page's L-test: $L_{13,3}$ = 172, P < 0.001) and were highest for the 30-μm surface (6.10 ± 0.90 mN). Forces remained comparatively lower for beetles with claws removed, but they did increase in comparison to micro-rough surfaces (upward trend from 0.05 μm to 30 μm asperity size, $L_{9,7}$ = 1158, P < 0.01). Attachment forces on the casts of *R. obtusifolius* leaves were relatively large (3.18 ± 0.56 mN; n=4 beetles) and similar in magnitude to the smooth surface measurements.

4.3.2 Claw morphology

The morphology of the claws in *G. viridula* can be seen in Fig. 4.1C. Claw length and tip radius were measured from SEM images of beetle hind legs to allow comparison to the asperity sizes used. Claws were 110.6 ± 3.2 μm long from base to tip and had a tip radius of 1.3 ± 0.1 μm (mean ± s.e.m. calculated from eight measurements from four claws).

4.4 DISCUSSION

4.4.1 Rough surface attachment

These findings show that the beetles' adhesive hairs did not make full surface contact and produced only little adhesion at all levels of substrate roughness, but in particular on micro-rough substrates. The size of asperities on these surfaces was well below the diameter of the hair tips (~6 μm), suggesting that even with some bending (Persson and Gorb, 2003), the tip elements were unable to make full

contact. A similar reduction in adhesion for micro-rough surfaces has been noted by previous authors (Gorb, 2001; Peressadko and Gorb, 2004b; Voigt et al., 2008).

On the micro-rough surfaces, no significant difference was observed between beetles with and without claws, confirming that the claws were unable to interlock with these small asperities. This is consistent with the measured claw tip radius of 1.3 μm, as claw tips are only able to grip when their tip radius is approximately equal or smaller than the radius of surface asperities (Dai et al., 2002).

Surprisingly, these findings differ from those of Voigt et al. (2008), who investigated the effect of claw removal in potato leaf beetles and reported an overall 30% reduction in attachment forces on smooth and rough surfaces. As Voigt et al. removed the whole pretarsus, it is likely that the unguitractor tendon was cut and the claw flexor muscle lost its ability to move the tarsus (Gorb, 1996). Moreover, the relatively short recovery time allowed for the beetles (1 hour) may have generally reduced attachment performance. As the tarsus was left intact in this study and only the claws were clipped, no significant change was observed in forces on the smooth surface. This suggests that the manipulation had no damaging effects.

These results show an increase in attachment forces with increasing particle size for beetles with clipped claws, in agreement with Voigt et al. (2008). This suggests that the surface profile at these size ranges is relatively smooth on the level of the hair tip, allowing good contact for the majority of hairs through the flexibility of the fibrillar system (Autumn et al., 2006c). However, the exact nature of the roughness profile used in most studies, including this one, is not precisely defined. Quantification of roughness levels is non-trivial and it often remains unclear whether surfaces have fractal properties or possess roughness only on a limited range of length scales (Gagnepain and Roques-Carmes, 1986; Greenwood, 1992; Peressadko et al., 2005). Thus, it is not known how smooth these substrates are at length scales smaller than the quoted nominal asperity size. Further investigation using substrates of surface roughness well defined at every length scale would help to address this problem.

It is likely that as asperities become larger than the length of the setae (~50 μm) adhesion properties will be further reduced as hairs will be unable to deform enough for the whole pad to contact the substrate (see Fig. 4.4B). However, large scale asperities are likely to benefit the use of the claws. In fact, interlocking of claws with larger asperities was confirmed by these results on the coarse rough surfaces. Here the beetles with claws did reach significantly higher forces than those with claws removed and forces increased for larger asperity sizes.

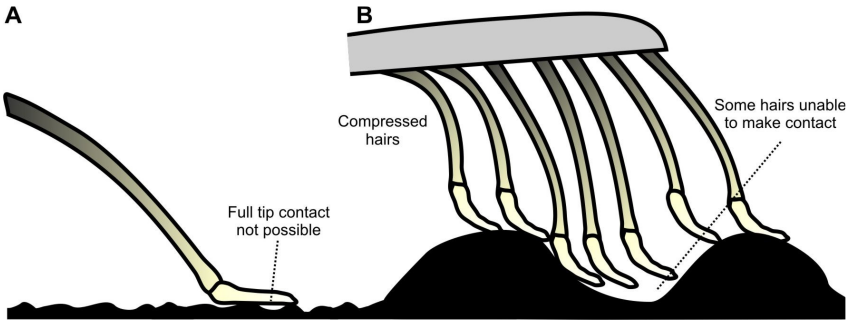

Figure 4.4: Setae in contact with either (A) small or (B) large scale surface roughness. For small surface irregularities, hair tips are unable to make full contact. For larger scale surface roughness, hairs will need to bend to allow contact.

It has been suggested that hairy systems are better adapted than smooth pads to cope with surface irregularities. A recent study on the trapping structures of the carnivorous plant genus *Nepenthes* indicates that the surface roughness of the wax crystal layer on the inner pitcher wall alone disrupts adhesion for smooth adhesive pads of stick insects (Scholz et al., 2010). Measurements on stick insects without claws have shown effects similar to the ones reported here for beetles, implying a similar susceptibility of these adhesive organs. However, direct comparisons between smooth and hairy pads (on the same rough surfaces) are needed to assess the ability of both adhesive systems to compensate surface roughness.

It is interesting to note that attachment forces on the surface replica of the beetle's host plant *R. obtusifolius* were relatively high compared to the other substrates. This suggests that the beetle's adhesive system compensates well the roughness levels found on the leaves of its host plant, despite a high average roughness R_a value (Table 4.1). This seeming contradiction highlights the need for a more detailed quantification of surface roughness profiles. The most widely quoted roughness value is the arithmetic mean roughness R_a which gives a measure for the amplitude of the asperities. However, large flat asperities still allow good contact for adhesive pads despite their relatively high profile depth. Clearly, other parameters must be taken into account to describe not only the height but also the width and spacing of asperities. Table 4.1 gives the peak spacing of the surfaces used. It can be seen that the dock leaf replica had a larger mean spacing than the 1 μm and 12 μm polishing paper replicas, explaining why the beetles' hairs were still able to adhere despite the high R_a value.

In recent years many significant advances have been made in the field of biomimetic adhesives and climbing robots. However the performance of these systems has so far been mainly tested on smooth substrates (e.g. Kim et al., 2008; Murphy and Sitti, 2007).

Whilst attempts have been made to include claw-like spines into biomimetic climbing robots (e.g. Asbeck et al., 2006; Spenko et al., 2008), a combination of adhesive and interlocking devices will be essential for a robot to be able to climb a wide variety of surfaces.

5

FIBRILLAR TARSAL ADHESIVE PADS IN THE DOCK BEETLE *GASTROPHYSA VIRIDULA*: DIVISION OF LABOUR AND SEX DIFFERENCES

Summary

Many beetles employ arrays of adhesive setae to control attachment during locomotion. It was investigated whether and how variation in seta structure, both between sexes and between tarsal pads on the same leg, determines the mechanical properties and adhesive performance of fibrillar arrays. Individual adhesive pads were vertically compressed to determine their effective elastic modulus. Distal adhesive arrays were significantly softer than middle and proximal ones. Variation in stiffness was mainly due to different seta diameters, while calculated elastic moduli of seta cuticle were relatively constant at 5-16 GPa. Consistent with their greater compliance, distal pads generated higher adhesion and friction on rough substrates. However, the greater stiffness of proximal pads conveys a superior ability to push. Proximal pads of males were less direction-dependent than distal pads and generated larger pushing forces in the distal and lateral directions. In females, proximal pads also produced higher friction forces than distal pads, but only in the lateral direction. Video recordings of vertically climbing beetles confirmed that each pad was used differently. When legs above the body centre of gravity (COG) were pulling, beetles mainly engaged the distal pads, whereas legs below the COG mainly pushed with the proximal pads. Attachment performance was additionally compared between sexes on different substrates. These findings demonstrate the presence of sex-specific specialisations of the fibrillar system as well as a division of labour between different adhesive pads on the same tarsus.

5.1 INTRODUCTION

Many insects, spiders and lizards employ a fibrillar system of adhesion, consisting of dense arrays of microscopic adhesive setae. In insects alone, hairy adhesives have evolved at least three times independently (Beutel and Gorb, 2001) and the fibrillar

morphology appears to represent a design optimised for dynamic attachment. Tarsal attachment pads not only have to adhere well on many different surface profiles but must also detach effortlessly during locomotion. Research into the fibrillar adhesive systems, both by biologists and engineers, has recently intensified, as it has become clear that they outperform conventional adhesives in several respects. For instance, they may maximise adhesion via contact splitting (Arzt et al., 2003; Jagota and Bennison, 2002), adapt to different levels of surface roughness (Chapter 4; Persson and Gorb, 2003), exhibit 'self-cleaning' properties (Chapter 3; Hansen and Autumn, 2005), and offer dynamic adhesion, easily controllable through shear forces (Chapter 2; Autumn et al., 2006a; Autumn and Hansen, 2006; Autumn et al., 2006b; Federle, 2006).

The dock beetle *Gastrophysa viridula* De Geer (Coleoptera) has been investigated as a model organism for fibrillar adhesion (Chapters 2-4; Eimüller et al., 2008; Gorb, 2001; Peressadko and Gorb, 2004b). As is common in the superfamily Chrysomeloidea, it possesses three adhesive pads on the proximal three tarsal segments of each leg. These tarsal pads are morphologically distinct, and bear setae of different designs (Betz, 2003; Stork, 1980c; Stork and Evans, 1976; Voigt et al., 2008). Distal pads mainly contain spatula-tipped hairs, whereas proximal pads bear large numbers of hairs with simple, pointed tips. Furthermore, as for many other beetles, there is a conspicuous sexual dimorphism, with male-specific discoidal setae present in all three pads (though mainly in the first, proximal pad) (Pelletier and Smilowitz, 1987; Stork, 1980a; Stork, 1980c; Voigt et al., 2008). One consequence of this morphological diversity observed in previous studies is the fact that males produce stronger attachment forces (Pelletier and Smilowitz, 1987; Stork, 1980a; Voigt et al., 2008). However, the functional implications and adaptive value of the different seta and pad designs have remained largely unclear. Is each type of pad or seta optimised for a different function?

The different morphology of setae on the three tarsal segments suggests that they are specialised for different tasks. A division of labour between different attachment pads on the same foot has recently been found in cockroaches (Clemente and Federle, 2008). Here, the pretarsal arolium (at the foot tip) is used for pulling and generating adhesive forces, whereas the tarsal euplantulae are mainly used for pushing when the foot is pressed onto the surface, i.e. in a situation where no adhesion is needed. A similar specialisation for pushing and pulling appears to be present in spiders, where tarsal and pretarsal setae are morphologically adapted for pushing and pulling, respectively (tarsal setae bear microtrichia with spatula ends on the setal surface facing in the distal direction of the leg, while microtrichia are on the opposite

side for the pretarsal claw tuft setae (Hill, 1977; Niederegger and Gorb, 2006).

However, no such obvious opposite orientation of setae appears to be present in leaf beetles. The distal adhesive pad of *G. viridula* is highly direction-dependent, with friction forces towards the body greatly exceeding those away from it (see Chapter 2). Direction-dependent attachment has also been observed in the fibrillar adhesive foot pads of geckos and flies (Autumn et al., 2006a; Autumn et al., 2000; Hill, 1977; Niederegger and Gorb, 2003), and it is an important principle enabling rapid and efficient detachment during locomotion. Whilst the rapid control of attachment and detachment by shear forces is clearly beneficial for walking and running, it has the possible adverse effect that legs are unable to push. Legs have to produce pushing forces both during walking on horizontal surfaces and during vertical climbing. It is unclear how beetles combine direction-dependent, controllable adhesion with the need to generate pushing forces and whether the different morphology of tarsal setae plays any role for this problem.

To determine whether and how the three adhesive pads of leaf beetles (both male and female) are functionally different, their stiffness as well as their adhesive and frictional performance were measured. Similar to a previous study in geckos (Autumn et al., 2006c) the spring constants and effective elastic moduli of individual pads of live beetles were quantified using loading experiments. Friction and adhesion of single pads was measured in different directions as well as on rough and smooth surfaces. The following questions were addressed: 1. Do beetle adhesive pads differ in their mechanical properties? 2. Do pads differ in their ability to adhere to smooth and rough surfaces and in their direction-dependence? 3. How are pads designed to resolve the conflict between effortless detachment and the need to generate pushing forces in the distal and lateral directions?

5.2 METHODS

5.2.1 Morphology of adhesive pads

The three adhesive pads of each sex of *G. viridula* were imaged using scanning electron microscopy (SEM). Freshly amputated legs were fixed with 4% glutaraldehyde at 4°C for 24 hours. Samples were washed with distilled water and gradually dehydrated with steps of increasing ethanol concentration before critical point drying. To enable accurate measurements of seta width and length, some hairs were removed using the sharpened point of a fractured glass pipette. By 'shaving' the left half of the pad clean of hairs, side views of the medial, sagittal plane of the array were obtained. Samples were mounted on SEM stubs, sputter coated with 20 nm

thick gold and studied with an FEI XL30-FEG (FEI, Hillsboro, OR, USA) at 2 or 5 kV.

Seta dimensions were measured from SEM images of side views of the array's medial, sagittal plane, from one beetle of each sex, using custom MATLAB (The Mathworks, Natick, MA, USA) scripts. Hairs were measured at three equally spaced points along the proximal-distal axis (in the middle of the pad and at two points 50 μm proximal and distal from it). Seta diameter was measured in the middle of the setal shaft and seta tip width measured at its widest point. Angles were measured in sagittal view relative to the horizontal plane of the pad. Lateral hair orientation was recorded in ventral view for each hair of the pad, as the absolute value of the angle relative to the proximal-distal axis. 'Pad composition' was calculated from the area of the pad occupied by one particular seta type and setal density (i.e. the number of setae per unit pad area) was obtained by manually counting the total number of hairs.

5.2.2 General set-up

G. viridula beetles were taken from laboratory colonies and weighed (body mass, males: 10.8 ± 0.3 mg, females: 19.7 ± 1.9 mg, means ± s.e.m.). As the material properties of arthropod cuticle are highly dependant on hydration (Vincent and Wegst, 2004) and excised tarsi rapidly lose adhesion (Jiao et al., 2000), all experiments were performed with live insects. Beetles were mounted on a glass cylinder using blu-tack and parafilm tape as described in Chapter 2. The blu-tack (Bostik, Leicester, UK) was used to fix one rear leg, isolating it and allowing the forces to be measured from each individual foot pad. This was achieved by aligning the pad parallel to the test substrate attached to the end of the force transducer (see Fig. 5.1). Additional blu-tack was used to restrain the tarsus to prevent contact from neighbouring pads or claws.

The experimental set-up allowed the measurement of single-pad adhesion and shear forces, as well as a simultaneous recording of contact area (Chapter 2; Fig. 5.1). Forces were measured using a 2D strain gage force transducer fixed to a 3D motor positioning stage M-126PD (Physik Instrumente, Karlsruhe, Germany). The motors were controlled with a custom LabVIEW (National Instruments, Austin, TX, USA) program which included a feedback mechanism allowing normal force to be kept constant. Voltage output was amplified (ME-Meßsysteme, Henningsdorf, Germany) and sampled at 1000 Hz with an I/O board PCI-6035E (National Instruments). Foot pad forces were measured whilst in contact with a glass plate or other substrates (see below), attached to the transducer. On glass, 'maximal setal' contact area (the total real contact area of the hairs) was visualised with a coaxially-illuminated stereomicroscope (Federle et al., 2002b). Images were

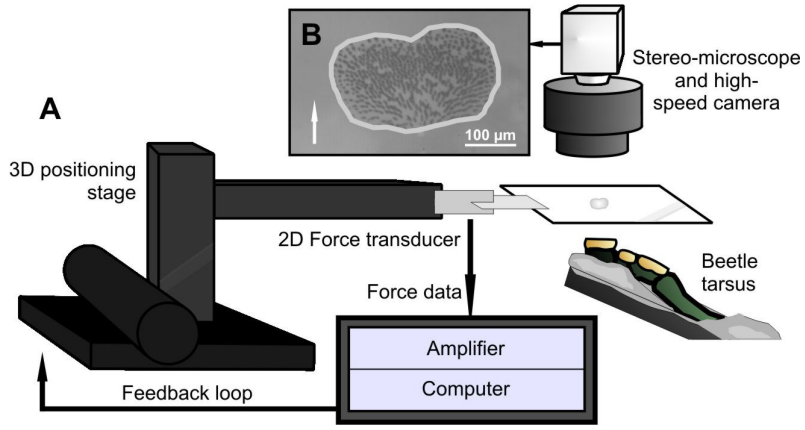

Figure 5.1: (A) Experimental set-up for measuring single-pad friction, adhesion and contact area. (B) Contact area image. Arrow indicates the distal direction of the pad; the line polygon marks the projected contact area.

recorded using a HotShot PCI 1280 B/W camera (NAC image technology, Simi Valley, CA, USA) and were analysed in MATLAB. A 'projected' pad area was also measured by manually drawing a polygon around the contact zone of the whole array, allowing values to be normalised for total pad area (Fig. 5.1).

5.2.3 Pad spring constant and effective elastic modulus

In order to quantify the stiffness and effective elastic modulus of the adhesive pads of *G. viridula*, force-distance curves were recorded for small-strain compressions of each fibrillar pad. The glass plate of the force transducer was lowered into contact with each mounted pad for 10 seconds with a normal force feedback of 1.0 mN. The force feedback was then set to zero for 10 seconds, reducing the load so that the hairs were no longer compressed, but still in contact. The motor position in this situation was defined as the zero point for the displacement. The motors then compressed the pad by distances of 20 or 50 µm at a constant speed of 0.5 μms^{-1}. To test for the presence of viscoelastic behaviour of the setal array, pads were left in compression for 2 minutes, and then the plate was withdrawn at the same velocity. A self-built force transducer consisting of two cut plates of carbon-manganese steel joined at right angles to form a 2D bending beam was used. Two mounted full bridges of 420 Ω semiconductor strain gauges (Micron Instruments, Simi Valley, CA, USA) allowed force measurement (see Fig. 5.2), calibrated as a function of lever arm length by applying milligram weights and defined displacements. The beam's spring constant (at the position where measurements were taken) of 452 Nm^{-1} was significantly higher than those obtained for each array (estimated from preliminary experiments) allowing small displacements of the fibrillar arrays to be investigated. Force-

distance curves were recorded for all three pads of *G. viridula* hind legs (*n*=10 males, *n*=3 females). The projected contact area of the pad was simultaneously measured throughout the experiments to monitor the adhesive contact and to allow the spring constant to be normalised for area giving the effective elastic modulus. Force data were filtered with a lowpass second-order Butterworth filter with sample frequency 100 Hz and cut-off frequency 0.25 Hz.

The recorded force-distance curves represent the behaviour of a system of springs in series, consisting of the force transducer, the setal array, the beetle's tarsal segment and the blu-tack mounting material. The blu-tack mount in this experiment behaved effectively as an incompressible solid so that its contribution could be safely neglected. This was confirmed with control tests where the above movement pattern was repeated with a small piece of

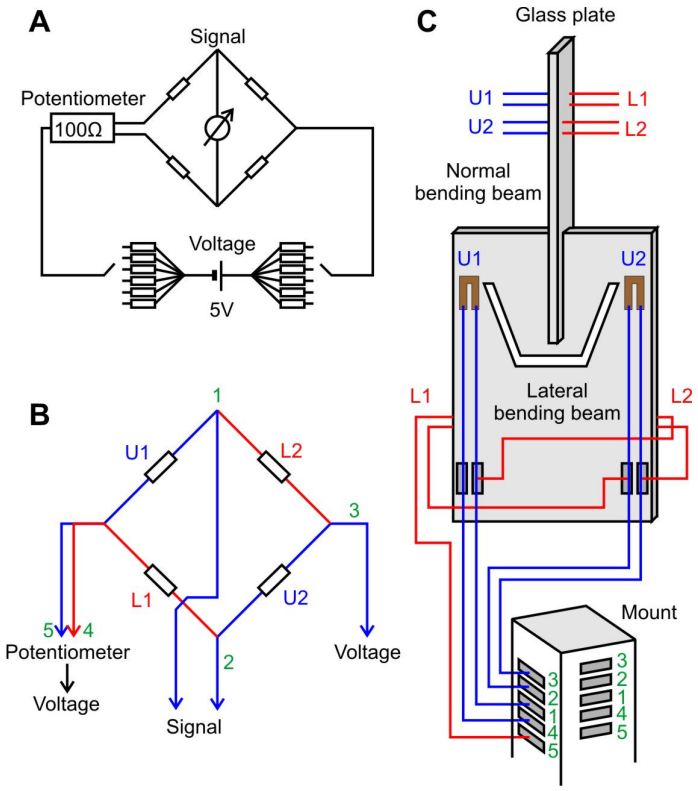

Figure 5.2: the set-up for the self-built 2D strain gauge force sensor showing the complete circuit diagram (A), bending beam wiring layout (B) and resulting physical set up. In A, the 100 Ω potentiometer allows the Wheatstone bridge to be balanced whereas the multiple resistors (of 0, 330, 510, 1000, 2000 and 4700 Ω respectively) allow the sensitivity to be adjusted. B shows the comparison between the circuit diagram and physical set-up, the numbers 1-5 corresponding to soldering terminals on the bending beam. U (1 and 2) and L (1 and 2) denote the strain gauges on the upper and lower sides of the beam. An identical full bridge set-up makes up the normal channel. C shows the positioning of the wiring and of the stain gauge sensors. Neither the potentiometer nor the multiple resistors are illustrated in C.

glass in place of the beetle pad (the glass piece had approximately the same dimensions as the beetle tarsus, and was mounted in the same way). This showed a very high spring constant of approximately 4500 N/m for motor compressions of the blu-tack bed. Blu-tack may exhibit some creep (Comyn, 1997) but this effect was found to be negligible within the range of normal forces in this experiment. The regression slope of the 20 μm compression experiments was used to measure the total spring constant k_{total}, from which the spring constant k_{pad} of each beetle pad was calculated:

$$k_{pad} = \frac{k_{beam} k_{total}}{k_{beam} - k_{total}} \qquad [5.1]$$

The effective elastic modulus of the setal array was calculated as:

$$E_{eff} = \frac{k_{pad} h}{A} \qquad [5.2]$$

where E_{eff} is the effective elastic modulus, k_{pad} the calculated spring constant, A the projected pad contact area and h the height of the array.

Two methods were used to model the bending-beam behaviour of the hairs; the full elastica cantilever model (Frisch-Fay, 1962) and the linear, small-strain cantilever model. From the equations presented in Autumn et al. (2006c) for the elastica model, the force vs. displacement relationship for an oblique, cylindrical bending beam with radius r, length l, elastic modulus E and a range of angles θ to the horizontal was calculated. This was compared with the small-strain cantilever model, which (ignoring compression along the beam) predicts perpendicular displacement δ to be (Glassmaker et al., 2004; Persson, 2003; Sitti and Fearing, 2003):

$$\delta = \frac{4 l^3 F \cos^2 \theta}{3 \pi r^4 E} \qquad [5.3]$$

where F is the normal force per seta.

The elastic modulus of the seta cuticle from the measured force-displacement relationships for a ~20 μm compression of the different beetle pads and the dimensions of the setae was estimated. Values were initially calculated from the small-strain cantilever model (Equation 5.3). As the strain was too large to be described satisfactorily by the small-strain model, correction factors were calculated from a linear regression to the first 20 μm of the full elastica model for the measured seta angle in each case.

5.2.4 Friction performance and direction-dependence

To investigate the direction-dependence of attachment for all three pads of both sexes, shear movements were performed on a glass surface in the pulling, pushing and lateral directions. Pulling slides (corresponding to a movement of the leg towards the body) were performed at 500 μms^{-1} over 10 mm with the force feedback employed to keep the load constant at 0.1 mN during the slide (n=5 beetles of each sex). Pushing slides (corresponding to a distal push of the leg away from the body) were additionally preceded by a short, 0.5 mm pulling movement to ensure proper contact of the hairs (n=5, both sexes). To investigate the effect of hair orientation, lateral (transverse) slides were performed as for the pull-push slides but with the pad rotated by first 90° and then 270° (n=2 beetles of each sex). At the end of every slide a 5 s pause was left before performing a 500 μms^{-1} perpendicular pull-off to measure adhesion forces.

To test the attachment performance on a rough surface, pulling and pushing slides were performed (n=5 further beetles of each sex) on aluminium oxide polishing paper of 1 μm nominal asperity size (Ultra Tec, Santa Ana, CA, USA) glued to the glass coverslip on the force transducer. This particle size is smaller than the tips of the hairs, leading to reduced adhesive and frictional contact with the surface as shown in previous studies (Chapter 4; Peressadko and Gorb, 2004b; Voigt et al., 2008). The rough substrate prevented any recording of contact area. To estimate stresses, the mean values of maximal setal contact area recorded on glass were used. All slides were performed on a clean area of the substrate, and thus correspond to the 'little secretion' regime as described in Chapter 2. Sliding experiments were performed using a force transducer with a spring constant of 50 Nm^{-1}, equipped with 350 Ω foil strain gauges 1-LY13-3/350 (Vishay, Malvern, PA, USA).

5.2.5 Friction forces on female elytra

In addition to the slides recorded on smooth glass, friction and adhesion were measured for the proximal pads of male and female beetles on the smooth wing case of a female beetle (n=6 beetles of each sex). Wing cases were detached from freshly dead female beetles and glued to a cover slip attached to the force transducer. Pulling slides and pull-offs were performed as above although sliding velocity and distance were restricted to only 100 μms^{-1} and 0.5 mm due to the limited length of the elytra. Pulling slides were performed in both directions along the length of the wing case so as to control for any directionality or anisotropy of the elytra surface, and two repeats were taken for every slide. As for the rough surface slides, simultaneous area recordings could not be taken.

5.2.6 Locomotion recordings

In order to link these results on the function and performance of individual foot pads with whole insect locomotory behaviour, video recordings were taken of climbing beetles. Male and female beetles running up and down a smooth vertical surface were filmed in side view (n=16 runs from 6 beetles, with 145 steps analysed) with the HotShot high-speed camera. The stance phase of each step (from front and rear legs) was analysed by recording the amount of time each pad (distal or proximal) remained in surface contact as a percentage of the total stance time. This 'relative pad contact time' provided a measure of how the pads are used during climbing.

5.3 RESULTS

5.3.1 Morphology of adhesive pads and setae

The tarsus of *G. viridula* consists of five segments and a distal pretarsus with the claws. The fourth segment is reduced and obscured by the third tarsomere. The proximal three tarsomeres bear on their ventral side adhesive pads, and are referred to as

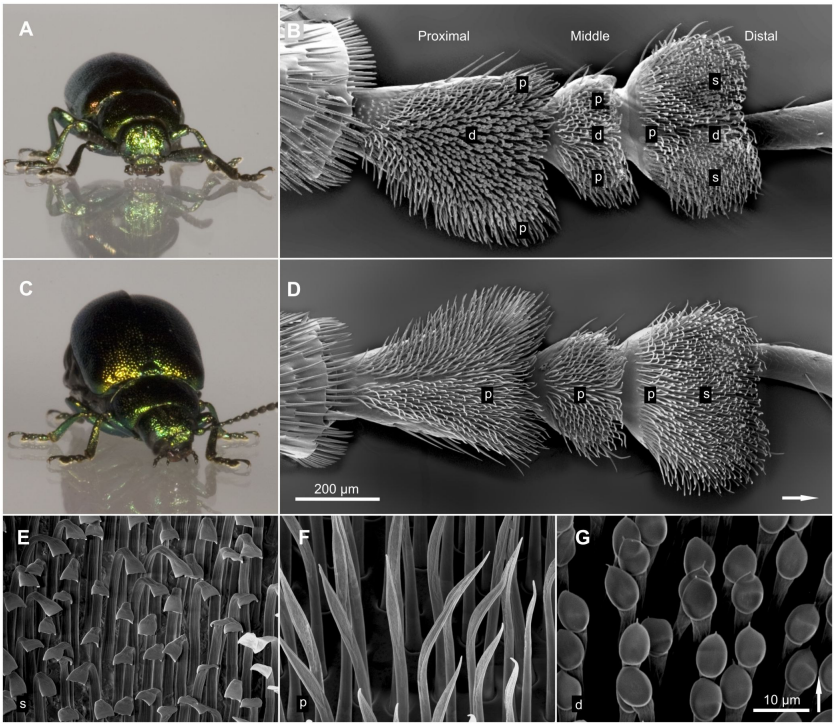

Figure 5.3: Male (A,B) and female (C,D) dock beetles (*Gastrophysa viridula*) and the attachment pads on their hind leg tarsus. E-G types of setae: spatula-tipped (E), pointed (F) and male-specific discoidal (G). Letters indicate hair type: s, spatula-tipped; p, pointed; d, discoidal. Arrows indicate distal direction. B,D and E,F,G respectively are of the same scale and orientation.

'proximal', 'middle' and 'distal' in this study. These pads are fibrillar arrays consisting of different seta types: a) spatula-tipped hairs, present on the distal-most tarsomere of both sexes, b) disk-tipped (discoidal) hairs, present on all pads of the male beetles only, and c) hairs with flattened and pointed tips, present in all pads (Fig. 5.3).

The distal-most pads of both sexes primarily contain thin, distally-oriented spatula-tipped hairs, with a small number of pointed hairs around the edges. The males additionally have a cluster of discoidal hairs in the centre of the pad. The small middle pads are populated by pointed hairs which point distally and laterally. A small number of discoidal hairs also exist on the middle pads of males. In the proximal pads there is the greatest sexual dimorphism. The female proximal pads are similar to the middle pads with pointed hairs that are oriented distally and laterally. The male pads however bear a large continuous field of discoidal hairs, fringed on the edges with pointed hairs (Fig. 5.3). In all pads, the hair tips form almost a perfect (horizontal) plane, meaning that hairs are slightly longer where the underlying pad cuticle curves away from the surface (Fig. 5.4). Array height was approximately 40 μm across all pads of both sexes, with the exception of male proximal pads, where the discoidal setae in the centre of the pad are considerably shorter and form a second plane set-in by ~15 μm from the longer pointed setae (see side sections Fig. 5.4).

From the side view images, both the pointed and the spatulate hairs appear to have a non-adhesive default position,

Table 5.1: Morphological properties of the three tarsal adhesive pads in *Gastrophysa viridula.* Seta dimensions and angles given as mean ± s.e.m. (*n*=3), measurements taken from one beetle of each sex.

			seta properties (μm)			seta angle to
Sex	Pad		array height	hair diameter	max. tip width	horizontal (°)
Male	Distal	spatula	37.5 ± 1.1	1.4 ± 0.1	4.1 ± 0.4	49.7 ± 2.1
	Middle	pointed	38.6 ± 0.8	2.2 ± 0.2	2.2 ± 0.3	45.3 ± 3.6
	Proximal	pointed	39.8 ± 1.4	2.2 ± 0.1	2.7 ± 0.2	53.6 ± 4.6
		discoidal	25.7 ± 0.3	2.3 ± 0.1	6.0 ± 0.6	58.3 ± 1.0
Female	Distal	spatula	38.1 ± 1.6	1.5 ± 0.0	3.8 ± 0.3	57.0 ± 2.4
	Middle	pointed	42.2 ± 2.5	2.2 ± 0.1	2.5 ± 0.1	54.8 ± 1.7
	Proximal	pointed	40.4 ± 0.4	2.6 ± 0.2	2.7 ± 0.2	52.9 ± 0.5

		approx. number of setae		pad composition by seta type			lateral seta orientation
Sex	Pad	total	density (mm^{-2})	spatula	pointed	discoidal	deviation (°) from proximal-distal axis
Male	Distal	550	8500	77.60%	10.30%	12.10%	8.2 ± 0.5
	Middle	200	7500	0%	95.80%	4.20%	45.0 ± 3.3
	Proximal	700	8000	0%	41.20%	58.80%	22.4 ± 1.3
Female	Distal	650	9500	83.80%	16.20%	0%	12.2 ± 0.7
	Middle	150	5500	0%	100%	0%	46.5 ± 1.5
	Proximal	300	4500	0%	100%	0%	52.2 ± 1.2

with the seta tip contact zones oriented not only perpendicularly to the surface but even slightly away from it, so that the setal surface facing in the distal direction of the leg points towards the surface. This would imply that these hairs cannot be brought into contact with a simple perpendicular approach and that a small proximal shear (pull) should be needed (as observed for gecko setae (Autumn and Hansen, 2006)). However, contact area imaging during the elastic modulus recordings showed that good contact was made by all hairs during a purely vertical compression. Hence, the extreme tip positions seen here may partly result from drying or preparation artefacts. By contrast, the tips of the discoidal hairs were aligned perfectly parallel with the substrate, suggesting that their default position is adhesive.

Spatula-tipped hairs (found on the distal pads of both sexes) were distinctly thinner (stalk diameter 1.4 to 1.5 μm) than middle and proximal pad hairs (diameters 2.2 to 2.6 μm). Measurements of mean lateral hair orientation (the absolute value of the angle relative to the proximal-distal axis of the pad in ventral view) showed that distal pads have hairs pointing mainly in the distal direction, whereas the middle pads of both sexes and the proximal pads of females have more laterally oriented hairs. The proximal pads of males are intermediate in this respect. Measurements of pad and seta properties are summarised in Table 5.1.

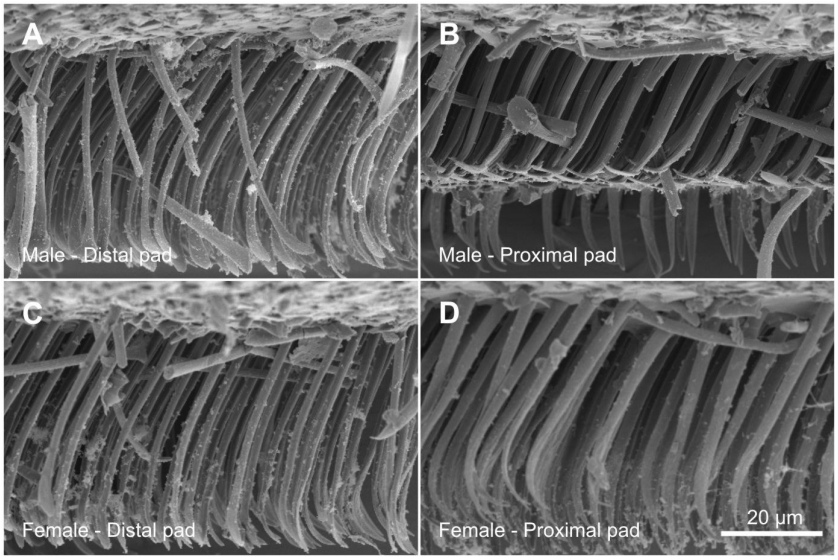

Figure 5.4: Side views of adhesive pads in *Gastrophysa viridula.* A, male distal pad; B, male proximal pad; C, female distal pad; D, female proximal pad. Half the setae of the pad were shaved off to image setae in the medial plane of the pad. Note (in B) the two different planes formed by seta tips in the proximal pad of the male beetle (discoidal setae shorter and pointed setae longer). The spatula-tipped setae of the distal pads (A,C) are visibly thinner than the discoidal and pointed setae on the other pads.

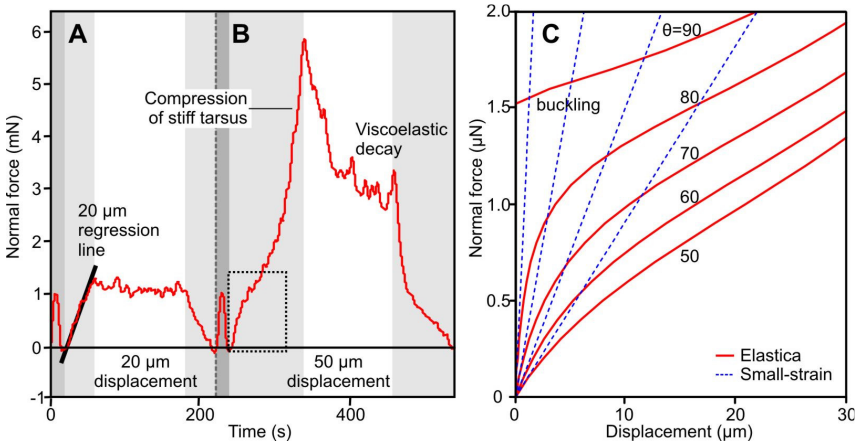

Figure 5.5: Example force trace showing the compression of a distal adhesive pad of a female *Gastrophysa viridula* beetle for 20 µm (A) and 50 µm (B) motor displacement. The slope of the regression line was used to calculate the spring constant of the setal array. Dark grey areas indicate the initial 1.0 mN loading and feedback mechanism for reaching the zero point, light grey the compression, and white the 2 minute pause before retraction. Viscoelastic decay is clearly visible in the 50 µm compression experiment. (C) Force-displacement relationship of a cylindrical cantilever beam with length 50 µm, radius 1 µm, and elastic modulus 2 GPa, as predicted by the full elastica model (red) and small-strain model (blue) plotted for different angles. The shape of the initial part of the force-displacement curve (dashed box in B) was well predicted by the full elastica model, using the observed seta angles of between 40° and 60° (see Table 5.1).

5.3.2 Pad spring constant and effective elastic modulus

To determine the material properties of the adhesive pads of *G. viridula*, perpendicular compressions of the fibrillar arrays were performed whilst simultaneously recording normal force and contact area. Two different compression depths were achieved with motor movements of 20 µm and 50 µm amplitude, resulting in actual seta tip displacements of 17.0 ± 0.3 and 42.3 ± 0.7 µm (mean ± s.e.m.). An example force trace is plotted in Fig. 5.5A,B. The large depth (50 µm, on the scale of the total array height) was chosen to characterise the compression behaviour of the system. The short depth (20 µm) was used to measure the array spring constant and effective elastic modulus.

During the 50 µm compression, forces increased non-linearly; with the slope initially decreasing (at ~15 µm) and then strongly increasing towards the end of the compression (see Fig. 5.5B). The initial decrease of the force-displacement slope may be explained by the similarly nonlinear shape exhibited by the full elastica cantilever model (Frisch-Fay, 1962) (see Fig. 5.5C). As the depth of the 50 µm compression exceeded the initial height of the setal array (approx. 40 µm), the setae will in this situation be pressed against the underlying tarsal cuticle, leading to a strong

increase of the apparent stiffness. This was visible by the steep increase of forces when the motor displacement exceeded ~30 μm. Only a moderate decay of force (by 32.4 ± 2.1% mean ± s.e.m.) was observed during the 2 minute pause after the 20 μm motor compression. This indicates that beetle setae deformed largely elastically. Viscoelastic creep would be recognised by a decrease of the force over time as previously demonstrated for the smooth adhesive pads of bushcrickets (Gorb et al., 2000). The large force decay observed after the 50 μm motor compression suggests that in this situation, deformation occurred in another component of the system that exhibits creep. The most likely explanation of this result is that the tarsus itself deforms viscoelastically.

From the results of the 20 μm compression, a first estimate of the elastic modulus of the seta cuticle was calculated using the small-strain cantilever model. From Equation 5.3, the elastic modulus of a cylindrical hair of length 50 μm, radius 1 μm, angle 50° and spring constant 0.1 Nm^{-1} is estimated to be 2.27 GPa. Taking into account that for large strains, setae are less stiff than predicted by the small-strain model, these results were corrected with a factor derived from a linear regression of the first 20 μm compression of the full elastica prediction (Fig. 5.5C). Corrected cuticle elastic modulus values calculated for each pad are presented in Table 5.2; they varied only slightly between 5.2 and 16.1 GPa.

For both sexes, the spring constants of the proximal pads were significantly higher than those of the distal and middle pads (male; repeated measures ANOVA: F_2=36.492, P<0.001, Bonferroni-corrected paired t-tests for proximal vs. distal: t_9=-7.332, P<0.001 and proximal vs. middle: t_9=-6.185, P<0.001) (see Table 5.2 and Fig. 5.6A). Unlike hemispherical smooth pads that increase contact area when pressed against a surface (Drechsler and Federle, 2006;

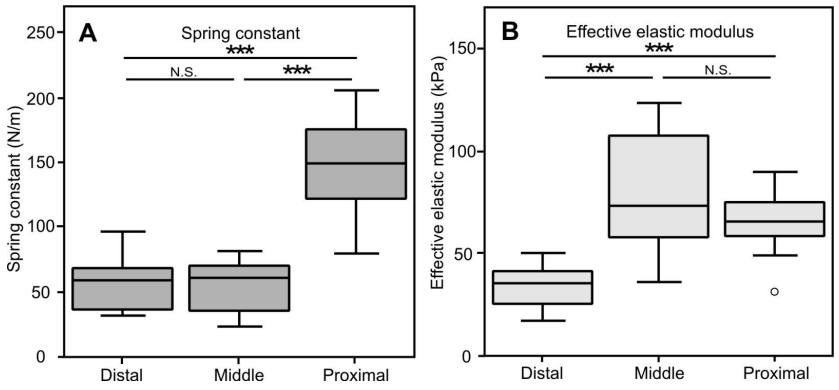

Figure 5.6: Spring constant (A) and effective elastic modulus (B) data for all three pads of male beetles (n=10). Plot shows medians (centre lines), interquartile ranges (boxes), and the largest and smallest values (whiskers) that are not outliers (>3 standard deviations from the mean) (circles). Significance levels: * P<0.05, ** P<0.01, *** P<0.001, N.S. not significant.

Table 5.2: Spring constant, projected contact area and elastic modulus for proximal, middle and distal pads of male and female *Gastrophysa viridula* beetles. Measured values given as means ± s.e.m..

Sex:	Male (n=10)			Female (n=3)		
Pad:	Distal	Middle	Proximal	Distal	Middle	Proximal
Spring constant (Nm^{-1})	57.1 ± 6.4	53.7 ± 6.7	145.4 ± 12.7	82.1 ± 7.0	55.3 ± 5.6	150 ± 11.9
Projected contact area (μm^2)	65277 ± 2802	26121 ± 1737	87856 ± 2169	66016 ± 2512	27027 ± 956	69692 ± 4876
Effective elastic modulus (kPa)	34.2 ± 3.2	81.1 ± 9.5	65.1 ± 5.4	53.6 ± 6.1	88 ± 10.5	92.3 ± 5.5
Estimated cuticle modulus (GPa)	16.14	10.42	5.24	10.46	11.39	8.3

Gorb et al., 2000), the beetle's planar fibrillar array showed little or no change in projected contact area during compression. Thus, a constant area was used for the calculation of the array's effective elastic modulus. The effective elastic modulus of the proximal pads was still approximately twice as high as that of the distal pads. The smaller middle pads also had a high effective elastic modulus, significantly higher than that of the distal pads (repeated measures ANOVA: F_2=14.176, P<0.001; Bonferroni corrected paired t-test: proximal vs. distal, t_9=-5.803, P<0.001; middle vs. distal t_9=-4.929, P<0.001) (see Table 5.2 and Fig. 5.6B).

5.3.3 Friction performance and direction-dependence

To quantify the frictional and adhesive performance of the pads of male and female beetles, friction slides were performed on smooth and rough substrates, both along the leg and in the lateral direction. The results are summarised in Fig. 5.7 and Tables 5.3 to 5.5.

Smooth surface

Comparing between sexes, male beetles produced higher forces than females for friction slides on the smooth surface. This was most pronounced for pulls of proximal pads where males generated a 2.3 times greater friction than females (difference highly significant, see Table 5.3). Comparing between pads, the pulling forces of the (larger) proximal pads were similar to those of the distal pads, and in the case of the males, significantly larger (see Table 5.3 and Fig. 5.7). Steady sliding was observed, and no stick-slip behaviour as has been proposed for the sliding of individual gecko spatulae (Yamaguchi et al., 2009).

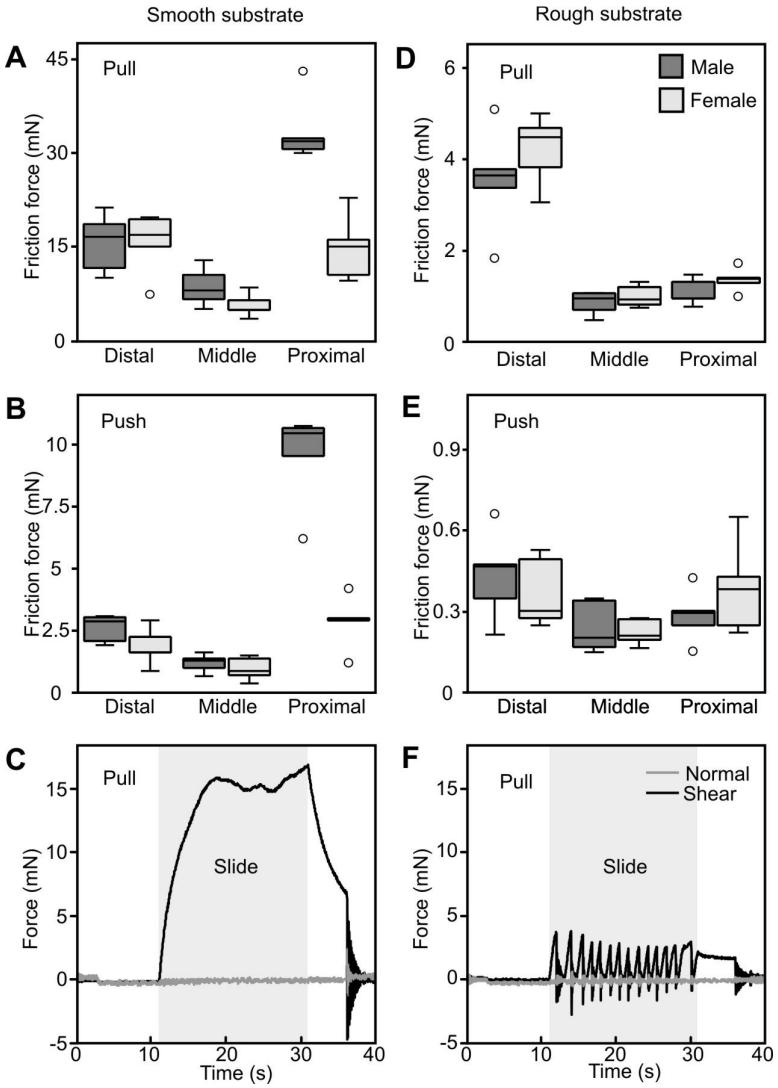

Figure 5.7: Friction force measurements of *Gastrophysa viridula* on smooth glass (A-C) and a rough, 1 μm grain polishing paper substrate (D-F). Values correspond to the peak force occurring during a 10 mm, 0.5 mms^{-1} pulling (A,D) or pushing slide (B,E). *n*=5. Plot shows medians (centre lines), interquartile ranges (boxes), and the largest and smallest values (whiskers) that are not outliers (>3 standard deviations from the mean) (circles). (C) and (F) show typical raw data curves for a pull of the distal pad of a female beetle on smooth (C) and rough (F) substrates. Shear (black) and normal (grey) forces are plotted. The grey area indicates the 10 mm slide (0.1 mN normal force feedback), followed by a 5 s pause and 500 μms^{-1} perpendicular pull-off, as described in the methods.

Rough surface

Presumably due to a lower real contact area, forces were much lower than on the smooth substrate (see Chapter 4). This is consistent with findings from other studies comparing the effect of rough and smooth substrates on a fibrillar system (Voigt et al., 2008). An unsteady, macroscopic 'stick-slip' movement was

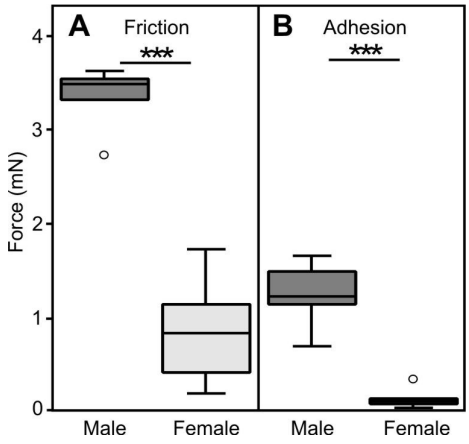

Figure 5.8: Pulling slides (0.5 mm at 100 μms^{-1}) of the proximal pads on a detached female elytra case. The comparison between males and females is presented for both friction forces (A) and adhesive forces (B). *n*=6. Plot shows medians (centre lines), interquartile ranges (boxes), and the largest and smallest values (whiskers) that are not outliers (>3 standard deviations from the mean) (circles). Significance levels: * P<0.05, ** P<0.01, *** P<0.001.

observed, contrary to the steady sliding on the smooth substrate. On the rough surface, males no longer generated significantly higher forces, and females even produced significantly greater shear stress during pulls (Table 5.3 and Fig. 5.7). Contrary to the smooth surface results, distal pads produced much higher forces than proximal pads (pulling friction: 3.5 fold in males, 3.1 fold in females; adhesion: 3.5 fold in males, 5.8 fold in females). Forces were higher despite the generally smaller size of distal pads, translating to an even larger difference in shear stress.

Friction forces on female elytra

The proximal pads of male and female beetles were tested on the fixed surface of the female wing case. No anisotropy of the elytra surface was found and no significant difference was seen for pulling slides up or down the elytra in either males or females (male: friction t_5=-1.618, P = 0.166, adhesion t_5=-1.952, P = 0.108, female: friction t_5=0.108, P = 0.918, adhesion t_5=0.513, P = 0.630, paired *t*-tests). Therefore data for pulling slides was pooled to test for significance between sexes. As for the smooth surfaces, the slides on the elytra gave much greater forces in the males than in the females (friction 3.9, adhesion 9.5 times greater; see Fig. 5.8). Sex differences were highly significant (friction: $t_{8.2}$=9.65, P<0.001; adhesion: $t_{7.8}$=6.00, P<0.001, unpaired *t*-tests). Due to the shorter amplitude and smaller velocity, the forces on the elytra could not be directly compared with those measured on the other surfaces.

Table 5.3: Friction force (mN) and shear stress (kPa) for all pads of male and female beetles (*n*=5 in all cases). On the rough surface, contact area could not be measured therefore shear stress was calculated using the mean maximal setal contact area of the same pad on glass. Values given as means ± s.e.m..

Friction		Sex:	Male			Female		
		Pad:	Distal	Middle	Proximal	Distal	Middle	Proximal
Smooth surface	pull	force	15.54 ± 2.10	8.50 ± 1.38	33.55 ± 2.42	15.60 ± 2.26	5.52 ± 0.85	14.76 ± 2.35
		stress	642 ± 99	1088 ± 219	1093 ± 68	613 ± 111	761 ± 150	747 ± 114
	push	force	2.58 ± 0.25	1.18 ± 0.16	9.51 ± 0.85	1.84 ± 0.34	0.95 ± 0.21	2.84 ± 0.48
		stress	203 ± 18	535 ± 172	585 ± 92	144 ± 38	413 ± 162	589 ± 177
Rough surface	pull	force	3.80 ± 0.52	0.90 ± 0.12	1.08 ± 0.13	4.29 ± 0.35	0.99 ± 0.11	1.38 ± 0.12
		stress	143 ± 21	105 ± 14	36 ± 4	157 ± 13	122 ± 14	68 ± 6
	push	force	0.43 ± 0.07	0.24 ± 0.04	0.29 ± 0.04	0.37 ± 0.06	0.22 ± 0.02	0.39 ± 0.08
		stress	26 ± 4	57 ± 10	14 ± 2	21 ± 3	62 ± 6	46 ± 9

Table 5.4: Adhesion (mN) and adhesive stress (kPa) for all pads of male and female beetles (*n*=5 in all cases) (data corresponding to friction values presented in Table 5.3). Again, for the rough surface, area was estimated using the mean maximal setal contact area on glass. Values given as means ± s.e.m..

Adhesion		Sex:	Male			Female		
		Pad:	Distal	Middle	Proximal	Distal	Middle	Proximal
Smooth surface	pull	force	2.25 ± 0.66	0.52 ± 0.14	4.24 ± 0.34	1.30 ± 0.31	0.29 ± 0.10	1.01 ± 0.34
		stress	100 ± 27	68 ± 18	142 ± 11	53 ± 10	53 ± 21	55 ± 18
	push	force	0.22 ± 0.07	0.30 ± 0.13	0.37 ± 0.19	0.19 ± 0.07	0.14 ± 0.07	0.14 ± 0.06
		stress	33 ± 12	47 ± 20	27 ± 9	19 ± 5	57 ± 18	32 ± 12
Rough surface	pull	force	0.49 ± 0.17	0.14 ± 0.04	0.13 ± 0.02	0.69 ± 0.10	0.09 ± 0.03	0.12 ± 0.04
		stress	20 ± 7	18 ± 5	4 ± 1	26 ± 4	11 ± 3	6 ± 2
	push	force	0.13 ± 0.02	0.11 ± 0.03	0.11 ± 0.03	0.10 ± 0.03	0.10 ± 0.03	0.09 ± 0.04
		stress	8 ± 1	26 ± 6	5 ± 1	6 ± 1	27 ± 8	11 ± 4

Direction-dependence of forces

Pulls, pushes and lateral slides were used to investigate the direction-dependence of the pads. Pulling and pushing slides in the distal pads of male *G. viridula* beetles have been previously recorded (see Chapter 2) and this is extended in the present study to include all three pads of both sexes. A strong direction-dependence was found for all pads of the beetles in all conditions

Table 5.5: Statistics comparing pulls of proximal and distal pads (for males and females), male and female beetles (for proximal pads only, as no significant differences are found between sexes for distal pads) and pulls and pushes.

			Smooth		Rough	
Proximal vs. distal pads (paired t-test)	Males	friction slides	t_4=-4.753	P=0.009	t_4=4.897	P=0.008
		shear stress	t_4=-3.939	P=0.017	t_4=5.317	P=0.006
		adhesion	t_4=-2.719	P=0.053	t_4=2.132	P=0.100
		adhesive stress	t_4=-1.599	P=0.185	t_4=2.272	P=0.086
	Females	friction slides	t_4=0.283	P=0.791	t_4=8.746	P<0.001
		shear stress	t_4=-2.400	P=0.074	t_4=7.385	P=0.002
		adhesion	t_4=0.733	P=0.504	t_4=6.437	P=0.003
		adhesive stress	t_4=-0.123	P=0.908	t_4=6.220	P=0.003
Males vs. females proximal pads (unpaired t-test)		friction slides	$t_{8.0}$=5.575	P<0.001	$t_{7.9}$=-1.542	P=0.162
		shear stress	$t_{6.5}$=2.613	P=0.037	$t_{7.3}$=-4.470	P=0.003
		adhesion	$t_{8.0}$=6.725	P<0.001	$t_{5.6}$=0.030	P=0.977
		adhesive stress	$t_{6.5}$=4.131	P=0.005	$t_{4.7}$=-1.145	P=0.307

		Males					
	pad:	Distal		Middle		Proximal	
Pushing vs. pulling friction force (paired t-test)	smooth	t_4=6.163	P=0.004	t_4=5.280	P=0.006	t_4=10.084	P<0.001
	rough	t_4=5.598	P=0.005	t_4=4.313	P=0.013	t_4=5.763	P=0.004
		Females					
	pad:	Distal		Middle		Proximal	
	smooth	t_4=6.717	P=0.003	t_4=6.288	P=0.003	t_4=5.142	P=0.007
	rough	t_4=10.646	P<0.001	t_4=6.505	P=0.003	t_4=8.689	P<0.001

(see Tables 5.3-5.5 and Fig. 5.7). However, it is important to note that for the proximal pads in males, this direction-dependence was weaker and relatively high forces were observed for pushing on a smooth surface. The higher stability of proximal pads in non-pulling directions was confirmed by lateral (transverse) slides (on the smooth surface, two beetles of each sex tested for all three pads), indicating stability in multiple directions. Proximal pads of both sexes appeared to support higher lateral friction (mean ± s.e.m., male, 11.85 ± 2.73 mN; female, 6.50 ± 1.18 mN) than the other pads, but forces were low (as for pushes) for the distal pads (males, 4.44 ± 0.61 mN; females, 2.00 ± 0.38 mN).

5.3.4 Use of adhesive pads during vertical climbing

The use of the three tarsal adhesive pads was investigated by filming male beetles climbing up a vertical smooth substrate. In most steps (n=43) all three segments appeared to be in contact with the surface. However the selective usage of proximal and distal adhesive pads was visible when pads did not remain in contact for the whole duration of the stance phase of the step (Fig. 5.9 A-C). During upward walking, the front, 'pulling' legs were slammed firmly onto the surface and remained in contact until they peeled and detached from the proximal edge, the distal pads remaining in

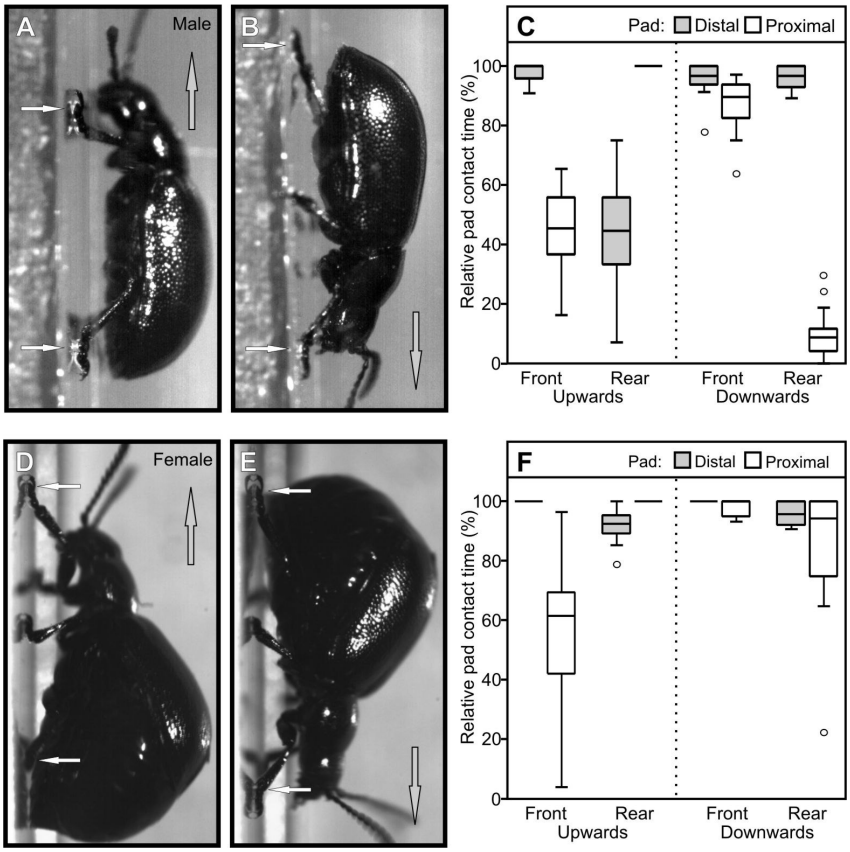

Figure 5.9: *Gastrophysa viridula* male (A,B) and female (D,E) beetles climbing up (*n*=43 steps) (A,D) and down (*n*=47 steps) (B,E) a smooth vertical surface. The white arrows indicate pads contacting the surface (upwards: the distal pad for the front, 'pulling' leg and the proximal pad for the rear, 'pushing' leg; downwards: both pads for the front leg, the distal pad for the rear leg). (C,F) boxplots showing the percentage time each pad (distal, grey; proximal, white) remained in contact with the surface, relative to the total duration of the stance phase of the step for male (C) and female (F) beetles. Results presented for front and rear legs, as well as upwards and downwards climbing.

contact for almost the whole stance phase of the step (mean percentage of step time in contact ± s.e.m.: 98.2 ± 0.6%). By contrast, proximal pads were little used and were in contact for less than half the stance phase of the step (mean: 43.6 ± 3.0%). In the rear, 'pushing' legs, however, proximal pads made almost continuous contact (mean: 98.1 ± 1.2%), often slightly laterally oriented, whereas distal pads were lifted from the surface before the end of the step (mean: 42.5 ± 4.2%).

During downwards walking all pads of the front legs were in contact for most of the stance phase of the step (*n*=47 steps). Contrary to the upwards climbing, the proximal pads appeared to be used almost continuously (mean: 85.7 ± 2.5%). In the rear legs, the distal pads were engaged almost exclusively (mean: 95.9 ± 0.8%), with the proximal pads making hardly any contact (mean:

10.6 ± 2.1%). At the end of the stance phase, the foot was detached from the distal edge and pulled along close to the surface.

This behaviour was also observed for female beetles (Fig. 5.9 D-F), with the exception that in the rear legs, both pads stayed in contact for most of the stance phase. This is likely explained by the additional mass that female beetles, heavily loaded with eggs, need to support (1.8 times that of the males). The large female beetles moved more slowly than the males, using a 'wave' rather than a 'tripod' gait. However, the distal pads were still in all cases employed during pulling and the proximal pads for pushing.

5.4 DISCUSSION

These findings indicate that the fibrillar adhesive pads on the tarsal segments of *G. viridula* beetles have developed a functional division of labour similar to that recently reported for the smooth attachment pads of cockroaches (Clemente and Federle, 2008). The three adhesive pads of the same tarsus are not only composed of morphologically different types of setae, but also differ in their effective elastic modulus and adhesive/frictional performance. Video recordings of freely walking beetles climbing upwards and downwards confirmed that proximal and distal pads are used differently and selectively during locomotion. Tarsi placed above the body centre of gravity (COG) mainly made contact with the distal pads, whereas feet below the COG primarily used their proximal pads. This suggests that the distal pads are mainly used for pulling and adhesion, whereas the proximal pads are used when legs have to push laterally or away from the body.

5.4.1 Direction dependence of tarsal adhesive pads

All three tarsal pads of *G. viridula* showed a clear direction-dependence, with forces being larger in the pulling than in the pushing direction. However, the stiffer proximal pads were less anisotropic and thus supported larger forces when pushed laterally or away from the body. The direction-dependence of many insect adhesive pads may be explained by the chain-like construction and flexibility of the tarsus (Snodgrass, 1935). Distal segments cannot exert large distal or lateral pushing forces, because the tarsus would easily buckle or bend (Chapter 2; Clemente and Federle, 2008). By contrast, the proximal tarsus has greater stability and allows more distal and lateral pushing before buckling occurs. When the foot is pulled towards the body, a force on the distal adhesive pad will straighten the tarsus and align it to the force vector. If all three tarsal pads are in contact with the surface during a pulling stride, the peel force will be concentrated on the proximal pad, causing it to lift and detach from the surface earlier. The greater width of

distal adhesive pads in many insects (e.g. bushcrickets (Beutel and Gorb, 2001), cockroaches (Clemente and Federle, 2008) and beetles (Stork, 1980c) appears to support this function, as the peel force is proportional to pad width.

Direction-dependence of shear forces caused by tarsal buckling occurs both in cockroaches (*N. cinerea*, Clemente and Federle, 2008) as well as stick insects and beetles (see Chapter 2). However, the adhesive pads of both insects differ when tested 'fixed' (i.e. fully immobilised). While the fixed cockroach arolium and the euplantulae produced forces and shear stresses on a smooth surface that were similar during pushing and pulling (Clemente and Federle, 2008), all three tarsal pads in *G. viridula* showed higher forces in the pulling direction.

As discussed in Chapter 2, this direction-dependence on the level of the adhesive pad itself appears to be based on the fibrillar pad design and the asymmetrical structure of seta tips. Seta tips align with the substrate when the pad is pulled. When pads are strongly pushed away from the body, setae deflect so that their tips are no longer able to align with the substrate. In many cases, the unstressed default orientation of seta tips is non-adhesive, so that they require a pull towards the body to become aligned (Autumn et al., 2006a; Autumn and Hansen, 2006; Federle, 2006). It is likely that this non-adhesive default state results in a particularly effortless, 'automatic' detachment as soon as the shear force towards the body is released. Interestingly, Fig. 5.4 suggests that only the pointed and spatulate setae in *G. viridula* have this relatively non-adhesive default position and this may explain the weaker direction-dependence of the proximal pads in males. In general, direction-dependence of adhesive pads allows animals to switch easily and rapidly between attachment and detachment by performing gross leg movements toward the body or away from it. These findings suggest that the detachment of the proximal pads in *G. viridula* should be more cumbersome, but more detailed observations of tarsal movements in freely walking beetles and of ground reaction forces are needed to test this prediction.

When viewed from the ventral side, the spatula-tipped hairs of the beetle's distal pad are more exactly aligned in the proximal-distal direction than those of the proximal pad. This orientation may also be responsible for the clearer direction-dependence of distal pads, with strong 'pulling' forces (when setae are loaded in tension) and easy detachment when 'pushing' (where setae are compressed along their axis) (see Chapter 2). By contrast, setae on the proximal pads were oriented more transversely and consistently, proximal pads were able to produce higher lateral forces (in both sexes) and, at least for the males, higher pushing forces.

Although force vectors typically point along the legs to minimise torques about the joints (Full et al., 1991), lateral forces may be important in some situations, for example in middle or hind legs during climbing (Goldman et al., 2006). In the lateral sliding tests, at least half of the pointed hairs (those on the side opposite to the sliding direction) may be able to contact the surface in tension, corresponding to substantial frictional and adhesive forces. This may well provide an elegant solution to the problem of how to push without sacrificing direction-dependent detachment (Fig. 5.10).

Specialisation of attachment pads for pushing and pulling (as in cockroaches and spiders) may correlate with a specialisation for friction and adhesion, respectively. To be able to climb on natural surfaces which usually exhibit some degree of surface roughness, insects may have to evolve more compliant pads, allowing them to conform better to the surface profile. As discussed in Chapter 4, the fibrillar design may be inherently well suited for this purpose for several reasons. Firstly, long and flexible setae bend easily so that their tips can make contact with an irregular substrate without the need for high normal forces. Secondly, the small size of seta tips makes fibrillar pads insensitive to roughness with a larger length scale. Lastly, contact to even smaller length scales of surface roughness may be facilitated by the bending of spatula tips, which are usually very thin (Eimüller et al., 2008; Persson and Gorb, 2003).

However, enhanced compliance may come at a cost, because soft adhesive pads will be more susceptible to wear, in particular when softer materials are used. Pads of climbing animals have to resist considerable shear forces over many steps in an entire lifetime. Abrasion and wear probably represent a significant problem for soft attachment pads (e.g. Ridgel et al., 2003; Slifer, 1950), calling for a more robust and thus less compliant pad design. Fibrillar adhesive systems are to some extent able to achieve compliance with relatively stiff and wear-resistant materials, but here too compliance may be limited by the condensation or 'self-matting' of hairs (Appendix A.2; Glassmaker et al., 2004; Persson, 2003; Sitti and Fearing, 2003; Spolenak et al., 2005). If pads are primarily used under compression to generate friction forces, wear resistance will be even more critical but the requirement for compliance may be relaxed, because on rough substrates high friction forces can be achieved by interlocking even with little adhesion. Stiffer proximal pads may also provide better stability when compressed by the insect's body weight. If the beetle was walking only on its distal pads (with three legs in contact at any one time), the setae would be deflected by 0.64 μm for males and 0.82 μm for females. Whilst this is small and well within the elastic range of the hairs, support from stiffer proximal pads may prove

beneficial for situations with additional loads. Thus, a division of labour between soft, adhesive pads and more robust and wear-resistant friction pads may evolve as a consequence of a trade-off between compliance and wear-resistance. The occurrence of a similar division of labour between proximal and distal tarsal pads in beetles (this study), cockroaches (Clemente and Federle, 2008) and presumably spiders (Hill, 1977; Niederegger and Gorb, 2006) suggests that this is a fundamental principle widespread among arthropods.

5.4.2 Array stiffness and performance on rough surfaces

These measurements of the effective elastic modulus of individual adhesive pads in *G. viridula* show that the distal pads of *G. viridula* are about twice as compliant as the middle and proximal pads. This difference in stiffness supports the observed functional division of labour between adhesive pads on the same foot. Greater compliance enhances a pad's ability to adapt to rough substrates (see Chapter 4). Consistently, on the rough substrate for the smaller, yet softer, distal pads three to five times higher forces and stresses were measured than for the proximal pads in both males and females. The adhesive and frictional performance of the different tarsal pads in *G. viridula* is based both on the structure of the seta tips and on the compliance of seta stalks. For large deformations, array stiffness is mainly affected by the bending of seta stalks. Seta bending is thus responsible for the ability of pads to conform to large-scale surface roughness. On a smaller length scale, adhesion will be mainly determined by the geometry, size and material properties of the seta tips (see Chapter 4). The higher compliance of the distal pads coincides with a primarily spatulate tip design. The spatulae are very thin and thus ensure a high flexibility that can compensate small-scale surface roughness (Persson and Gorb, 2003). To enable adhesion to natural surfaces with many length scales of surface roughness, a combination of seta stalk compliance and flexible tips is required, and this explains that both features are present in distal pads of beetles.

It should be noted that during free walking on a rough surface, other parts of the tarsus and pretarsus may be used. In all insects, the pretarsal claws contribute to pulling (Dai et al., 2002) and many insects (including *G. viridula*) have distally oriented, stiff spines on the tibia (near the tibia-tarsus joint), which regularly contact the ground and are probably used for pushing (e.g. froghoppers: Burrows, 2006).

Despite the variation in stiffness, all three pads of *G. viridula* were so compliant that their effective elastic moduli fell within Dahlquist's criterion for tack (E_{eff} < 100 kPa) (Dahlquist, 1969). This empirical criterion was introduced for bulk adhesive materials. For

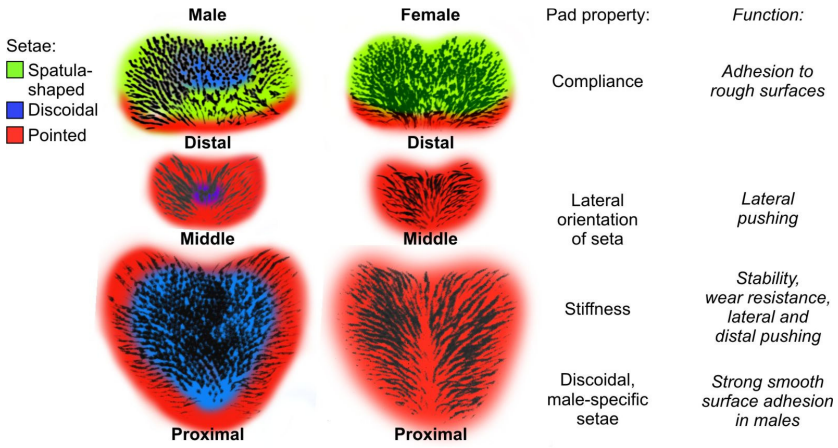

Figure 5.10: Summary of the proposed functional properties for each pad (distal, middle and proximal) of both sexes of *Gastrophysa viridula*. Epi-illumination contact area images; colours mark the position of the different seta types.

fibrillar adhesives, however, this condition is necessary but not sufficient for good adhesion, as the adhesive contact also depends on the geometry of the seta tips, which can vary independently of the array's effective elastic modulus. The values measured here for *G. viridula* are close to results obtained for gecko fibrillar arrays (E_{eff} = 83 ± 4.0 kPa; (Autumn et al., 2006c)).

5.4.3 Material properties of seta cuticle

Using the measured pad spring constants, the elastic modulus of the seta cuticle was estimated to range from 5.2-16.1 GPa. This is slightly higher than the range estimated by Orso et al. (2006) for a hydrated seta (2-6 GPa) but is consistent with their figure calculated from tensile tests of a dried seta of 13.3 ± 1.0 GPa. Although this comparison between elastic modulus values measured in a tensile and a bending test may have limited validity, it suggests that the stiffness of a hydrated seta is not very different from that of a dried one. This suggests that the seta cuticle is quite hydrophobic and may contain little water *in vivo*.

A similar effect has been reported for locust wings, where the cuticle of the thin wing membrane was found to be unusually insensitive to hydration (Smith et al., 2000). Being unaffected by dehydration may also be biologically advantageous in an adhesive system, because setae may be particularly exposed to the environment and to a wide range of humidity conditions. The elastic modulus measured here is strikingly high, and is in fact close to the highest values ever reported for insect cuticle (20 GPa measured in the locust tibia (Ker, 1977; Vincent and Wegst, 2004)). A high elastic modulus of the cuticle making up the adhesive pad

may provide increased wear resistance during repeated steps. It should be noted that in addition to bending, setae may also deflect by rotating in their socket, i.e. the hair socket could act as a hinge. This would result in an even higher predicted value for the cuticle modulus. Further work is needed to investigate whether adhesive seta cuticle is indeed less hydration-dependent than other types of insect cuticle and if so, how this property relates to the cuticle's chemical composition.

The calculated Young's modulus of seta cuticle varied only slightly between pads. Instead, the greater compliance of the distal pad appears to be achieved mainly by thinner seta stalks. This may be the simplest and most effective way to increase seta compliance, because seta radius appears to the fourth power in Equation 5.3. Hence, a small decrease in hair thickness will strongly reduce the array's effective elastic modulus. The same change would require a much larger relative change of cuticle modulus, and whilst cuticle may be a highly variable material (Vincent and Wegst, 2004), a strong hydration dependence is undesirable as discussed above. Interestingly, the elastic modulus of the gecko's setal β-keratin also appears to be relatively conserved across species (at approximately 1.5 GPa), again implying a reliance on morphological parameters rather than material properties (Peattie et al., 2007). The hydration dependence of gecko seta material has not been investigated but the elastic modulus of avian keratin is also only moderately dependent on humidity (Taylor et al., 2004).

5.4.4 Sex specific differences of attachment

Beetle seta design does not only differ between different tarsal segments of the same foot but also between sexes. The wide-spread sexual dimorphism can be explained by the need of males to maintain a firm and long-lasting hold on the relatively smooth elytra of females during copulation. An adhesive system adapted to generate large forces on smooth surfaces is clearly advantageous for this purpose (Pelletier and Smilowitz, 1987; Stork, 1980a; Voigt et al., 2008). As a consequence of sexual conflict, females of diving beetles have evolved surface corrugations on their elytra that make it more difficult for males to adhere, triggering further modifications of the male adhesive system (Bergsten et al., 2001) but no such effects are presently known for leaf beetles.

In this study the stronger adhesion of males to female elytra and smooth surfaces on the level of individual pads was confirmed. Consistent with the setal composition, the greatest difference in forces on a smooth surface was found for the proximal pads which possess many discoidal setae in males but not in females. On smooth glass, males were able to generate over twice the friction force of the females (or 1.5 times the shear stress) and an even

stronger difference was found for the friction produced on female elytra. This confirms the important role of discoidal setae on male proximal pads in the attachment to the smooth surface of females during mating.

The absence of discoidal setae in the proximal pads of females suggests that their presence might entail a cost for males. Firstly, male proximal pads achieved slightly smaller shear forces and stresses than female ones on the rough surface (see also Voigt et al. (2008)). Secondly, the weaker direction-dependence of male proximal pads might make it more difficult for the pads to detach rapidly from a smooth surface.

5.4.5 Outlook

Despite a large number of recent studies and efforts to 'mimic' biological fibrillar adhesives (see Appendix A.1), there is still very little actually known about the properties and the performance of the natural systems. In fact many synthetic adhesives do not fall within the parameter space of biological adhesives (with respect to size and stiffness of setae) and their performance often falls short of the natural systems. This may be partly due to a lack of understanding of the biological systems which are being imitated. Only little information is available on the material properties of adhesive setae (although see: Orso et al., 2006; Peattie et al., 2007). For many systems, the frictional and adhesive performance is unknown, making it impossible to test available theoretical models. Analysing the material properties of natural adhesive pads as well as their adhesive performance and locomotion represents an essential step towards the development of biomimetic fibrillar adhesives.

6

FIBRILLAR TARSAL ADHESIVE PADS IN THE FLEA BEETLE *ALTICA LYTHRI*: JUMPING FROM A SMOOTH SURFACE

This work was conducted in collaboration with Christofer J. Clemente and Gregory P. Sutton. All jumping performance measurements in this study were performed in conjunction with them.

Summary

Flea beetles are able to jump to escape from predators. Like other leaf beetles, they possess hairy pads on their tarsi allowing them to cling to smooth plant surfaces. Here it was shown that flea beetles successfully combine the conflicting requirements of surface adhesion and jumping, achieving take-off velocities of 0.74 ms^{-1} (male beetles) from a smooth glass substrate and jumps from inverted surfaces. High-speed video observations showed that the beetles' hind leg tarsi made contact almost exclusively with their proximal pads while accelerating for take-off. These pads exhibited extremely rapid attachment and detachment, with an upper limit on detachment times as low as 0.16 ± 0.02 ms. Single, proximal pad friction force measurements surprisingly showed that forces were higher in the pulling direction, against the direction of the jump. Nevertheless, proximal pads were able to withstand pushing forces higher than those occurring during take-off. Flea beetles have a similar sexual dimorphism to other Chrysomelidae with males possessing large numbers of discoidal setae in the centre of their proximal pads. When tested on rough and smooth substrates, males and females showed similar jumping performances. However, the take-off speed of males was significantly lower on glass than on rough sandpaper. This effect may be based on a behavioural adaptation of males for jumping. They were observed to supinate their tarsus before jumping, resulting in a reduced contact area of the proximal pads and of the sticky discoidal hairs in particular.

6.1 INTRODUCTION

Flea beetles (Alticini), unlike most other groups of beetles have impressive jumping abilities, helping them to escape predators. Using a metafemoral spring mechanism (Furth, 1982; Furth et al., 1983) they can jump with take-off accelerations of between 10 and 270 g (Brackenbury and Wang, 1995). Flea beetles possess tarsal adhesive structures similar to those found in many other insects and spiders (Beutel and Gorb, 2001; Scherge and Gorb, 2001), consisting of fine arrays of adhesive hairs (setae) and allowing them to climb over smooth plant surfaces where claws would be unable to grip (Dai et al., 2002; Stork, 1980a). Flea beetles can be seen jumping off leaves when disturbed, suggesting that they are capable of jumping from smooth surfaces, but the detailed mechanisms underlying this ability have not been investigated.

Jumping from a smooth surface should present considerable biomechanical difficulties for insects. First, the strong forward accelerations during take-off are only possible if feet can generate sufficient traction on the ground. If jumpers from smooth surfaces relied on classical friction only, their take-off angle would be constrained by the friction coefficient μ:

$$\tan\theta = \frac{F_{\perp}}{F_{\parallel}} = \frac{1}{\mu} \qquad [6.1]$$

so that for typical values of μ<0.3, insects would slip for all but the steepest jumps (θ>73°), strongly limiting maximum jumping distance. In the absence of surface roughness, the only possible solution to this problem is to strengthen the foot contact by adhesive forces. Consistently, many jumping insects possess adhesive organs on their feet (Beutel and Gorb, 2001). However, while feet adhering to the substrate give a higher traction during acceleration, this might make it more difficult for the insect to detach from the surface for take-off. Given the considerable take-off velocities of arthropod jumpers, the time available for detachment is extremely short.

Most animal adhesive pad structures achieve rapid and effortless detachment by their direction-dependent properties. In most cases, pads make full adhesive contact when pulled toward the body, but detach when pushed away from it. Thus, attachment and detachment can be controlled by shear forces, minimising normal preload and pull-off forces. Animals with hairy adhesive pads have been found to produce negligible normal detachment forces when running up smooth vertical surfaces (Autumn et al., 2006b). In Chapters 2 and 5 the direction-dependence of hairy adhesive pads in the non-jumping leaf beetle *Gastrophysa viridula*

De Geer (Coleoptera) was investigated. Like flea beetles, dock beetles possess three fibrillar attachment pads on each tarsus. The distal pads in dock beetles were found to be strongly direction-dependent, with friction forces 7.8 times lower in the pushing than in the pulling direction (Chapter 2). This direction-dependence facilitates foot detachment for the beetles, as found for other hairy adhesive systems (Autumn et al., 2006a).

However, foot detachment by pushing presents a potential problem for climbing insects, where legs regularly need to push during upward and downward locomotion (Clemente and Federle, 2008; Goldman et al., 2006). Jumping presents perhaps the clearest example of the importance of pushing forces: all insects jumping with legs (including flea beetles) propel themselves by pushing with their hind legs, thereby exposing their hind tarsi to large pushing forces, against the typical preferred direction of adhesive pads. Several groups of insects have solved the problem of direction-dependence via a division of labour between proximal and distal pads on the tarsus, which are specialised for pushing and pulling, respectively (Chapter 5; Clemente and Federle, 2008).

The analysis for dock beetles showed that all three pads, including the proximal ones, showed the same direction-dependence with higher friction forces in the pulling direction. However, proximal pads were found to be less direction-dependent than distal pads; they were also stiffer and more stable against buckling. These properties allow dock beetles to use their proximal pads for pushing. In contrast, distal pads were compliant and highly direction-dependent, allowing them to detach easily. It is unclear whether jumping flea beetles use the same principle when producing large pushing forces with their hind legs.

As common in other leaf beetles (Pelletier and Smilowitz, 1987; Stork, 1980a; Stork, 1980c; Voigt et al., 2008), a strong sexual dimorphism is present in the adhesive pads of dock beetles. Male beetles possess large numbers of flat, discoidal hairs on their proximal pads, likely facilitating strong attachment to the smooth elytra of female beetles during mating (Chapter 5; Pelletier and Smilowitz, 1987; Stork, 1980a; Voigt et al., 2008). However, the strong adhesion to smooth surfaces and the weaker direction-dependence of proximal pads may make it difficult for walking beetles to detach from surfaces (Chapter 5). In contrast, female proximal pads consist mainly of pointed setae and do not generate excessive adhesive forces. It was investigated whether a similar sexual dimorphism is present in the pads of *Altica lythri* Geoffroy (Coleoptera). Given that for an effective jump, rapid take-off is of crucial importance (Burrows, 2009), the implications of any morphological variation for jumping performance were assessed.

To investigate how flea beetles use their adhesive organs to jump from smooth surfaces, the following questions were

addressed: 1. Can flea beetles jump from smooth surfaces upright and inverted, using their adhesive pads? 2. Which tarsal pads do they use for jumping and how quickly do these pads attach and detach? 3. Do flea beetles show the same division of labour between tarsal pads as other insects? 4. Do tarsal pads of flea beetles show a sexual dimorphism and is there any difference in jumping performance or behaviour between male and female beetles?

6.2 METHODS

6.2.1 Tarsal morphology

Male and female *Altica lythri* beetles were collected from hairy willowherbs (*Epilobium hirsutum*) near Cambridge and kept on leaves of their host plant in the laboratory. The average weight of male beetles was 8.1 ± 0.4 mg; females weighed 11.5 ± 0.5 mg (means ± s.e.m.). The proximal adhesive pads of the front and rear legs of male and female beetles were imaged using scanning electron microscopy (SEM). Samples were mounted on SEM stubs, sputter coated with 20 nm thick gold and studied with an FEI XL30-FEG (FEI, Hillsboro, OR, USA) at 5 kV (see Fig. 6.1). Pad dimensions were measured from ventral view SEMs of the tarsus, from one beetle of each sex.

6.2.2 Measurement of friction in individual pads

In order to measure the forces supported by individual pads, live beetles were attached by their back to a glass rod using blu-tack (Bostik, Leicester, UK) and parafilm tape. One rear leg was isolated and fixed with blu-tack so that friction forces could be measured from individual foot pads as described in Chapter 2. Friction forces were measured on a glass substrate using a 2D foil strain gauge force transducer mounted on a 3D motor positioning stage M-126PD (Physik Instrumente, Karlsruhe, Germany). Data acquisition, video and motor movements were controlled using a custom LabVIEW (National Instruments, Austin, TX, USA) program which included a feedback mechanism allowing normal force to be kept constant during slides. All force measurements were performed with live beetles. Slides of 10 mm were performed at 500 μms^{-1} velocity with feedback-controlled load of 0.3 mN. Tests were carried out separately for both the distal and proximal pads of male (n=5) and female (n=6) beetles. All slides were performed for both the pulling (towards the body) and pushing (away from the body) directions.

6.2.3 Jumping performance of whole animals

Adhesive contact area

Two separate experiments were used to investigate the beetles' ability to jump from a smooth surface. Firstly, the adhesive contact areas of each pad were imaged during upright and inverted jumps using high-speed video cameras. Adhesive contact area (the total setal contact of the pads) was visualised using light microscopy with brightfield epi-illumination via a direct-current 100 W high-pressure mercury burner, which provided sufficient and flicker-free light even for high-speed recordings. For upright jumping, beetles were allowed to walk on a glass microscope slide on an inverted Leica DMIRBE microscope (Leica Microsystems GmbH, Wetzlar, Germany). Contact area during each jump was filmed with a 5x objective at 5000 Hz using a FASTCAM 1024 PCI high-speed camera (Photron Ltd, Marlow, UK). For inverted jumping, beetles were placed on the underside of a glass coverslip under a Leica DMR upright microscope. Here, contact area was filmed at 3000 Hz using a HotShot PCI 1280 B/W camera (NAC image technology, Simi Valley, CA, USA). The beetles' jumping escape response was triggered using a single paintbrush fibre. From the video recordings, a 'projected' pad area was measured in MATLAB (The Mathworks, Natick, MA, USA) by manually drawing a polygon around the contact zone of the whole array.

Take-off velocity

Secondly, take-off velocity was quantified for beetles of each sex (n=10 males, n=11 females) jumping from both smooth and rough substrates. Beetles were placed in randomised order on either a smooth glass plate or a rigid rough aluminium oxide substrate with 30 μm nominal asperity size (Ultra Tec, Santa Ana, CA, USA). Jumps were triggered as above and filmed in both lateral and dorsal views using two synchronised, levelled Redlake PCI 1000 B/W cameras (Redlake, Tallahassee, FL, USA) at 1000 Hz. These were digitised using the DLTdataViewer2 program (Hedrick, 2008) giving 3D velocity vectors for each sex and surface. Two jumps were recorded for each beetle and the maximum velocity taken to provide a measure of peak jumping performance. Jumps from the edge of the platform were excluded to ensure tarsal contact with the level surface. All jumping measurements were performed in collaboration with C. J. Clemente and G. P. Sutton.

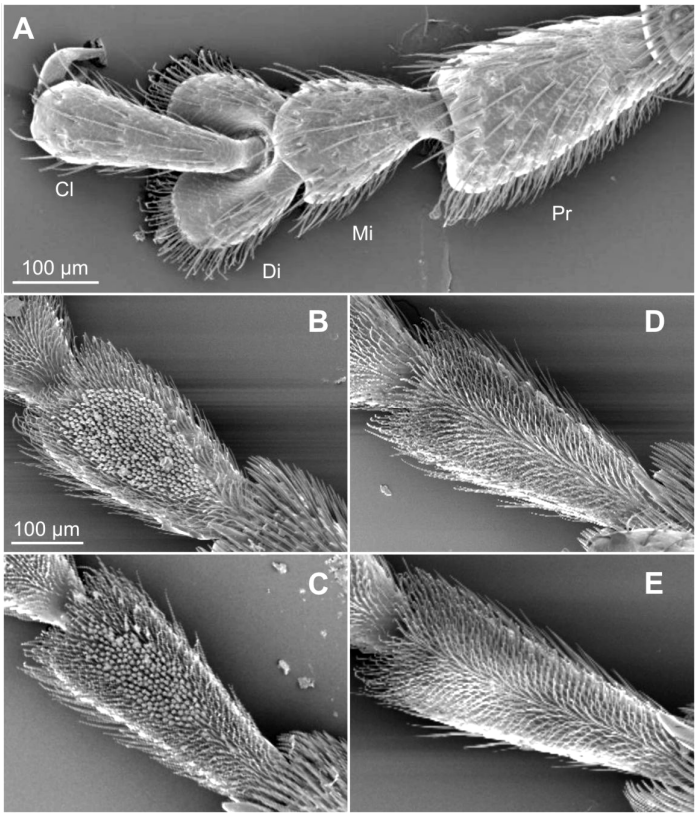

Figure 6.1: SEMs showing the tarsi of male (A-C) and female (D-E) flea beetles *Altica lythri*. (A) dorsal view of a male front leg tarsus (Cl: claws, Di: distal pad, Mi: middle pad, Pr: proximal pad). (B,D) proximal pads from the front legs (C,E) proximal pads from the rear legs. Note the different size and shape of proximal pads in the front and rear legs and the high density of discoidal hairs in the male pads (B,C). Images (B-E) presented to the same magnification.

6.3 RESULTS

6.3.1 Morphology of adhesive pads

The tarsal morphology of the flea beetle *A. lythri* is similar to that of other leaf beetles (Fig.6.1; Chapter 5; Stork, 1980c; Voigt et al., 2008). The three tarsal pads show a sexual dimorphism with large numbers of flat, disk-shaped hairs covering all but the outer edges of the male proximal pads. In both sexes the proximal pads on the rear legs were longer than those on the front legs (front leg pad length 291.3 ± 3.2 µm males, 361.9 ± 3.6 µm females; rear leg pad length 331.3 ± 2.8 µm males, 411.4 ± 3.5 µm females, means ± s.e.m., 5 measurements from 1 beetle of each sex).

6.3.2 Friction performance of individual pads

Friction tests revealed that the pads of the flea beetles showed direction-dependent properties similar to those of the dock beetles

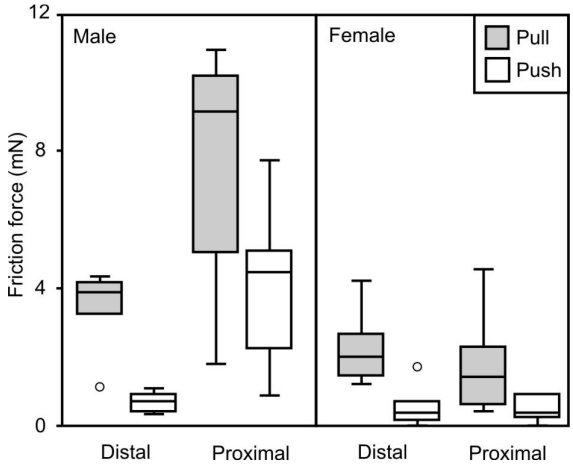

Figure 6.2: Friction force measurements of *Altica lythri* on a smooth glass substrate. Values correspond to the peak force occurring during a 10 mm, 0.5 mms^{-1} pulling or pushing slide of either the distal or proximal pad, n=5 for each sex. Plot shows medians (centre lines), interquartile ranges (boxes), and the largest and smallest values (whiskers) that are not outliers (circles).

(see Fig. 6.2 for flea beetles and Chapter 5 for dock beetles). In all cases pulls generated higher shear forces than pushes (all pads $P \leq 0.05$, paired t-tests). As in dock beetles however, the proximal pads showed the weakest direction dependence and were able to support the largest pushing forces. These high pushing forces imply the same division of labour properties as seen for dock beetles (Chapter 5). Males generated significantly higher pulling forces than those of females (all pads $P \leq 0.05$ unpaired t-tests).

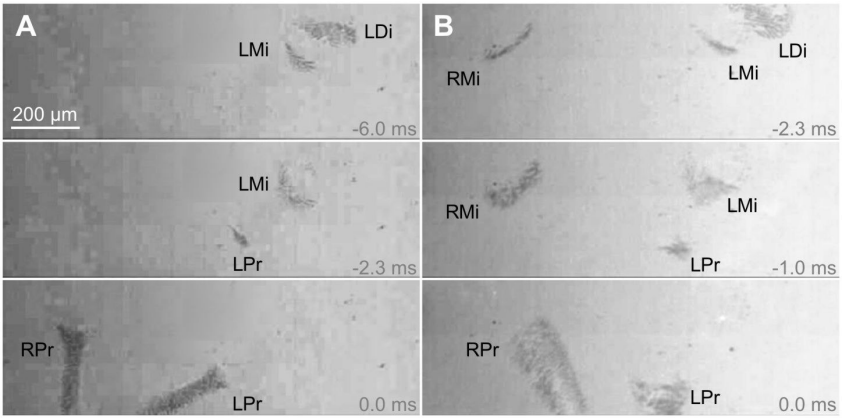

Figure 6.3: Contact areas of jumping male (A) and female (B) flea beetles from the inverted position, showing the change from distal, through middle, to proximal pads. Numbers denote the time until the final frame before detachment. In females, proximal pads can be seen to make contact with their full width, whereas only the outer sides of each pad make contact in male jumps. Letters denote the different tarsal pads (L,R: left right, Di: distal, Mi: middle, Pr: proximal). All images to the same magnification.

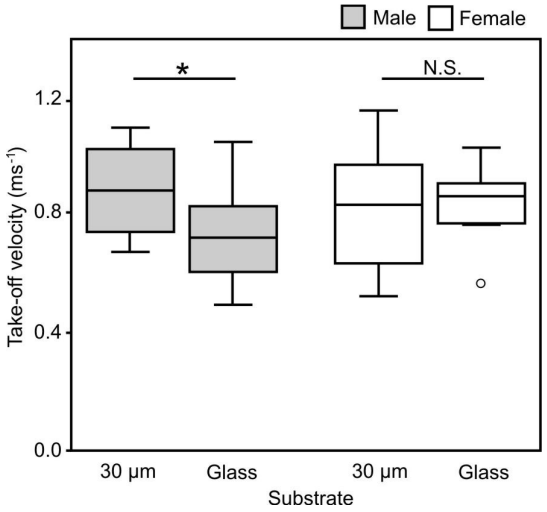

Figure 6.4: Maximum recorded take-off velocities for male (*n*=10) and female (*n*=11) beetles jumping from smooth (glass) and rough (30 µm sandpaper) substrates. Plot shows medians (centre lines), interquartile ranges (boxes), and the largest and smallest values (whiskers) that are not outliers (circles). Significance levels: * $P<0.05$, ** $P<0.01$, *** $P<0.001$, N.S. not significant.

6.3.3 Jumping performance

All recorded jumps showed that both sexes of the flee beetle *A. lythri* were capable of jumping from smooth surfaces and were even able to jump from an inverted position. No instances of foot slipping were observed in either case (as seen in other jumping insects (e.g. locusts: Sutton and Burrows, 2008)). Videos of the pad contact area during jumping revealed that beetles always accelerated with the proximal pads in surface contact (see Fig. 6.3). During inverted jumping, beetles initially adhered using the distal pads. Immediately before take-off, this pad detached and the contact changed to the middle and finally proximal pad, which was used to provide propulsion during the jump (Fig. 6.3A,B). In all cases, the contact times of the individual pads overlapped, and there was no period without contact.

An attempt was made to estimate 'detachment time' for upright jumping as the time elapsed between the frame showing 50% of the maximal pad contact area achieved during the jump and complete detachment (Federle and Endlein, 2004). However, in the final frame before detachment (recorded at 5000 fps), pad contact area still averaged 73% of the maximal pad contact area. Hence an upper limit for pad detachment time was estimated by interpolation (assuming a linear decrease in area to zero over the final contact frame for each beetle), giving 0.16 ± 0.02 ms. Upper limits for detachment times for inverted jumps (recorded at 3000 Hz and estimated in the same way) were 0.45 ± 0.18 ms (difference not significant).

Table 6.1: Take-off velocity, acceleration, acceleration time, force and pressure (force per projected pad contact area) calculated from the averaged maximum recorded take-off velocities for male and female beetles jumping from smooth and rough surfaces.

	Male		Female	
	30 μm	glass	30 μm	glass
Take of velocity (ms^{-1})	0.89	0.74	0.82	0.84
Acceleration (ms^{-2})	132.8	93.1	112	116.5
Acceleration time (ms)	6.65	8.00	7.39	7.21
Force (mN)	1.08	0.75	1.29	1.34
Pressure (kPa)	116.3	81.5	52.0	54.0

During both upright and inverted jumping, males were observed to make contact with a smaller fraction of their proximal pads than females. The pad was visibly tilted from the surface so that only the outer edge of the pad made contact (see Fig. 6.3A). This indicates that the tarsus was supinated before jumping, likely as a result of a gross leg movement. As a result, maximal projected proximal pad contact area during a jump (n=8 male, n=9 female jumps recorded from 5 individuals) was much smaller for males (9250 ± 1480 μm^2) than for females (24800 ± 3180 μm^2) ($t_{11.3}$=-4.427, $P \leq 0.001$ unpaired t-test).

Maximum take-off velocities from both rough and smooth substrates are plotted in Figure 6.4. The velocities were significantly different between rough and smooth substrates for males but not for females (males t_9=2.560, P=0.031; females t_{10}=-0.236, P=0.818 paired t-test). Take-off angle was similar for different sexes and substrates: smooth, males 35.3 ± 5.6°, females 41.0 ± 4.1°; rough, males 35.9 ± 7.8°, females 38.8 ± 6.7°; means ± s.e.m. (all differences not significant in paired t-tests). This result implies that the take-off force vectors are outside the narrow 'friction cone' (see Equation 6.1).

Acceleration, force and pressure (force per projected pad contact area) were calculated from the maximum recorded take-off velocities (see Table 6.1). Mean leg lengths were estimated as the sum of tibia and femur length from side-view recordings of the jumps giving 2.96 ± 0.18 mm for males and 3.03 ± 0.10 mm for females (mean ± s.e.m., n=7). Mean values of acceleration, a and acceleration time, t were calculated using the standard equations of motion:

$$a = \frac{v^2}{2l} \quad \text{and} \quad t = \frac{2l}{v} \qquad [6.2]$$

where v is the overall mean take-off velocity and l the mean leg length as an approximation of the distance over which the acceleration occurred. As the beetles likely reach maximal velocity

before the complete extension of their legs, the accelerations may be slightly underestimated. Acceleration was converted to a force using the mean measured body mass of the beetles. The pressure on the proximal pad was calculated as the force divided by the mean projected pad contact area during take-off as recorded above (see Table 6.1).

6.4 DISCUSSION

In this study it was shown that both sexes of the flea beetle *A. lythri* were able to jump effectively from a smooth glass surface without slipping. The glass provides no opportunity for the beetles to interlock their claws or tarsal spines (Dai et al., 2002; Spagna et al., 2007) and given that the take-off angle is outside the friction cone, the setal attachment pads are necessary for the jump. In fact, female beetles were able to jump with similar take-off velocities on both rough and smooth substrates. Extremely fast detachment times were observed for take-off from the glass surface and impressively, flea beetles were even able to jump upside down from a glass plate.

6.4.1 Division of labour

As observed for dock beetles, all pads of the flea beetles displayed direction dependent properties. As proposed for other hairy systems, this direction-dependence likely originates from the arrangement of the setae being angled in the distal direction, and often exhibiting asymmetrical spatulate tips. Hence, a pull of the pad towards the body maintains good substrate contact whereas a push away from the body buckles the hairs, peeling them from the surface (Chapter 2; Autumn and Hansen, 2006; Federle, 2006). This is likely an important mechanism for the detachment of adhesive pads which are able to adhere with high safety factors when attached (Eisner and Aneshansley, 2000).

However, as discussed in Chapter 5, this may pose a problem during locomotion when beetles need to push with their pads to provide propulsion for either a step, or in this case, a jump. It was proposed that similar to the division of labour system used by cockroaches (Clemente and Federle, 2008), dock beetles may use different tarsal segments for pushing and pulling during locomotion. This division of labour system allows the easily detachable distal pad to be used to attach and pull, whereas the stable proximal pads (located on the first tarsal segment preventing buckling of the tarsal chain) can be used for pushing. This principle was shown to be consistent for dock beetle locomotion (filmed in the sagittal view climbing a smooth vertical plate) and has now been demonstrated for flea beetle jumping. The high-speed observations of pad contact area during jumps show that only the

proximal pads made contact during the final stages of the jump. They are therefore responsible for generating the pushing thrust.

The pushing forces on each foot calculated from the maximal take-off velocities were around 0.38 mN for males and 0.67 mN for females. This is below the mean measured friction forces generated by the beetles' proximal pads (4.25 mN males, 1.30 mN females, see Fig. 6.2) on a glass substrate and therefore consistent with the beetles' observed ability to jump without slipping. However, the highest jumping forces for the female beetles were close to the lowest single pad pushing forces. This raises an interesting question. Among the seven species of flea beetle investigated by Brackenbury and Wang (1995), *A. lythri* had the lowest take-off acceleration and four species (*A. atrocaerulea, P. affinis, L. gracilis* and *P. dulcamarae*) exhibited accelerations that were more than an order of magnitude higher. High performance in locomotory tasks is often a result of greater specialisations (Biewener and Daniel, 2010; Dickinson et al., 2000). Hence unless they possess further specialisations of their adhesive pads towards pushing, females of these species should slip when jumping from a smooth surface. It will be worth exploring the detailed adaptations of these faster jumpers in future studies. It is possible that our single-pad measurements underestimated the maximal pushing force in females. Given that the mean take-off angle for females was 41°, the normal force component is approximately 0.9 mN for female beetles on glass. This is three times higher than the normal force used during the friction slides. Female proximal pads are made up of pointed hairs (Fig. 6.1) which lie flat when pressed against a surface (Chapters 2 and 5; Geiselhardt et al., 2009b). While the detailed effect of load on the contact of pointed hairs is still unknown, it is likely that a higher normal force increases the contact area of these hairs and therefore the shear force supported by the pad during pushing.

6.4.2 Sexual dimorphism in jumping performance

As observed in dock beetles, friction slides confirmed that male flea beetles generated significantly higher pulling forces on smooth surfaces than females. This is explained by the presence of large numbers of flat discoidal hairs on the proximal pads, which are believed to be an adaptation allowing strong adhesion to the smooth surface of the female elytra during mating. As discussed above, jumping from adhesive pads requires detachment to be rapid with minimal forces, or else the beetle will lose momentum. In fact jumping plant hoppers (*Issidae*) have been shown to decelerate during the final stages of take-off, hinting at a possible difficulty in leaving the surface (Burrows, 2009). Hence even small losses in take-off velocity could give rise to adaptations. The higher

attachment forces shown by the male proximal pads should therefore result in a reduced jumping performance. Male beetles were shown to jump with slower take-off velocities from the smooth surface than from the rough surface (no significant difference for females). A distinction was also observed between jumping behaviour in male and female beetles with male beetles jumping from a smaller fraction of the possible contact area of their pads. This behaviour prevented contact from being made with the discoidal hairs in the centre of the pad and may be a behavioural adaptation to jumping, allowing male beetles to retain their highly adhesive pads. By using only the side hairs for pushing, thereby avoiding contact with the majority of the discoidal hairs, the force required for detachment may be reduced.

6.4.3 Detachment mechanisms

The exact mechanism of detachment at such remarkable speeds is still unclear as is the full effect of the forces generated on the stability of the pads. As shown in Fig. 6.2 for both sexes, forces are very large for pulling proximal pads even though this is the direction in which they detach. Hence the question arises as to whether the beetle's inertia is sufficient to break this bond, and what effect this has on the take-off velocity of the beetle. The velocity a male beetle would lose if it was decelerated with the recorded proximal pad pulling force (~16 mN for two feet) over the duration of the proximal pad's detachment time (~0.2 ms) was estimated. Equation A.10 from Appendix A.3 shows that beetles of mass ~8 mg should lose about 0.2 ms^{-1} velocity. This is only around 20% of the recorded take-off velocity and while this still seems significant, the estimate of deceleration time is only an upper limit (due to a maximum camera recording rate) and is likely too high. Hence even with this high pulling force, the beetle will experience only a very small deceleration. Thus the beetle's inertia alone may be sufficient to break the adhesive bond. As a result, no special mechanisms may be required to facilitate detachment.

The topic of jumping from a smooth surface using adhesive pads has as yet remained largely unexplored and many questions still remain. As mentioned above, clarification is required as to whether flea beetles of other species capable of generating high take-off accelerations (Brackenbury and Wang, 1995) are able to jump from smooth surfaces without slipping, and whether insects with other pad designs use similar principles. Answering these questions on the mechanisms of jumping insect adhesive systems will provide valuable insight into the workings of biological adhesives in general. Their use in an application as demanding as jumping only serves to underline the impressive versatility of these biological structures.

7

IN VIVO ADHESION MEASUREMENTS ON INDIVIDUAL SETAE OF VARYING MORPHOLOGIES: DIFFERENCES IN STIFFNESS AND ATTACHMENT PERFORMANCE

Summary

Leaf beetles are able to climb on smooth and rough surfaces using arrays of micron-sized adhesive setae of varying morphology. The first *in vivo* measurements of individual setae in the beetle *Gastrophysa viridula,* using a glass capillary micro-cantilever are reported. The beetles possess three distinct adhesive pads on each leg which differ in both function and setal morphology. Continuous visualisation of pull-offs allowed forces to be compared between three different tarsal hair types. Male discoidal hairs were shown to adhere with the highest forces (919 ± 104 nN) to a smooth polystyrene sphere, followed by spatulate (582 ± 59 nN), and pointed (127 ± 19 nN) hairs. Discoidal hairs also proved to be stiffer (0.693 ± 0.111 Nm^{-1}) than spatulate (0.364 ± 0.039 Nm^{-1}) or pointed (0.192 ± 0.044 Nm^{-1}) hairs. This implies a greater smooth surface adhesion and stability for this hair morphology. A comparison of pull-off forces measured at the single seta and whole pad (array) levels revealed similar values of adhesive stress. This suggests that beetles may be able to distribute the load across their feet so that detachment through peeling is prevented.

7.1 INTRODUCTION

Insects, spiders and lizards are well equipped to climb almost any natural surface thanks to their highly specialised foot pads, containing arrays of fine adhesive hairs or 'setae'. These biological fibrillar adhesive systems are considered promising models for novel man-made adhesives. They are different in several respects to conventional synthetic bonders; for example they adapt well to surface roughness (Chapter 4; Persson and Gorb, 2003), exhibit controllable adhesion (Chapter 2; Autumn et al., 2006a; Autumn and Hansen, 2006; Autumn et al., 2006b; Federle, 2006) and show a resistance to contamination (Chapter 3; Hansen and Autumn, 2005).

Adhesive pads of leaf beetles are not uniform arrays of hairs, but consist of several morphologically different types of setae, which occur in a specific distribution across the three tarsal pads. At least three types of hairs have been identified: spatula-tipped, pointed and discoidal (Betz, 2003; Stork, 1980c; Stork and Evans, 1976; Voigt et al., 2008). The discoidal setae are only found in males. In *Gastrophysa viridula* De Geer (Coleoptera, Chrysomelidae), the proximal pads are dominated by discoidal setae in males, and pointed hairs in females, whereas the distal adhesive pads in both sexes are covered mainly by spatula-tipped hairs (Fig. 7.1). In Chapter 5 it was found that proximal pads differ considerably from distal ones in their performance on smooth and rough surfaces, suggesting diverse functional roles for each pad type. It is likely that this variation is based on the different types of setae dominating on the pads. On a smooth surface, pads containing mainly pointed setae generated lower adhesive forces than pads with large numbers of discoidal setae. However, as most pads contain a mixture of different seta types, array level measurements alone cannot clarify exact roles played by each seta type.

Force measurements from single hairs of varying type should therefore help to explain their properties on an individual level. Previous studies have provided single seta or single spatula measurements for dry gecko adhesives (Autumn et al., 2000; Huber et al., 2005a), although these methods have relied on detached, dehydrated setae. Insect cuticle is known to increase in stiffness when dehydrated (Vincent and Wegst, 2004), detrimental to adhesive function. Consistently, smooth insect adhesive pads were found to lose adhesion with dehydration (Jiao et al., 2000). *In vivo* measurements are therefore critical to achieve biologically meaningful results. The study by Huber et al. (2005a) used a focused ion beam (FIB) system to isolate individual gecko spatulae and measured forces with an atomic force microscope (AFM); AFM adhesion measurements were also performed on single spider setulae (Kesel et al., 2004). In both studies, the small size of the hair tips did not allow visualisation of the pull-offs. As a consequence, the number of spatulae measured and the quality of their contact before pull-off could only be estimated indirectly. This study therefore attempted to visualise the single-hair pull-offs, which is facilitated by the relatively larger size of the beetles' setae.

Several theoretical models have been developed for fibrillar adhesion, but most of their predictions still require testing in natural attachment systems. One such idea is the principle of 'force scaling' (Arzt et al., 2003). This idea is based on existing contact models, for example the Johnson-Kendall-Roberts model, which states that for a peeling adhesive, attachment forces will scale with contact length and not area (Johnson et al., 1971). This result

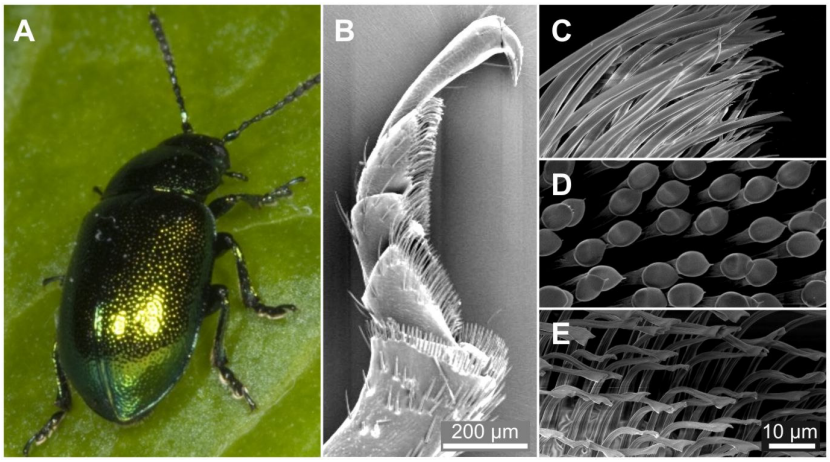

Figure 7.1: The adhesive pad morphology of the dock beetle Gastrophysa viridula (A), showing the three tarsal pads of the hind leg (B) and three hair morphologies; pointed (C), discoidal (D) and spatula tipped (E). (C-E) are presented to the same scale.

implies that the division of contact area will actually enhance adhesive force (Arzt et al., 2003; Autumn et al., 2002; Spolenak et al., 2004). However, gain of adhesion by contact splitting requires that the stresses are distributed evenly across the contact zone so that there is no peeling of the pad during detachment (Federle, 2006; Hui et al., 2004). It is as yet unclear under which situations this condition applies. If force scaling is to occur in natural systems, adhesive stresses should be similar whether measured at the level of individual contacts or of the whole pad. This study therefore additionally aims to compare the stresses generated by single hairs with individual pad recordings.

7.2 METHODS

7.2.1 Individual seta forces

In order to measure the adhesive force of a single beetle seta a method similar to the single gecko seta adhesion measurements of Autumn et al (2000) was used. For *in vivo* testing, individual hairs could not be removed from the pads as in Autumn et al (2000) or Orso et al. (2006). Hence two finely drawn glass capillaries (length 5 mm, approximate taper 5°, diameter at tip 11.5 µm) were used as micro-cantilevers. A 25 µm diameter polystyrene microsphere (Polysciences Inc., Warrington, PA, USA) was attached to the tip of each capillary using two-component epoxy glue 45705 (UHU, Bühl, Germany) to allow contact with individual hairs of the planar beetle foot pad (see Fig. 7.2). Glueing was performed under magnification using two precision micromanipulators.

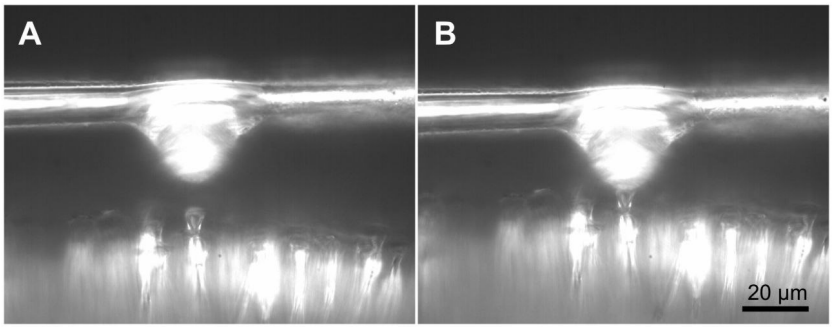

Figure 7.2: The glass capillary micro-cantilever with spherical tip before (A) and during (B) contact with a single spatula tipped hair.

The beams' spring constants were measured using a MC5 microbalance (Sartorius, Goettingen, Germany). The capillary was mounted on a closed-loop piezo positioning stage P-611.ZS (Physik Instrumente, Karlsruhe, Germany), attached to a micromanipulator. The microsphere tip was brought into contact with the weighing pan of the balance, observed from the side with a Leica MZ16 stereomicroscope (Leica Microsystems GmbH, Wetzlar, Germany). The weighing pan of the balance, accurate to the nearest µg, is protected from air movements by a draft shield, leaving only a small window free to allow access. The piezo stage was controlled using LabVIEW (National Instruments, Austin, TX, USA) software. The capillary tip was moved towards the balance in steps of 10 µm up to a maximum displacement of 100 µm and the readout of the balance recorded. The compliance of the balance itself was assessed by using an inflexible steel rod in place of the capillary (maximum displacement 20 µm), recording a spring constant of 578 Nm^{-1} for the balance. A linear regression line (R^2=0.99) was fitted to the data for each capillary. After subtracting the displacement of the balance from the total displacement, the spring constant of the beam was calculated. Two beams of spring constants 0.238 and 0.182 Nm^{-1} were used.

G. viridula beetles were restrained using blu-tack (Bostik, Leicester, UK), and a single distal pad of the rear leg isolated and immobilised. Beetles were then mounted on a glass tube and attached to an open-loop piezo drive controlled manually via an amplifier P-280-30 and E-663 (Physik Instrumente). The open-loop piezo was used as it allowed manual position control via a turning knob. The piezo stage was mounted beneath a Leitz Secolux compound microscope (Leica Microsystems Gmbh) so that a side view of the setae was obtained using a 50x objective. The cantilever was brought level with the beetle foot using a micromanipulator. Using the piezo drive, the insect pad was moved towards the beam, allowing the tip to make contact with a single hair. It was then withdrawn (at ~10 μms^{-1}) and the resulting deflection of the beam

recorded using a HotShot PCI 1280 B/W high-speed camera (NAC image technology, Simi Valley, CA, USA) at 120 fps. The full movement of the cantilever tip was digitised and tracked using the DLTdataViewer2 program (Hedrick, 2008), giving complete force curves for each pull-off. From the peak deflection and the beam spring constant the adhesive force of the single seta was calculated. The compression and following extension of the individual hairs during pull-offs were used to determine the spring constant of the seta as the slope of the Model II regression of force against displacement. A single pixel corresponded to 0.238 μm, corresponding to a force of 43.2 nN. A total number of 54 single hair measurements from 8 animals were performed.

In order to investigate the adhesive properties of each seta type, individual recordings were made from hairs on all parts of the distal foot pad, allowing measurements to be taken from the spatula-tipped (n=24), pointed (n=13) and discoidal (n=11) hairs. The hair type could be seen with the microscope during testing. To gain access to discoidal hairs, located in the centre of the male pads, some of the outer (pointed and spatula-tipped) hairs were 'shaved' off under a stereomicroscope prior to testing using a sharp glass pipette fragment.

The effect of a proximal shear movement before pull-off on the spatula-tipped hairs was tested. A small synchronous motor 336-438 (RS Components Ltd., Corby, UK) was attached to the micromanipulator, allowing a slow (~5 μms^{-1}) and vibration-free proximal-distal movement of the cantilever tip. The cantilever tip could therefore be brought into contact with the beetle seta and given a short 3 μm shear movement before detachment (distally along the pad, corresponding to a pull of the foot towards the body) (n=6).

7.2.2 Single-pad forces

To compare the forces of individual setae with those produced by arrays of hairs, forces were measured from individual pads of live beetles (n=25 measurements from 6 animals) using a strain gauge force transducer as described in Chapter 2. Beetles were restrained as above with the single distal-most pad of the rear leg isolated and immobilised. They were then mounted on a glass tube and fixed below the glass plate at the end of the force transducer. To test the pads on the same substrate as the individual setae, a substrate consisting of a glass plate, spin-coated at 30 rps for 60 s with polystyrene (Sigma-Aldrich, St. Louis, MO, USA), prepared as a 5% w/w solution with toluene and cured at 50° for 12 hours was used. The force transducer consisted of a 2D bending beam strain gauge fixed to a motor positioning stage M-126PD (Physik Instrumente) controlled with custom LabVIEW software. A feedback loop was

used to load the pad with a normal force of between 0.3 and 0.5 mN ensuring proper contact of the whole pad (see Chapter 2). Perpendicular pull-offs were then performed at 500 μms^{-1} to measure adhesive forces. Contact area was visualised using a stereomicroscope with coaxial illumination (Federle et al., 2002b) and recorded using the HotShot high-speed camera. In order to allow calculation of seta adhesive stress, setal contact area was measured from the contact images of single pads.

7.3 RESULTS

7.3.1 *In vivo* single seta measurements

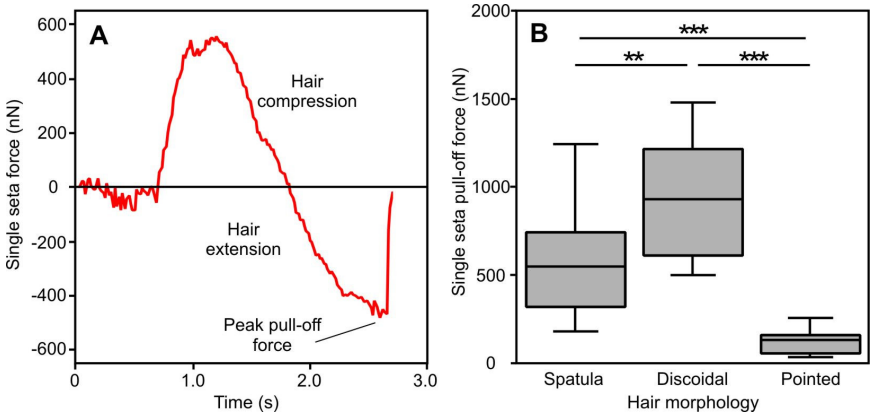

Figure 7.3: (A) a typical force curve showing the full pull-off trace from a single spatula hair. (B) *In vivo* single hair forces for the three seta types (n=24, 11, and 13 respectively) found on the distal pad of *Gastrophysa viridula*. Plot shows medians (centre lines), interquartile ranges (boxes), and the largest and smallest values (whiskers) that are not outliers. Significance levels: * P<0.05, ** P<0.01, *** P<0.001.

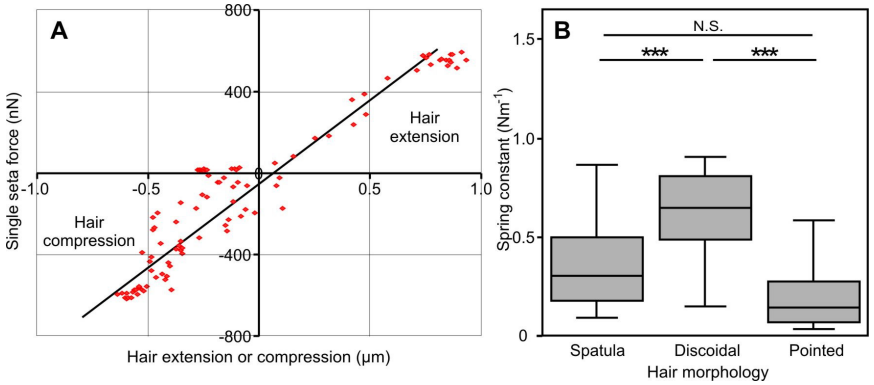

Figure 7.4: (A) typical force vs. extension curve for a single spatula tipped hair, allowing the calculation of spring constant from the gradient of the calculated model II regression line (plotted). The graph gives both the compression and extension sections of the curve. (B) spring constant values for each seta type (n=24, 11, and 13 respectively). Plot shows medians (centre lines), interquartile ranges (boxes), and the largest and smallest values (whiskers) that are not outliers (not shown). Significance levels: * P<0.05, ** P<0.01, *** P<0.001, N.S. not significant.

Single seta pull-off forces were recorded for each of the three hair morphologies of *G. viridula*. These are presented in Fig. 7.3 along with a typical force curve of the pull-off. Hairs showed highly significant differences in attachment performance (one way ANOVA: $F_{2,45}$=27.295, P≤0.001). Discoidal, male specific hairs produced significantly higher adhesive forces than spatula-tipped hairs (Tukey HSD test: P=0.003). The tips of the pointed hairs however gave 4.5 times lower values than spatula-tipped hairs (P≤0.001).

To test the effect of a preceding shear movement, 3 μm pulling slides were performed before the pull-off in 6 recordings on spatula-tipped hairs. Forces averaged 510 ± 76 nN showing no evidence for an increase in pull-off forces (Mann Whitney U test: U_{29}=63, P=0.641).

Force values were used to calculate the spring constant of each hair using their observed compression and extension before detachment. A typical force vs. extension plot is shown in Fig 7.4A. The spring constant measured for each hair type are plotted in Fig 7.4B. The differences were significant (one way ANOVA: $F_{2,51}$=13.208, P≤0.001) with discoidal hairs showing significantly higher spring constants than spatula-tipped hairs (Tukey HSD test: P≤0.001). However spring constants of spatula and pointed hairs were not significantly different (P=0.091).

7.3.2 Comparison of the hierarchical attachment levels

Measurements of attachment force were made at the single pad level; recording a pull-off force of 0.30 ± 0.03 mN (mean ± s.e.m.). Actual spatula hair contact area was recorded from contact area images as 40.1 ± 1.9 μm² and used to calculate adhesive stress in

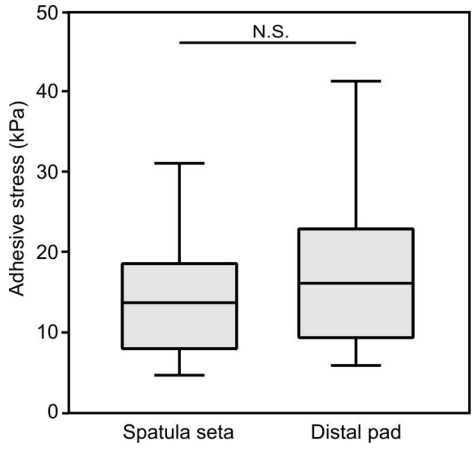

Figure 7.5: Adhesive stress recordings from single seta (n=24) and whole pads (n=25). Plots show medians (centre lines), interquartile ranges (boxes), and the largest and smallest values (whiskers) that are not outliers. Significance levels: * P<0.05, ** P<0.01, *** P<0.001, N.S. not significant.

these hairs. Stresses are presented above (Fig. 7.5), with no significant differences found between these hierarchical levels ($t_{26.2}$=-1.297, P=0.206, unpaired t-test).

7.4 DISCUSSION

7.4.1 Single hair forces

The ability to visualise and measure forces from individual hairs allowed the performance and function of different hair types found on beetle adhesive pads to be investigated. In Chapter 5 it was shown that pads bearing different seta morphologies have differing adhesive abilities on smooth and rough surfaces. The adhesive forces of each hair type can shed light on the different roles played by these hairs. Discoidal hairs were more adhesive than either of the other hair types. They were also stiffer which may help to increase the adhesive forces by allowing them to distribute the load across the entire tip, reducing peeling. This supports previous data obtained at the pad level, which showed that male pads (containing discoidal hairs) generate significantly greater adhesion on smooth surfaces than female pads (where discoidal hairs are absent) (see Chapter 5). The stronger adhesion of discoidal hairs may be essential for elytra attachment during mating (Chapter 5; Pelletier and Smilowitz, 1987; Stork, 1980a; Voigt et al., 2008).

SEM images of the tips of the discoidal hairs show a default position parallel to the surface, allowing them to engage the surface with ease (see Fig. 7.1 and Chapter 5). Spatula-shaped setae however suggest a default position angled to the surface. This non-parallel orientation may require deformation of the tip to bring it into full contact, weakening attachment and further explaining the difference in adhesion seen between spatula and discoidal hair types. Gecko spatulae are also non-parallel suggesting a 'non adhesive' default position, with the spatulae shown to require a proximal shear in order to align their tips to the surface and generate forces (Autumn and Hansen, 2006; Autumn and Peattie, 2002). Beetle spatula hairs may therefore be similarly designed to allow rapid and effortless detachment. However, it should be noted that in the present study, no increase in force was observed for spatula hairs following a shear movement of the cantilever tip. Additionally previous measurements of the distal pad (containing mostly spatula hairs) show that pull-off forces can be generated without a shear movement (see Chapter 3). Hence it is unlikely that beetle spatula hairs are fully non-adhesive as default.

Perhaps unsurprisingly, the tapered, pointed hairs generated very little adhesive force when contacted at the tip. These hairs may therefore only contribute significantly to pad forces

when they make contact with the full length of the hair, rather than just the tip. This is also seen in the contact images of whole pads when pressed against the surface, where the pointed hairs are seen lying flat against the substrate (Chapters 2 and 5; Geiselhardt et al., 2009b). This property would make them mainly relevant for generating friction to prevent the pad from sliding.

7.4.2 Single hair spring constants

Spring constant measurements indicate a further functional difference between hair types, with discoidally tipped hairs proving to be 1.9 times stiffer than those with spatula tips. This confirms previous single pad results; effective elastic moduli recorded at the array level showed the proximal pads of males (containing the highest numbers of discoidal hairs) to be twice as stiff as the distal pads (containing predominately spatula hairs) (Chapter 5). This higher stiffness confirms an important biological function for the discoidal hairs. Although all *G. viridula* pads are direction-dependent with higher forces in the pulling direction, the proximal pads are more stable during pushing, providing strong shear forces in both directions (Chapter 5). The higher stability may be important for vertical climbing as it allows legs below the centre of mass to push (Chapter 5). Assuming that the hairs can be modelled as simple bending beams with radius r, length l, elastic modulus E and angle θ to the horizontal then their spring constant can be derived using the small-strain cantilever model (Glassmaker et al., 2004; Persson, 2003; Sitti and Fearing, 2003) as:

$$k_{hair} = \frac{3\pi r^4 E}{4l^3 \cos^2 \theta} \qquad [7.1]$$

This equation shows clearly that whilst the material properties of the hair will affect stiffness, increasing the radius (which appears to the fourth power) of the hairs will result in a far greater increase in spring constant. It is therefore likely that the increased stiffness of the discoidal hairs originates in a greater seta thickness. Indeed previous SEMs of the discoidal hairs from the stiff proximal pads of dock beetles have shown them to be thicker than the spatula hairs from the soft distal pads (see Chapter 5).

The low spring constant of the spatula hairs may allow adaptability towards surface roughness. Again, this supports previous array level data with male beetles generating higher attachment forces on rough substrates with their distal pads than with their proximal pads (Chapter 5). The thin flexible design of the spatula tips may also allow the hairs to compensate for fine scale surface roughness (Eimüller et al., 2008; Persson and Gorb, 2003).

This could be tested further with a rough or patterned substrate attached to the cantilever tip.

The spring constant of pointed hairs was not significantly higher than spatula hairs. As proximal pads of female beetles, which contain only pointed hairs showed high effective elastic moduli (Chapter 5) this result is less well explained by array level data. However in the present study measurements were performed only at the tips of the pointed hairs. As these hairs taper towards the end, the tips may be more flexible allowing them to bend and increase surface contact during compression, whereas the base may remain stiff providing pushing stability.

7.4.3 Array level adhesive stresses

Comparisons can be made between seta and array attachment levels and these results allow an approximate test of the principal requirement for force scaling; equal load sharing between setae (Federle, 2006; Hui et al., 2004). Stresses were found to be comparable between individual hairs and single pads, implying that the requirement holds in this system. If the stresses were concentrated along the edge of the pad contact zone, the total force of pad or whole animal measurements would be less than the forces measured from single hairs multiplied by the numbers of hairs present. However, in Chapter 2 no evidence of force scaling was found when comparing smooth and hairy systems. Other requirements are necessary for the force scaling model to hold and these may not be met in this system. For example, the adhesive forces of individual setal contacts might not scale with their width or radius but with contact area (e.g. if the tip geometry is concave). Further work is needed before it can be established whether force scaling plays a role in the maximisation of adhesion in the beetle attachment system.

Interestingly, gecko hairs have shown a significant decrease in performance when comparing the shear stresses supported at the array (Gravish et al., 2008) and single seta (Autumn et al., 2000; Hansen and Autumn, 2005) levels. This result appears to imply that geckos are unable to follow the force scaling model. The larger size of gecko pads (measured total pad sizes are approximately 227.1 mm^2 (Irschick et al., 1996) as compared to around 0.47 mm^2 for beetles (Chapter 5)) may make it difficult for them to resist peeling. The large force decrease in geckos may also result from their pad design which contains folds of adhesive arrays possibly preventing full setal contact to a surface on the macroscopic scale.

The methodology employed in this study allowed *in vivo* recordings of the adhesive performance of individual hairs of a beetle foot pad. These combined with single pad and whole insect recordings provide a more complete set of measurements detailing

the performance of these natural adhesives. However, much work is still needed in order to understand the functional morphology of these biological adhesives. This is particularly important given the rapid advances being made in the synthetic replication of these fibrillar systems using patterned and moulded polymers or carbon nano-tubes (see Appendix A.1). For developing such biomimetic adhesives, it will be essential to achieve a better understanding of the detailed properties and functions of the biological systems that are being mimicked.

8

CONCLUDING SUMMARY

A large number of animals make use of adhesive systems to climb across smooth surfaces. Insects in particular have developed a wide range of tarsal structures allowing them to exploit their habitats. Highly specialised smooth or fibrillar adhesive pads have repeatedly evolved in many orders. They out-perform synthetic adhesives in several important respects, combining highly controllable and effective attachment with reusability and resistance to contamination, making them important subjects for biomimetics. Hairy pads in particular are thought to possess many impressive properties resulting from the division of contact which allows compliance, high contact perimeter and specialised tip designs. Previous studies have investigated the fibrillar adhesive system of the gecko (see: Autumn, 2006b) but less focus has been directed towards the performance and mechanisms of hairy adhesive systems in insects. The fibrillar pads of leaf beetles were therefore used as a model system for this study. Various methodologies were used to measure and quantify the adhesive and frictional forces generated by insect attachment systems at every hierarchical level; whole animal, individual tarsal pad and single hair.

To investigate the functions of the fibrillar pad design, the attachment performance of the hairy pads of the leaf beetle *Gastrophysa viridula* was compared with that of the smooth arolia of the stick insect *Carausius morosus*. Three measures of attachment performance were compared; the attachment stresses supported by the pads, the ability of the pads to detach and their ability to resist contamination and self-clean.

Absolute adhesive and frictional stresses were found to be remarkably similar between the two systems. This contradicts the theoretical concept of contact splitting, which predicts higher adhesive stresses for fibrillar adhesives. A possible explanation for this is the detachment mode of the pad; if peeling occurs this will result in a stress concentration at the pad edge. This behaviour would invalidate the assumptions of the force scaling model which requires an even load distribution. The finding shows that contact splitting is unable to explain the performance of insect pads, at least under the investigated conditions.

In order to run on smooth surfaces with their adhesive pads, insects must also possess highly dynamic attachment systems. Detachment ability was therefore compared between smooth and hairy systems. The fibrillar pads showed a greater direction-dependence of friction forces than smooth pads. This property may allow the animal to attach and detach its feet via simple proximal-distal movements. The mechanisms of this increased direction-dependence may be explained by the opportunities for morphological variation offered by a system of divided contacts. For example angled hairs with asymmetric tips will buckle and peel when pushed but not when pulled. This property allows for a passive mechanism to effectively control attachment and effortless detachment in insect hairy pads.

As well as being highly dynamic, insect adhesive systems must also possess some mechanism to prevent contamination or they would rapidly clog with dirt particles and become useless after just a few steps. A self-cleaning ability was tested by contaminating pads of beetles and stick insects with microspheres of varying sizes. Although forces dropped by up to 90% following contamination, pads began to recover their adhesive properties after several simulated steps on a smooth surface. Analysis of footprints showed that they had shed much of the contamination confirming for the first time a self-cleaning ability in insect adhesive pads. This ability was comparable to that previously observed for geckos and may even exceed it in efficiency. The fibrillar system showed significantly faster rates of recovery, possibly as a result of the small seta tips which may allow particles to be moved to the edge of each contact via microscale movements. In contrast a smooth pad may deform around a contaminating particle, trapping it within the contact zone. Only for particles with diameters corresponding to the inter-setae distances (~10 μm) was self-cleaning reduced in hairy systems, explained by the tendency of particles to lodge between the hairs. The presence of an adhesive fluid is likely important in the self-cleaning process of both systems as this may allow contamination to be 'washed' from the pad.

Whilst obviously limited to only one representative of each group, the model hairy system studied was therefore shown to outperform the smooth system in two important respects; level of direction-dependence and rate of self-cleaning. However, the smooth system did still demonstrate both of these properties and showed similar levels of maximal adhesive stress. Clearly smooth pads are also well developed natural adhesives and are consequently found in a wide range of insect orders. This to some extent challenges the assumption that hairy systems may dramatically outperform smooth systems. However, a more dynamic attachment system could allow slightly higher running speeds at a lower energetic cost and a more efficient self-cleaning

mechanism may allow colonisation of habitats containing extreme levels of contamination. Further work would be needed to investigate whether these properties represent limiting factors for locomotion employing a smooth adhesive system.

The above studies addressed attachment performance on smooth surfaces. However, few natural surfaces are perfectly smooth and any biological attachment system must be capable of adapting to some degree of substrate roughness. The ability of the beetle hairy system to adhere was therefore tested over a wide range of roughness levels by quantifying whole-body attachment forces on a series of moulded substrates. Whilst the insects could adhere with forces of over forty times their body weight on smooth surfaces, attachment was significantly reduced for all length scales of surface roughness. Attachment was minimal for asperities smaller than the hair tips, where only partial contact could be made. An increase in attachment was however shown for larger particle sizes. This is in agreement with previous studies and suggests that the surface profile at these asperity sizes is relatively smooth for the seta tips. Good contact for the majority of hairs is then achieved due to the flexibility of the hairs. High attachment was also observed on the beetle's host plant, despite its 'average roughness' value underlining the importance of different parameters for accurately characterising the properties of surface profiles. For coarse rough surfaces, claws were able to take over from adhesive hairs and are clearly an important component of the beetles' attachment systems allowing them to climb on a diverse range of rough and smooth substrates.

Many models of fibrillar adhesion describe only generalised arrays of uniform setae. However, these models face limitations when dealing with actual biological attachment systems. *G. viridula*, as typical of the Chrysomelidae, possesses three fibrillar adhesive pads on each leg and displays variation in hair morphology both within and between pads as well as between the sexes. In fact, three distinct hair types are found across the pads; spatula tipped, discoidally tipped and pointed hairs.

The material properties of each pad were investigated with the proximal-most pad proving stiffer than the distal pad. This was shown to allow higher friction forces whilst sliding in the pushing direction. The soft distal pad, on the other hand, was highly directionally-dependent and was able to better conform to rough surfaces. This difference between pads provides evidence for a division of labour between tarsal segments in the dock beetle allowing the beetle to climb rapidly over smooth or rough surfaces. Video recordings of free climbing beetles confirmed that the distal pads were used for pulling whereas the proximal pads were used

for pushing. Using the measured pad spring constants, the elastic modulus of the hair cuticle was also estimated, and found to be strikingly high despite the low effective moduli of the distal pads. Hence the high aspect ratio of the hairs allows soft arrays to be formed from stiff wear resistant setae. Given that a strong sexual dimorphism is present, with male beetles possessing large numbers of discoidally tipped hairs on the proximal pad, attachment performance was also compared between males and females. The discoidal hairs have flat tips aligned parallel to the surface and are likely used for firm attachment to the smooth elytra of the female during mating. Male proximal pads were shown to generate stronger attachment forces to smooth substrates and showed less direction-dependence than those of female beetles. This implies a specialisation of the male system towards adhesion during mating, at the cost of a weaker attachment to rough surfaces and less rapid detachment.

The conflict between detachment and the need to push, solved via the division of labour system, was further investigated in the extreme case of jumping in flea beetles. The pads of males and females of the flea beetle *Altica lythri* were shown to possess the same direction-dependence properties as the dock beetles. Whilst jumping from a smooth surface, beetles exclusively used the proximal pads. They were even able to jump from an inverted position, by switching from the distal pads whilst resting to the proximal ones when jumping. Flea beetles show a similar sexual dimorphism of setae. However, male beetles jumped with significantly lower take-off velocities from smooth surfaces and even showed a behavioural difference to females by jumping only from the outer edge of their proximal pads. This behaviour may derive from the highly adhesive discoidal setae which could otherwise hamper detachment.

To investigate the properties of different seta morphologies and to understand how they influence whole-animal and array level performance, single hair forces were measured. Using a glass capillary cantilever, pull-off forces were quantified for each seta type of the beetles. The discoidal, male-specific hairs were shown to be stiffer and to provide the strongest attachment to the smooth cantilever tip. This likely affects array level performance and contributes to the overall pad stability and attachment strength. Pointed hairs generated only weak attachment forces at their tips and may instead be designed to support friction forces when lying flat, compressed along the length of the hair.

In summary, the hairy adhesive systems of insects are highly developed structures, which allow them to climb across many different surfaces. They allow rapid and dynamic attachment and detachment, are able to self-clean and, in combination with the

animals' claws, allow attachment to a wide range of substrate profiles. Hairy pads were similar to smooth pads in the magnitude of adhesive stresses supported yet they out performed them in detachability and self-cleaning.

There are however large differences in morphology and performance even within setal arrays of a single beetle. Through the investigation of the tarsal pads of different leaf beetles, attachment properties were shown to be divided across separate tarsal pads allowing direction-dependence and rough surface attachment, as well as the ability to effectively push. This underlies the importance of specific models of fibrillar adhesion which take into account the varying hair designs and specialised adaptations. Through the study of biological systems we can better understand these impressive natural adhesives, which will be important for developing biomimetic structures.

"*These hairy feet are of great use to this little insect…!*"

Benedict Jaeger (1854)

Aksak, B., Murphy, M. P. and Sitti, M. (2007). Adhesion of biologically inspired vertical and angled polymer microfiber arrays. *Langmuir* 23, 3322-3332.

Amontons, G. (1709). Histoire de l'Académie Royale des Sciences avec les Mémoires de Mathématique et de Physique, 1699-1708. Amsterdam: Chez Gerald Kuyper.

Arzt, E., Gorb, S. and Spolenak, R. (2003). From micro to nano contacts in biological attachment devices. *Proceedings of the National Academy of Sciences, USA* 100, 10603-10606.

Asbeck, A. T., Kim, S., Cutkosky, M. R., Provancher, W. R. and Lanzetta, M. (2006). Scaling hard vertical surfaces with compliant microspine arrays. *International Journal of Robotics Research* 25, 1165-1179.

Autumn, K. (2006a). How gecko toes stick. *American Scientist* 94, 124-132.

Autumn, K. (2006b). Properties, principles, and parameters of the gecko adhesive system. In *Biological Adhesives* eds. A. M. Smith and J. A. Callow, pp. 225-256. Berlin, Heidelberg: Springer-Verlag.

Autumn, K. (2007). Gecko adhesion: structure, function, and applications. *MRS bulletin* 32, 473-478.

Autumn, K., Dittmore, A., Santos, D., Spenko, M. and Cutkosky, M. (2006a). Frictional adhesion: a new angle on gecko attachment. *Journal of Experimental Biology* 209, 3569-3579.

Autumn, K. and Hansen, W. (2006). Ultrahydrophobicity indicates a non-adhesive default state in gecko setae. *Journal of Comparative Physiology A* 192, 1205-1212.

Autumn, K., Hsieh, S. T., Dudek, D. M., Chen, J., Chitaphan, C. and Full, R. J. (2006b). Dynamics of geckos running vertically. *Journal of Experimental Biology* 209, 260-272.

Autumn, K., Liang, Y. A., Hsieh, S. T., Zesch, W., Chan, W. P., Kenny, T. W., Fearing, R. and Full, R. J. (2000). Adhesive force of a single gecko foot-hair. *Nature* 405, 681-685.

Autumn, K., Majidi, C., Groff, R. E., Dittmore, A. and Fearing, R. (2006c). Effective elastic modulus of isolated gecko setal arrays. *Journal of Experimental Biology* 209, 3558-3568.

Autumn, K. and Peattie, A. M. (2002). Mechanisms of adhesion in geckos. *Integrative and Comparative Biology* 42, 1081-1090.

Autumn, K., Sitti, M., Liang, Y. A., Peattie, A. M., Hansen, W. R., Sponberg, S., Kenny, T. W., Fearing, R., Israelachvili, J. N. and Full, R. J. (2002). Evidence for van der Waals adhesion in gecko setae. *Proceedings of the National Academy of Sciences, USA* 99, 12252–12256.

Barnes, W. J. P. (1999). Tree frogs and tire technology. *Tire Technology International* March 99, 42-47.

Barnes, W. J. P. (2007). Functional morphology and design constraints of smooth adhesive pads. *MRS bulletin* 32, 479-485.

Barnes, W. J. P., Riehle, M. O., Smith, J. M. and Federle, W. (2004). Wet adhesion in tree frogs. *Comparative Biochemistry and Physiology Part A: Molecular & Integrative Physiology* 137, S87.

Barnes, W. J. P., Smith, J., Oines, C. and Mundl, R. (2002). Bionics and wet grip. *Tire Technology International* Dec 2002, 56-60.

Bergsten, J. and Miller, K. B. (2007). Phylogeny of diving beetles reveals a coevolutionary arms race between the sexes. *PLoS ONE* 2, e522.

Bergsten, J., Toyra, A. and Nilsson, A. N. (2001). Intraspecific variation and intersexual correlation in secondary sexual characters of three diving beetles (Coleoptera: Dytiscidae). *Biological Journal of the Linnean Society* 73, 221-232.

Betz, O. (2002). Performance and adaptive value of tarsal morphology in rove beetles of the genus *Stenus* (Coleoptera, Staphylinidae). *Journal of Experimental Biology* 205, 1097–1113.

Betz, O. (2003). Structure of the tarsi in some *Stenus* species (Coleoptera, Staphylinidae): External morphology, ultrastructure, and tarsal secretion. *Journal of Morphology* 255, 24-43.

Beutel, R. G. and Gorb, S. N. (2001). Ultrastructure of attachment specializations of hexapods (Arthropoda): evolutionary patterns inferred from a revised ordinal phylogeny. *Journal of Zoological Systematics and Evolutionary Research* 39, 177-207.

Biewener, A. and Daniel, T. (2010). A moving topic: control and dynamics of animal locomotion. *Biology Letters* 6, 387-388.

Bogue, R. (2008). Biomimetic adhesives: a review of recent developments. *Assembly Automation* 28, 282-288.

Bohn, H. F. and Federle, W. (2004). Insect aquaplaning: *Nepenthes* pitcher plants capture prey with the peristome, a fully wettable water-lubricated anisotropic surface. *Proceedings of the National Academy of Sciences, USA* 101, 14138-14143.

Brackenbury, J. and Wang, R. (1995). Ballistics and visual targeting in Flea-Beetles (Alticinae). *Journal of Experimental Biology* 198, 1931-1942.

Burrows, M. (2006). Morphology and action of the hind leg joints controlling jumping in froghopper insects. *Journal of Experimental Biology* 209, 4622-4637.

Burrows, M. (2009). Jumping performance of planthoppers (Hemiptera, Issidae). *Journal of Experimental Biology* 212, 2844.

Calmet, A. (1730). Dictionnaire historique, critique, chronologique, géographique et littéral de la Bible. Paris: Bousquet.

Chung, J. Y. and Chaudhury, M. K. (2005). Roles of discontinuities in bio-inspired adhesive pads. *Journal of The Royal Society Interface* 2, 55-61.

Clemente, C. J. and Federle, W. (2008). Pushing versus pulling: division of labour between tarsal attachment pads in cockroaches. *Proceedings of the Royal Society B* 275, 1329-1336.

Coddington, J. A. and Levi, H. W. (1991). Systematics and evolution of spiders (Araneae). *Annual Review of Ecology and Systematics* 22, 565-592.

Comyn, J. (1997). Adhesion Science. Cambridge: Royal Society of Chemistry.

Crisp, D. J., Walker, G., Young, G. A. and Yule, A. B. (1985). Adhesion and substrate choice in mussels and barnacles. *Journal of Colloid and Interface Science* 104, 40-50.

Crosby, A. J., Hageman, M. and Duncan, A. (2005). Controlling polymer adhesion with "pancakes". *Langmuir* 21, 11738 -11743.

Dahlquist, C. A. (1969). Pressure-sensitive adhesives. In *Treatise on Adhesion and Adhesives, Vol. 2* ed. R. L. Patrick, pp. 219-260. New York: Marcel Dekker.

Dai, Z., Gorb, S. N. and Schwarz, U. (2002). Roughness-dependent friction force of the tarsal claw system in the beetle *Pachnoda marginata* (Coleoptera, Scarabaeidae). *Journal of Experimental Biology* 205, 2479–2488.

del Campo, A., Alvarez, I., Filipe, S. and Wilhelm, M. (2007). 3D microstructured surfaces obtained by soft-lithography using fast-crosslinking elastomeric precursors and 2D masters. *Advanced Functional Materials* 17, 3590.

del Campo, A. and Arzt, E. (2007). Design parameters and current fabrication approaches for developing bioinspired dry adhesives. *Macromolecular Bioscience* 7, 118-127.

Del Campo, A. and Greiner, C. (2007). SU-8: a photoresist for high-aspect-ratio and 3D submicron lithography. *Journal of Micromechanics and Microengineering* 17, 81.

Dickinson, M. H., Farley, C. T., Full, R. J., Koehl, M. A. R., Kram, R. and Lehman, S. (2000). How animals move: an integrative view. *Science* 288, 100-106.

Dirks, J. H., Clemente, C. J. and Federle, W. (2009). Insect tricks: two-phasic foot pad secretion prevents slipping. *Journal of The Royal Society Interface* 7, 587-593.

Drechsler, P. and Federle, W. (2006). Biomechanics of smooth adhesive pads in insects: Influence of tarsal secretion on attachment performance. *Journal of Comparative Physiology A* 192, 1213-1222.

Edwards, P. B. (1982). Do waxes on juvenile *Eucalyptus* leaves provide protection from grazing insects? *Australian Journal of Ecology* 7, 347-352.

Eimüller, T., Guttmann, P. and Gorb, S., N. (2008). Terminal contact elements of insect attachment devices studied by transmission X-ray microscopy. *Journal of Experimental Biology* 211, 1958-1963.

Eisner, T. and Aneshansley, D. J. (2000). Defense by foot adhesion in a beetle (*Hemisphaerota cyanea*). *Proceedings of the National Academy of Sciences, USA* 97, 6568-6573.

Emerson, S. B. and Diehl, D. (1980). Toe pad morphology and mechanisms of sticking in frogs. *Biological Journal of the Linnean Society* 13, 199-216.

Farish, D. J. (1968). Cleaning movements in insects and more about bees. *Curious Naturalist* 7, 5-6.

Farish, D. J. (1972). The evolutionary implications of qualitative variation in the grooming behavior of the Hymenoptera (Insecta). *Animal Behaviour* 20, 662-676.

Federle, W. (1999). Significance of epicuticular wax barriers in ant-plants of the genus *Macaranga* (Euphorbiaceae). *Zoology-Analysis of Complex Systems* 102, Supplement II, (DZG 92.1), 27.

Federle, W. (2006). Why are so many adhesive pads hairy? *Journal of Experimental Biology* 209, 2611-2621.

Federle, W., Barnes, W. J. P., Baumgartner, W., Drechsler, P. and Smith, J. M. (2006). Wet but not slippery: boundary friction in tree frog adhesive toe pads. *Journal of The Royal Society Interface* 3, 689-697.

Federle, W., Baumgartner, W. and Hölldobler, B. (2004). Biomechanics of ant adhesive pads: frictional forces are rate- and temperature-dependent. *Journal of Experimental Biology* 207, 67-74.

Federle, W., Brainerd, E. L., McMahon, T. A. and Hölldobler, B. (2001). Biomechanics of the movable pretarsal adhesive organ in ants and bees. *Proceedings of the National Academy of Sciences, USA* 98, 6215-6220.

Federle, W. and Endlein, T. (2004). Locomotion and adhesion: dynamic control of adhesive surface contact in ants. *Arthropod Structure & Development* 33, 67-75.

Federle, W., Maschwitz, U., Fiala, B., Riederer, M. and Hölldobler, B. (1997). Slippery ant-plants and skilful climbers: Selection and protection of specific ant partners by epicuticular wax blooms in *Macaranga* (Euphorbiaceae). *Oecologia* 112, 217-224.

Federle, W., Maschwitz, U. and Hölldobler, B. (2002a). Pruning of host plant neighbors as defence against enemy ant invasions: *Crematogaster* ant partners of *Macaranga* protected by 'wax barriers' prune less than their congeners. *Oecologia* 132, 264-270.

Federle, W., Riehle, M., Curtis, A. S. G. and Full, R. J. (2002b). An integrative study of insect adhesion: mechanics and wet adhesion of pretarsal pads in ants. *Integrative and Comparative Biology* 42, 1100-1106.

Federle, W., Rohrseitz, K. and Hölldobler, B. (2000). Attachment forces of ants measured with a centrifuge: better "wax-runners" have a poorer attachment to a smooth surface. *Journal of Experimental Biology* 203, 505-512.

Frisch-Fay, R. (1962). Flexible bars. London: Butterworths.

Full, R. J., Blickhan, R. and Ting, L. H. (1991). Leg design in hexapedal runners. *Journal of Experimental Biology* 158, 369-390.

Furth, D. G. (1982). The metafemoral spring of flea beetles (Chrysomelidae: Alticinae). *Spixiana* Suppl. No. 7, 11-27.

Furth, D. G., Traub, W. and Harpaz, I. (1983). What makes *Blepharida* jump? A structural study of the metafemoral spring of a flea beetle. *Journal of Experimental Zoology* 227, 43–47.

Gadelmawla, E. S., Koura, M. M., Maksoud, T. M. A., Elewa, I. M. and Soliman, H. H. (2002). Roughness parameters. *Journal of Materials Processing Technology* 123, 133-145.

Gagnepain, J. J. and Roques-Carmes, C. (1986). Fractal approach to two-dimensional and three-dimensional surface roughness. *Wear* 109, 119-126.

Gao, H., Wang, X., Yao, H., Gorb, S. and Arzt, E. (2005). Mechanics of hierarchical adhesion structures of geckos. *Mechanics of Materials* 37, 275-285.

Gao, H. and Yao, H. (2004). Shape insensitive optimal adhesion of nanoscale fibrillar structures. *Proceedings of the National Academy of Sciences, USA* 101, 7851-7856.

Gaume, L., Perret, P., Gorb, E., Gorb, S., Labat, J.-J. and Rowe, N. (2004). How do plant waxes cause flies to slide? Experimental tests of wax-based trapping mechanisms in three pitfall carnivorous plants. *Arthropod Structure and Development* 33, 103-111.

Geim, A. K., Dubonos, S. V., Grigorieva, I. V., Novoselov, K. S., Zhukov, A. A. and Shapoval, S. Y. (2003). Microfabricated adhesive mimicking gecko foot-hair. *Nature Materials* 2, 461-463.

Geiselhardt, S. F., Federle, W., Prüm, B., Geiselhardt, S., Lamm, S. and Peschke, K. (2009a). Impact of chemical manipulation of tarsal liquids on attachment in the Colorado potato beetle, Leptinotarsa decemlineata. *Journal of Insect Physiology* 56, 398-404.

Geiselhardt, S. F., Geiselhardt, S. and Peschke, K. (2009b). Comparison of tarsal and cuticular chemistry in the leaf beetle Gastrophysa viridula (Coleoptera: Chrysomelidae) and an evaluation of solid-phase microextraction and solvent extraction techniques. *Chemoecology* 19, 185-193.

Ghatak, A., Mahadevan, L., Yun, J., Chaudhury, M. and Shenoy, V. (2004). Peeling from a biomimetically patterned thin elastic film. *Proceedings of the Royal Society London A* 460, 2725-2735.

Glassmaker, N. J., Jagota, A., Hui, C.-Y., Noderer, W. L. and Chaudhury, M. K. (2007). Biologically inspired crack trapping for enhanced adhesion. *Proceedings of the National Academy of Sciences, USA* 104, 10786-10791.

Glassmaker, N. J., Jagota, A., Hui, C. Y. and Kim, J. (2004). Design of biomimetic fibrillar interfaces: 1. Making contact. *Journal of The Royal Society Interface* 1, 23-33.

Goldman, D. I., Chen, T. S., Dudek, D. M. and Full, R. J. (2006). Dynamics of rapid vertical climbing in cockroaches reveals a template. *Journal of Experimental Biology* 209, 2990-3000.

Gorb, E. V. and Gorb, S. N. (2002). Attachment ability of the beetle *Chrysolina fastuosa* on various plant surfaces. *Entomologia Experimentalis et Applicata* 105, 13–28.

Gorb, E. V. and Gorb, S. N. (2009). Effects of surface topography and chemistry of Rumex obtusifolius leaves on the attachment of the beetle Gastrophysa viridula. *Entomologia Experimentalis et Applicata* 130, 222-228.

Gorb, S., Jiao, Y. and Scherge, M. (2000). Ultrastructural architecture and mechanical properties of attachment pads in *Tettigonia viridissima* (Orthoptera Tettigoniidae). *Journal of Comparative Physiology A* 186, 821-831.

Gorb, S. and Scherge, M. (2000). Biological microtribology: anisotropy in frictional forces of orthopteran attachment pads reflects the ultrastructure of a highly deformable material. *Proceedings of the Royal Society London B* 267, 1239-1244.

Gorb, S., Varenberg, M., Peressadko, A. and Tuma, J. (2007). Biomimetic mushroom-shaped fibrillar adhesive microstructure. *Journal of The Royal Society Interface* 4, 271-275.

Gorb, S. N. (1996). Design of insect unguitractor apparatus. *Journal of Morphology* 230, 219-230.

Gorb, S. N. (1998). The design of the fly adhesive pad: distal tenent setae are adapted to the delivery of an adhesive secretion. *Proceedings of the Royal Society London B* 265, 747-752.

Gorb, S. N. (2001). Attachment devices of insect cuticle. Dordrecht, Boston: Kluwer Academic Publishers.

Gorb, S. N. (2007). Smooth Attachment Devices in Insects: Functional Morphology and Biomechanics. In *Insect Mechanics and*

Control eds. J. Casas and S. Simpson, pp. 81-116. London: Academic Press.

Gorb, S. N., Beutel, R. G., Gorb, E. V., Jiao, Y., Kastner, V., Niederegger, S., Popov, V. L., Scherge, M., Schwarz, U. and Vötsch, W. (2002). Structural design and biomechanics of friction-based releasable attachment devices in insects. *Integrative and Comparative Biology* 42, 1127–1139.

Gorb, S. N., Niederegger, S., Hayashi, C. Y., Summers, A. P., Vötsch, W. and Walther, P. (2006). Biomaterials: Silk-like secretion from tarantula feet. *Nature* 443, 407.

Gorb, S. N. and Varenberg, M. (2007). Mushroom-shaped geometry of contact elements in biological adhesive systems. *Journal of Adhesion Science and Technology* 21, 1175-1183.

Gravish, N., Wilkinson, M. and Autumn, K. (2008). Frictional and elastic energy in gecko adhesive detachment. *Journal of The Royal Society Interface* 5, 339-348.

Green, D. M. (1981). Adhesion and the toe pads of tree frogs. *Copeia* 1981, 790-796.

Green, D. M. and Simon, M. P. (1986). Digital microstructure in ecologically diverse sympatric microhylid frogs, genera *Cophixalus* and *Sphenophryne* (Amphibia: Anura), from Papua New Guinea. *Australian Journal of Zoology* 34, 135-145.

Green, P. B. and Linstead, P. (1990). A procedure for SEM of complex shoot structures applied to the inflorescence of snapdragon (Antirrhinum). *Protoplasma* 158, 33-38.

Greenwood, J. A. (1992). Contact of rough surfaces. In *Fundamentals of Friction: Macroscopic and Microscopic Processes* eds. I. L. Singer and H. M. Pollock, pp. 37–56. Dordrecht: Kluwer Academic Publishers.

Greiner, C., del Campo, A. and Arzt, E. (2007). Adhesion of bioinspired micropatterned surfaces: effects of pillar radius, aspect ratio, and preload. *Langmuir* 23, 3495-3502.

Griffith, A. A. (1921). The Phenomena of Rupture and Flow in Solids. *Philosophical Transactions of the Royal Society A: Mathematical, Physical and Engineering Sciences* 221, 163-198.

Groot, E. P., Sweeney, E. J. and Rost, T. L. (2003). Development of the adhesive pad on climbing fig (Ficus pumila) stems from clusters of adventitious roots. *Plant and Soil* 248, 85-96.

Haas, F. and Gorb, S. (2004). Evolution of locomotory attachment pads in the Dermaptera (Insecta). *Arthropod Structure & Development* 33, 45-66.

Hamaker, H. C. (1937). The London-van der Waals attraction between spherical particles. *physica* 4, 1058-1072.

Hanna, G. and Barnes, W. J. P. (1991). Adhesion and detachment of the toe pads of tree frogs. *Journal of Experimental Biology* 155, 103-125.

Hansen, W. R. and Autumn, K. (2005). Evidence for self-cleaning in gecko setae. *Proceedings of the National Academy of Sciences, USA* 102, 385-389.

Hedrick, T. L. (2008). Software techniques for two-and three-dimensional kinematic measurements of biological and biomimetic systems. *Bioinspiration & biomimetics* 3, 34001-34007.

Hertz, H. (1881). Über den Kontakt elastischer Körper. *Journal für Reine und Angewandte Mathematik* 92, 156–171.

Hill, D. E. (1977). The pretarsus of salticid spiders. *Zoological Journal of the Linnean Society* 60, 319-338.

Hooke, R. (1665). Micrographia. London: Martyn and Allestry.

Huber, G., Gorb, S. N., Hosoda, N., Spolenak, R. and Arzt, E. (2007). Influence of surface roughness on gecko adhesion. *Acta Biomaterialia* 3, 607-610.

Huber, G., Gorb, S. N., Spolenak, R. and Arzt, E. (2005a). Resolving the nanoscale adhesion of individual gecko spatulae by atomic force microscopy. *Biology Letters* 1, 2-4.

Huber, G., Mantz , H., Spolenak, R., Mecke, K., Jacobs, K., Gorb, S. N. and Arzt, E. (2005b). Evidence for capillarity contributions to gecko adhesion from single spatula nanomechanical measurements. *Proceedings of the National Academy of Sciences, USA* 102, 16293-16296.

Hui, C.-Y., Glassmaker, N. J. and Jagota, A. (2005). How compliance compensates for surface roughness in fibrillar adhesion. *Journal of Adhesion* 81, 699-721.

Hui, C.-Y., Glassmaker, N. J., Tang, T. and Jagota, A. (2004). Design of biomimetic fibrillar interfaces: 2. Mechanics of enhanced adhesion. *Journal of The Royal Society Interface* 1, 35-48.

Hui, C.-Y., Shen, L., Jagota, A. and Autumn, K. (2006). Mechanics of anti-fouling or self-cleaning in gecko setae. In *Proeedings of the 29th Annual Meeting of the Adhesion Society*, pp. 29-31. Blacksburg, VA, USA: Adhesion society, Inc.

Irschick, D. J., Austin, C. C., Petren, K., Fisher, R. N., Losos, J. B. and Ellers, O. (1996). A comparative analysis of clinging ability among pad-bearing lizards. *Biological Journal of the Linnean Society* 59, 21-35.

Israelachvili, J. (1992a). Interfacial forces. *Journal of Vacuum Science & Technology A* 10, 2961-2971.

Israelachvili, J. (1992b). Intermolecular and surface forces. London: Academic Press.

Jaeger, B. and Preston, H. C. (1854). The life of North American insects: illustrated by numerous colored engravings and narratives. Providence: Sayles, Miller and Simons.

Jagota, A. and Bennison, S. J. (2002). Mechanics of adhesion through a fibrillar microstructure. *Integrative and Comparative Biology* 42, 1140-1145.

Jagota, A., Hui, C.-Y., Glassmaker, N. J. and Tang, T. (2007). Mechanics of bioinspired and biomimetic fibrillar interfaces. *MRS bulletin* 32, 492-495.

Jeong, H. E., Lee, S. H., Kim, J. K. and Suh, K. Y. (2006). Nanoengineered multiscale hierarchical structures with tailored wetting properties. *Langmuir* 22, 1640-1645.

Jiao, Y., Gorb, S. and Scherge, M. (2000). Adhesion measured on the attachment pads of *Tettigonia viridissima* (Orthoptera, Insecta). *Journal of Experimental Biology* 203, 1887-1895.

Jin, M., Feng, X., Feng, L., Sun, T., Zhai, J., Li, T. and Jiang, L. (2005). Superhydrophobic aligned polystyrene nanotube films with high adhesive force. *Advanced Materials* 17, 1977-1981.

Johnson, K. L., Kendall, K. and Roberts, A. D. (1971). Surface energy and the contact of elastic solids. *Proceedings of the Royal Society London A* 324, 301-313.

Kendall, K. (1971). The adhesion and surface energy of elastic solids. *Journal of Physics D: Applied Physics* 4, 1186-1195.

Ker, R. F. (1977). Some structural and mechanical properties of locust and beetle cuticle. D Phil Thesis: University of Oxford.

Kesel, A. B., Martin, A. and Seidl, T. (2004). Getting a grip on spider attachment: an AFM approach to microstructure adhesion in arthropods. *Smart Materials and Structures* 13, 512-518.

Kier, W. M. and Smith, A. M. (2002). The structure and adhesive mechanism of Octopus suckers. *Integrative and Comparative Biology* 42, 1146-1153.

Kim, S. and Sitti, M. (2006). Biologically inspired polymer microfibers with spatulate tips as repeatable fibrillar adhesives. *Applied Physics Letters* 89, 261911.

Kim, S., Spenko, M., Trujillo, S., Heyneman, B., Santos, D. and Cutkosky, M. R. (2008). Smooth Vertical Surface Climbing With Directional Adhesion. *IEEE Transactions on Robotics* 24, 65-74.

Kustandi, T. S., Samper, V. D., Yi, D. K., Ng, W. S., Neuzil, P. and Sun, W. (2007). Self-assembled nanoparticles based fabrication of gecko foot-hair-inspired polymer nanofibers. *Advanced Functional Materials* 17, 2211-2218

Langer, M. G., Ruppersberg, J. P. and Gorb, S. (2004). Adhesion forces measured at the level of a terminal plate of the fly's seta. *Proceedings of the Royal Society London B* 271, 2209-2215.

Laplace, P. S. (1806). Theorie de l'action capillaire. In *Suppl. au livre X de la mécanique céleste* Paris: Courcier.

Lee, H., Lee, B. P. and Messersmith, P. B. (2007). A reversible wet/dry adhesive inspired by mussels and geckos. *Nature* 448, 338-341.

Lee, J. and Fearing, R. S. (2008). Contact Self-Cleaning of Synthetic Gecko Adhesive from Polymer Microfibers. *Langmuir* 24, 10587-10591.

Lee, J., Majidi, C., Schubert, B. and Fearing, R., S. (2008). Sliding-induced adhesion of stiff polymer microfibre arrays. I. Macroscale behaviour. *Journal of The Royal Society Interface* 5, 835-844.

Lees, A. D. and Hardie, J. (1988). The organs of adhesion in the aphid *Megoura viciae*. *Journal of Experimental Biology* 136, 209-228.

McFarlane, J. S. and Tabor, D. (1950). Adhesion of solids and the effect of surface films. *Proceedings of the Royal Society London A* 202, 224-243.

Menon, C. and Sitti, M. (2006). A biomimetic climbing robot based on the gecko. *Journal of Bionic Engineering* 3, 115-125.

Murphy, M. P., Aksak, B. and Sitti, M. (2007). Adhesion and anisotropic friction enhancements of angled heterogeneous micro-fiber arrays with spherical and spatula tips. *Journal of Adhesion Science and Technology* 21, 1281-1296.

Murphy, M. P., Aksak, B. and Sitti, M. (2009). Gecko-inspired directional and controllable adhesion. *Small* 5, 170–175.

Murphy, M. P. and Sitti, M. (2007). Waalbot: An Agile Small-Scale Wall-Climbing Robot Utilizing Dry Elastomer Adhesives. *IEEE/ASME Transactions on Mechatronics* 12, 330-338.

Niederegger, S. and Gorb, S. (2003). Tarsal movements in flies during leg attachment and detachment on a smooth substrate. *Journal of Insect Physiology* 49, 611-620.

Niederegger, S., Gorb, S. and Jiao, Y. (2002). Contact behaviour of tenent setae in attachment pads of the blowfly *Calliphora vicina* (Diptera, Calliphoridae). *Journal of Comparative Physiology A* 187, 961 –970.

Niederegger, S. and Gorb, S. N. (2006). Friction and adhesion in the tarsal and metatarsal scopulae of spiders. *Journal of Comparative Physiology A* 192, 1223-1232.

Northen, M. T. and Turner, K. L. (2005). A batch fabricated biomimetic dry adhesive. *Nanotechnology* 16, 1159-1166.

Northen, M. T. and Turner, K. L. (2006a). Batch fabrication and characterization of nanostructures for enhanced adhesion. *Current Applied Physics* 6, 379-383.

Northen, M. T. and Turner, K. L. (2006b). Meso-scale adhesion testing of integrated micro- and nano-scale structures. *Sensors and actuators* 130, 583-587.

Orso, S., Wegst, U. G. K., Eberl, C. and Arzt, E. (2006). Micrometer-scale tensile testing of biological attachment devices. *Advanced Materials* 18, 874–877.

Page, E. B. (1963). Ordered hypotheses for multiple treatments: A significance test for linear ranks. *Journal of the American Statistical Association* 58, 216-230.

Papov, V. V., Diamond, T. V., Biemann, K. and Waite, J. H. (1995). Hydroxyarginine-containing polyphenolic proteins in the adhesive plaques of the marine mussel Mytilus edulis. *Journal of Biological Chemistry* 270, 20183.

Parness, A., Soto, D., Esparza, N., Gravish, N., Wilkinson, M., Autumn, K. and Cutkosky, M. (2009). A microfabricated wedge-shaped adhesive array displaying gecko-like dynamic adhesion, directionality and long lifetime. *Journal of The Royal Society Interface* 6, 1223-1232.

Peattie, A. M. and Full, R. J. (2007). Phylogenetic analysis of the scaling of wet and dry biological fibrillar adhesives. *Proceedings of the National Academy of Sciences, USA* 104, 18595-18600.

Peattie, A. M., Majidi, C., Corder, A. and Full, R. J. (2007). Ancestrally high elastic modulus of gecko setal ß-keratin. *Journal of The Royal Society Interface* 3, 1071-1076.

Pelletier, Y. and Smilowitz, Z. (1987). Specialized tarsal hairs on adult male Colorado potato beetles, *Leptinotarsa decemlineata* (Say), hamper its locomotion on smooth surfaces. *Canadian Entomologist* 119, 1139-1142.

Peressadko, A. and Gorb, S. N. (2004a). When less is more: experimental evidence for tenacity enhancement by division of contact area. *Journal of Adhesion* 80, 247-261.

Peressadko, A. G. and Gorb, S. N. (2004b). Surface profile and friction force generated by insects. In *First International Industrial Conference Bionik 2004, Fortschritt-Berichte VDI 15, Nr.249*, pp. 257-263. Düsseldorf, Germany: VDI Verlag.

Peressadko, A. G., Hosoda, N. and Persson, B. N. J. (2005). Influence of surface roughness on adhesion between elastic bodies. *Physical Review Letters* 95, 124301.

Persson, B. N. J. (1999). Sliding friction. *Surface Science Reports* 33, 85-119.

Persson, B. N. J. (2003). On the mechanism of adhesion in biological systems. *Journal of Adhesion Science and Technology* 118, 7614-7620.

Persson, B. N. J. (2007). Biological adhesion for locomotion on rough surfaces: basic principles and a theorist's view. *MRS bulletin* 32, 486-490.

Persson, B. N. J., Albohr, O., Tartaglino, U., Volokitin, A. I. and Tosatti, E. (2005). On the nature of surface roughness with application to contact mechanics, sealing, rubber friction and adhesion. *Journal of Physics: Condensed Matter* 17, R1-R62.

Persson, B. N. J. and Gorb, S. (2003). The effect of surface roughness on the adhesion of elastic plates with application to biological systems. *Journal of Chemical Physics* 119, 11437-11444.

Qu, L., Dai, L., Stone, M., Xia, Z. and Wang, Z. L. (2008). Carbon nanotube arrays with strong shear binding-on and easy normal lifting-off. *Science* 322, 238 - 242.

Ridgel, A. L., Ritzmann, R. E. and Schaefer, P. L. (2003). Effects of aging on behavior and leg kinematics during locomotion in two species of cockroach. *Journal of Experimental Biology* 206, 4453-4465.

Riskin, D. K. and Fenton, M. B. (2001). Sticking ability in Spix's disk-winged bat, Thyroptera tricolor (Microchiroptera : Thyropteridae). *Canadian Journal of Zoology-Revue Canadienne De Zoologie* 79, 2261-2267.

Riskin, D. K. and Racey, P. A. (2009). How do sucker-footed bats hold on, and why do they roost head-up? *Biological Journal of the Linnean Society* 99, 233-240.

Rosenberg, H. I. and Rose, R. (1999). Volar adhesive pads of the feathertail glider, Acrobates pygmaeus (Marsupialia; Acrobatidae). *Canadian Journal of Zoology* 77, 233-248.

Rovner, J. S. (1978). Adhesive hairs in spiders: behavioral functions and hydraulically mediated movement. *Symposia of the Zoological Society, London* 42, 99-108.

Ruibal, R. and Ernst, V. (1965). The structure of the digital setae in lizards. *Journal of Morphology* 117, 271-294.

Russell, A. P. (1975). A contribution to the functional analysis of the foot of the Tokay, Gekko gecko (Reptilia: Gekkonidae). *Journal of Zoology London* 176, 437-476.

Russell, A. P. (2002). Integrative functional morphology of the gekkotan adhesive system (Reptilia: Gekkota). *Integrative and Comparative Biology* 42, 1154-1163.

Santos, R., Gorb, S., Jamar, V. and Flammang, P. (2005). Adhesion of echinoderm tube feet to rough surfaces. *Journal of Experimental Biology* 208, 2555-2567.

Scherge, M. and Gorb, S. N. (2001). Biological micro- and nanotribology: nature's solutions. Berlin, New York: Springer.

Scholz, I., Baumgartner, W. and Federle, W. (2008). Micromechanics of smooth adhesive organs in stick insects: pads are mechanically

anisotropic and softer towards the adhesive surface. *Journal of Comparative Physiology A: Neuroethology, Sensory, Neural, and Behavioral Physiology* 194, 373-384.

Scholz, I., Buckins, M., Dolge, L., Erlinghagen, T., Weth, A., Hischen, F., Mayer, J., Hoffmann, S., Riederer, M., Riedel, M. and Baumgartner, W. (2010). Slippery surfaces of pitcher plants: Nepenthes wax crystals minimize insect attachment via microscopic surface roughness. *Journal of Experimental Biology* 213, 1115-1125.

Schubert, B., Lee, J., Majidi, C. and Fearing, R. S. (2008). Sliding-induced adhesion of stiff polymer microfibre arrays. II. Microscale behaviour. *Journal of The Royal Society Interface* 5, 845-853.

Sethi, S., Ge, L., Ci, L., Ajayan, P. M. and Dhinojwala, A. (2008). Gecko-inspired carbon nanotube-based self-cleaning adhesives. *Nano Letters* 8, 822-825.

Sitti, M. and Fearing, R. S. (2003). Synthetic gecko foot-hair micro/nano-structures as dry adhesives. *Journal of Adhesion Science and Technology* 17, 1055-1073.

Slifer, E. H. (1950). Vulnerable areas on the surface of the tarsus and pretarsus of the grasshopper (Acrididae, Orthoptera) with special reference to the arolium. *Annals of the Entomological Society of America* 43, 173-188.

Smith, A. M. (1991). The role of suction in the adhesion of limpets. *Journal of Experimental Biology* 161, 151-169.

Smith, A. M. (1992). Alternation between attachment mechanisms by limpets in the field. *Journal of Experimental Marine Biology and Ecology* 160, 205-220.

Smith, A. M. (1996). Cephalopod sucker design and the physical limits to negative pressure. *Journal of Experimental Biology* 199, 949-958.

Smith, C. W., Herbert, R., Wootton, R. J. and Evans, K. E. (2000). The hind wing of the desert locust (Schistocerca gregaria Forskal). II. Mechanical properties and functioning of the membrane. *Journal of Experimental Biology* 203, 2933-2943.

Snodgrass, R. E. (1935). Principles of insect morphology. New York, London: McGraw-Hill Book Company.

Spagna, J. C., Goldman, D. I., Lin, P., Koditschek, D. E. and Full, R. J. (2007). Distributed mechanical feedback in arthropods and

robots simplifies control of rapid running on challenging terrain. *Bioinspiration and Biomimetics* 2, 9-18.

Spenko, M. J., Haynes, G. C., Saunders, J. A., Cutkosky, M. R., Rizzi, A. A., Full, R. J. and Koditschek, D. E. (2008). Biologically inspired climbing with a hexapedal robot. *Journal of Field Robotics* 25, 223-242.

Spolenak, R., Gorb, S. and Arzt, E. (2005). Adhesion design maps for bio-inspired attachment systems. *Acta Biomaterialia* 1, 5-13.

Spolenak, R., Gorb, S., Gao, H. and Arzt, E. (2004). Effects of contact shape on the scaling of biological attachments. *Proceedings of the Royal Society London A* 460, 1-15.

Stefan, J. (1875). Versuche über die scheinbare Adhäsion. *Annalen der Physik und Chemie* 230, 316-318.

Stork, N. E. (1980a). Experimental analysis of adhesion of *Chrysolina polita* (Chrysomelidae: Coleoptera) on a variety of surfaces. *Journal of Experimental Biology* 88, 91-107.

Stork, N. E. (1980b). Role of waxblooms in preventing attachment to brassicas by the mustard beetle, Phaedon cochleariae. *Entomologia Experimentalis et Applicata* 28, 100-107.

Stork, N. E. (1980c). A scanning electron microscope study of tarsal adhesive setae in the Coleoptera. *Zoological Journal of the Linnean Society* 68, 173-306.

Stork, N. E. (1983). A comparison of the adhesive setae on the feet of lizards and arthropods. *Journal of Natural History* 17, 829-835.

Stork, N. E. and Evans, E. G. (1976). Tarsal setae in Coleoptera. *International Journal of Insect Morphology and Embryology* 5, 219-221.

Sukontason, K. L., Bunchu, N., Methanitikorn, R., Chaiwong, T., Kuntalue, B. and Sukontason, K. (2006). Ultrastructure of adhesive device in fly in families Calliphoridae, Muscidae and Sarcophagidae, and their implication as mechanical carriers of pathogens. *Parasitology Research* 98, 477-481.

Sutton, G. P. and Burrows, M. (2008). The mechanics of elevation control in locust jumping. *Journal of Comparative Physiology A: Neuroethology, Sensory, Neural, and Behavioral Physiology* 194, 557-563.

Taylor, A. M., Bonser, R. H. C. and Farrent, J. W. (2004). The influence of hydration on the tensile and compressive properties of avian keratinous tissues. *Journal of Materials Science* 39, 939-942.

Taylor, C. and Wells, E. (1795). Augustin Calmet's Great Dictionary of the Holy Bible, Historical, Critical, Geographical, and Etymological. London: Published for C. Taylor.

Thewissen, J. G. M. and Etnier, S. A. (1995). Adhesive devices on the thumb of Vespertilionoid bats (Chiroptera). *Journal of Mammalogy* 76, 925-936.

Thompson, D. A. W. (1918). The works of Aristotle: Historia animalium. Oxford: The Clarendon Press.

Varenberg, M. and Gorb, S. (2007). Shearing of fibrillar adhesive microstructure: friction and shear-related changes in pull-off force. *Journal of The Royal Society Interface* 4, 721-725

Varenberg, M., Peressadko, A., Gorb, S. and Arzt, E. (2006). Effect of real contact geometry on adhesion. *Applied Physics Letters* 89, 121905.

Vincent, J. F. V. and Wegst, U. G. K. (2004). Design and mechanical properties of insect cuticle. *Arthropod Structure & Development* 33, 187-199.

Voigt, D., Schuppert, J. M., Dattinger, S. and Gorb, S. N. (2008). Sexual dimorphism in the attachment ability of the Colorado potato beetle *Leptinotarsa decemlineata* (Coleoptera: Chrysomelidae) to rough substrates. *Journal of Insect Physiology* 54, 765-776.

Vötsch, W., Nicholson, G., Müller, R., Stierhof, Y.-D., Gorb, S. and Schwarz, U. (2002). Chemical composition of the attachment pad secretion of the locust *Locusta migratoria*. *Insect Biochemistry and Molecular Biology* 32, 1605-1613.

Waite, J. H., Holten-Andersen, N., Jewhurst, S. and Sun, C. J. (2005). Mussel adhesion: finding the tricks worth mimicking. *Journal of Adhesion* 81, 297-317.

Williams, E. E. and Peterson, J. A. (1982). Convergent and alternative designs in the digital adhesive pads of scincid lizards. *Science* 215, 1509-1511.

Yamaguchi, T., Gravish, N., Autumn, K. and Creton, C. (2009). Microscopic Modeling of the Dynamics of Frictional Adhesion in

the Gecko Attachment System. *The Journal of Physical Chemistry B* 113, 3622-3628.

Yao, H. and Gao, H. (2006). Mechanics of robust and releasable adhesion in biology: bottom up designed hierarchical structures of gecko. *Journal of the Mechanics and Physics of Solids* 54, 1120-1146.

Yoon, E.-S., Singh, R. A., Kong, H., Kim, B., Kim, D.-H., Jeong, H. E. and Suh, K. Y. (2006). Tribological properties of bio-mimetic nano-patterned polymeric surfaces on silicon wafer. *Tribology Letters* 21, 31-37.

Young, T. (1805). An essay on the cohesion of fluids. *Philosophical Transactions of the Royal Society of London* 95, 65-87.

Young, T., Peacock, G. and Leitch, J. (1855). Miscellaneous works of the late Thomas Young. London: J. Murray.

Yurdumakan, B., Raravikar, N. R., Ajayan, P. M. and Dhinojwala, A. (2005). Synthetic gecko foot-hairs from multiwalled carbon nanotubes. *Chemical Communications* 2005, 3799-3801.

Zhao, Y., Tong, T., Delzeit, L., Kashani, A., Meyyappan, M. and Majumdar, A. (2006). Interfacial energy and strength of multiwalled-carbon-nanotube-based dry adhesive. *Journal of Vacuum Science & Technology B: Microelectronics and Nanometer Structures* 24, 331-335.

A

APPENDIX

A.1 DETAIL ON THE POTENTIAL FOR SYNTHETIC FIBRILLAR ADHESIVES

Biomimetic adhesives have in recent years come to represent an important and vibrant field of research. As discussed above, biological adhesives possess many desirable properties such as dynamic attachment, reusability and substrate tolerance. Hence the development of commercially viable biomimetic structures could satisfy the demands of applications as diverse as climbing robots, or microsystem assembly manipulation. In addition, as they allow the possibility of manipulation of parameters (such as seta size or stiffness), they also have the potential to shed light on the functions or the structures they seek to imitate.

Due to the perceived advantages of the hairy system as discussed in section 1.3, very few material scientists have focused on the replication of smooth systems (although see: Glassmaker et al., 2007). Instead, many groups have taken the hairy systems of geckos or insects as their inspiration. Several important advances have been made, relying on a variety of fabrication techniques. Initially these were based on the patterning or moulding of soft polymeric materials (e.g. PMA, PDMS, polystyrene or polyimide); for example by creating incisions on thin films (Chung and Chaudhury, 2005; Ghatak et al., 2004), casting soft-moulding polymers around a microfabricated template (Crosby et al., 2005; Glassmaker et al., 2004; Greiner et al., 2007; Peressadko and Gorb, 2004a; Sitti and Fearing, 2003), or hot embossing (Jeong et al., 2006; Yoon et al., 2006). Nanopore membranes are also used as commercially available moulds for the production of nano-meter sized fibres and then selectively dissolved away (Jin et al., 2005; Lee et al., 2008; Sitti and Fearing, 2003). Lithography and dry etching provide further techniques for the creation of fibres (Geim et al., 2003; Northen and Turner, 2005; Northen and Turner, 2006a) with a recent example involving the use of self-assembling microspheres as a mask for silicon etching (Kustandi et al., 2007). Techniques have also been developed that do not require the use of a template or mould, the most notable of these being the use of carbon nanotube (CNT) forests, fabricated via chemical vapour deposition

onto silicon substrates (Qu et al., 2008; Yurdumakan et al., 2005; Zhao et al., 2006).

Attempts have been made to replicate many of the detailed morphological structures of natural adhesive arrays. For example; angled fibres (Aksak et al., 2007), spatula, mushroom shaped or pyramidal tips (del Campo et al., 2007; Murphy et al., 2007; Murphy et al., 2009; Parness et al., 2009; Varenberg and Gorb, 2007), fluid covered surfaces (Lee et al., 2007) or hierarchical structures (Del Campo and Greiner, 2007; Jeong et al., 2006; Northen and Turner, 2006b). Polymer microfiber based adhesives have even begun to show some of the self-cleaning properties (Lee and Fearing, 2008) observed in geckos (Hansen and Autumn, 2005).

However, despite these significant advances, the majority of synthetic adhesives occupy a different parameter space with fabrication limitations making artificial setae either larger or stiffer than their natural counterparts. They also still fall short of the performance of the natural systems in terms of the magnitude of attachment stresses supported or reusability. This is due to a lack of understanding of the biological systems which are being imitated. With a few exceptions (e.g. see: Autumn et al., 2006c; Orso et al., 2006; Peattie et al., 2007) almost no information is available on the material properties of the natural hairs. In most cases, frictional and adhesive performance is unknown, making it impossible to test the proposed models. The exact functions of many of the observed morphologies are not yet recognised and many crucial design features are therefore still absent from synthetic studies.

A.2 ADDITIONAL MATHEMATICAL MODELS FOR MAXIMAL ADHESION

In addition to the force scaling model presented in section 1.3 of the introduction, two further theoretical concepts explain the idea that a fibrillar array may be able to maximise the overall adhesive force. These concepts are the crack arresting model and the work of adhesion model and are presented below.

A.2.1 The crack arresting model

Detachment of an adhesive and substrate can be modelled as a fracture between the two surfaces. The 'crack arresting' property of a fibrillar array states that when each contact is smaller than a critical crack length it will not be broken by the independent propagation of such fractures. This is because the elastic energy released will no longer be greater than the energy needed to form two distinct surfaces (Griffith, 1921).

As the area of a crack tip tends to zero, the stress should correspondingly approach infinity and any crack should always

break a solid. However, theoretical facture mechanics, as proposed by Griffith, states that the growth of a crack requires energy (proportional to the crack length, *CL*) in order to create two distinct surfaces (Griffith, 1921). This energy comes from the loss of strain energy (proportional to the square of the crack length) resulting from the relaxation of stresses as the crack propagates. Failure will therefore not occur when the crack is small enough that there is no longer sufficient energy to form two surfaces. Elastic energy released, *G* is given by

$$G = \frac{\pi\sigma^2 CL}{2E} \geq \gamma \qquad [A.1]$$

which must be bigger than γ, the surface energy (i.e. the energy needed to form two surfaces) for propagation. E is the elastic modulus and σ the applied stress. Hence the minimum crack length must be

$$CL \geq \frac{2\gamma E}{\pi\sigma^2} \qquad [A.2]$$

This implies that the division of the surface into contacts smaller than the critical crack length will prevent failure from crack propagation. Division of contact therefore helps to reduce susceptibility to flaws and to increase attachment forces (Gao and Yao, 2004; Hui et al., 2004). Some of the first synthetic fibrillar adhesives were formed by simply scoring a polymer film with a razorblade, creating rows of fibres. Upon subjecting them to peel tests, these patterned surfaces demonstrated a 20 times increase in the fracture energy compared to the smooth control and this was attributed to the crack arresting properties of a divided contact (Chung and Chaudhury, 2005; Ghatak et al., 2004).

A.2.2 The work of adhesion model

The 'work of adhesion' model is used to describe the detachment of a pad which peels from one edge loading the peel force on the peripheral setae (in contrast to the force scaling model which requires equal loading across all setae). As the hairs act as crack arrestors (Hui et al., 2004; Jagota and Bennison, 2002), the energy needed to detach each hair will be lost and the adhesion of the pad will depend on the force required to deform and detach each hair. The increased compliance of an array of flexible hairs will increase the normal adhesive force (or 'pull-off force') as energy must additionally be put in to bend the hairs (Jagota and Bennison, 2002). This allows significant adhesion even when relying on relatively

weak attachment mechanisms such as van der Waals forces. By dividing the contact into several fine, flexible hairs, the overall effective elastic modulus of the pad is decreased and, due to the greater displacement, the work of adhesion increases.

Several parameters will affect the amount of energy lost during stretching of a fibrillar array. The flexibility of the array, and hence its ability to deform, will depend on the radius, r and length, l of the hairs and the elastic modulus, E of the material. Additionally as hairs will be more easily bent when compressed or pulled perpendicularly to their axis, the hair angle, θ will also affect flexibility (Glassmaker et al., 2004; Persson, 2003). Effective work of adhesion, W is given by (Federle, 2006)

$$W \approx \frac{2F^2 N_A l^3}{3\pi r^4 E} \sin\theta \cos^2\theta \qquad [A.3]$$

Where F is the adhesive force to the surface and N_A the density of hairs. Hence longer, thinner hairs will contribute more to the work of adhesion. Many natural setal arrays are also angled or curved, affording greater compliance in the perpendicular direction (Glassmaker et al., 2004; Persson, 2003).

A.2.3 The self-matting constraint

All three of the above models are constrained by 'self-matting' or 'condensation' (Glassmaker et al., 2004; Persson, 2003; Sitti and Fearing, 2003; Spolenak et al., 2005) as this places a limit on seta miniaturisation. This is a result of overly flexible adhesive hairs sticking to each other, forming clumps which reduce attachment contact area. Several theories based on bending-beam models (Glassmaker et al., 2004; Persson, 2003; Sitti and Fearing, 2003; Spolenak et al., 2005) show that there is a maximal density of hairs (N_A) permissible before lateral collapse will occur. This is related to the flexibility of the hairs, for example by Sitti & Fearing (2003) as:

$$N_A = \frac{1}{d^2} \leq \frac{9\pi^2 r^8 E^2}{64 F^2 l^6} \qquad [A.4]$$

Where N_A is the maximal setal density, d the minimum distance between setae, F the adhesion between hairs (assumed to be equal to the adhesive force between the hairs and the substrate) and assuming hairs are small-strain bending beams of radius r, length l and elastic modulus E (as described in section 1.4). Hence thicker hairs with larger contacts are required, limiting each of the above models (Federle, 2006).

A.3 ESTIMATION OF THE DECELERATION DUE TO ADHESION ON A JUMPING INSECT

To estimate the maximum amount of deceleration the beetles would experience as a result of foot adhesion in the pulling direction, we assume that the beetle has reached a maximum velocity v_0 at the end of its acceleration phase, and its legs are in the extended position. The beetle will now be decelerated until detachment, when the pulling force on the pad has reached F_{max}. Assuming that the straight legs behave like a linear spring with spring constant k, the equation of motion during the deceleration phase is:

$$\ddot{s} = -\frac{k}{m}s, \qquad [A.5]$$

where s is the beetle's displacement along its trajectory and m its body mass. With initial conditions s=0 and v=v_0, the solution is:

$$s(t) = v_0\sqrt{\frac{m}{k}}\sin\left(\sqrt{\frac{k}{m}}t\right) \qquad [A.6]$$

and

$$v(t) = v_0\cos\left(\sqrt{\frac{k}{m}}t\right) \qquad [A.7]$$

Time until detachment (i.e. at F=F_{max}) is calculated by substituting Hooke's law F_{max}=ks into Equation A.6, giving:

$$t_{detach} = \sqrt{\frac{m}{k}}\arcsin\left(\frac{F_{max}}{v_0\sqrt{km}}\right) \qquad [A.8]$$

Substituting into equation A.7 gives final take-off velocity as:

$$v(t_{detach}) = \sqrt{v_0^2 - \frac{F_{max}^2}{km}} \qquad [A.9]$$

Equation A.9 shows that the decrease in take-off velocity caused by foot adhesion is inversely related to the leg's spring constant k. Estimating $F_{max} \approx 16$ mN (from two feet), $m \approx 8$ mg and $v_0 \approx 1$ m s^{-1}, the beetle would only be brought to a complete stop if the leg's spring constant was as small as 32 Nm^{-1}, and t_{detach} would be 0.8 ms. Whilst the spring constant of the extended flea beetle legs is not known, the deceleration time is clearly much shorter than this value.

In this range, velocity decreases approximately linearly as:

$$dv \approx -\frac{F_{\max} t}{2m} \qquad [A.10]$$

With an upper estimate of $t_{detach} \approx 0.2$ ms and the above values for F_{max} and m, $dv \approx 0.2$ m s^{-1}, i.e. the beetle would only lose a fraction of its initial velocity due to foot adhesion. It is likely that t is even shorter than this estimate, making the loss of momentum even more negligible.

List of symbols

F	force	N	seta number
R	radius	d	setal spacing
l	length	N_A	seta density
θ	angle	r	radius of curvature
k	spring constant	a	contact radius
E	elastic modulus	μ	coefficient of friction
K	bulk elastic modulus	n	number
ν	Poisson ratio	p	pressure
h	height or separation	s	displacement
δ	deflection	v	velocity
B	width	a	acceleration
A	area	m	mass
γ	surface energy	t	time
W	work of adhesion	CL	crack length
G	elastic energy	σ	stress
η	viscosity	A_H	Haymaker constant

List of abbreviations

SEM	scanning electron microscope
FIB	focused ion beam
AFM	atomic force microscope
COM	centre of mass
s.e.m.	standard error on the mean
PMA	Polymethyl acrylate
PDMS	Polydimethylsiloxane
CNT	carbon nanotube
PID	proportional–integral–derivative
I/O	input/output
PCI	peripheral component interconnect
w/w	weight/weight